SELF-POWERED BIO-SENSING PLATFORM WITH GLUCOSE ENERGY HARVESTING FUEL CELL

A thesis submitted for the degree of Doctor of Philosophy

By

Santos Bunga

Department of Electronic and Computer Engineering

Brunel University

May 2016

Supervision:

Dr Antonio Vilches

Dr Wenhui Song

Abstract

The design and implementation of self-powered, low power implant microcontroller, with wireless data transmitter system that captures data as subcutaneous bio-sensing platform has been achieved with glucose fuel cell (GFC) energy harvesting power solution. Data transfer is unidirectional, implant to reader and is initiated by a single transmission from the external reader. The implant's memory contents are transmitted as a stream of wireless pulses to the reader. This work explored two different approaches on current technologies used for designing self-powered bio medical devices (BMDs) and active implantable medical devices (IMDs), their processing, sampling data, transmission of data and energy hasting powering techniques with a view to identifying state-of-the art technologies and methods to improve the long-term powering and recharging of IMDs via a highly safe, efficient and convenient way.

The designed low power implant microcontroller, with wireless data transmitter system combines glucose energy harvesting technique by using materials with efficient catalyst capabilities based on platinum nanoparticles supported on Vulcan carbon cloth (PtVCC) as a cathode electrode for GFC configuration, while plain Platinum (Pt) mesh/sheet acted as anode. The PtVCC and Pt electro-reaction, catalytic activities and stability resulted in a design of a direct GFC with high output voltage and current, >0.4V and >300μA respectively per cell, and increased this voltage to value >4V, to power the implant system, by using a voltage booster; direct current to direct current (DC-DC) converter circuit, and a rechargeable battery. The innovative self-powered bio-sensing platform integrating GFC design, meets the self-powered IMDs expectations in terms of simplified fabrication and materials that allows one-compartment design that can directly be placed on the surface of medical implant to provide sufficient output power boosted by DC-DC converter to produced higher output voltage ten times greater than the input value, enough to power most efficient electronic devices.

This research therefore proposes the practicability and potential of designing and implementing a wireless bio-sensor system powered by an energy harvesting solution, based on GFC to produce a proof-of-concept design system and integration, including power management and data communication (sampling and transmission) platform suitable for self-low-powered periodically-activated IMD.

List of Abbreviations

AFC	Abiotic Fuel Cell
AIMD	Active Implantable Medical Devices
ADC	Analogue to Digital Converter
BFC	Bio Fuel Cell
BMD	Bio Medical Device
EMC	Electromagnetic Compatibility
ETSI	European Telecommunications Standards Institute
CMOS	Complementary Metal-Oxide Semiconductor
CAD	Computer Aided Design
CV	Cyclic Voltammetry
DI	Deionized
GDL	Diffusion Layers
DC	Direct Current
DGFC	Direct Glucose Fuel Cell
SEM	Electron Scanning Microscopy
EDS	Energy-Dispersive X-Ray Spectroscopy
FSK	Frequency-shift keying
FTIR	Fourier Transform Infrared
GFC	Glucose Fuel Cell
GOX	Glucose Oxidase
PTFE	Hydrophobic Treatment
ISM	Industrial, Scientific and Medical
IBFCs	Implantable Bio Fuel Cells
IBMDs	Implantable Biomedical Devices
IR	Infrared
IGFC	Implantable Glucose Fuel Cell
IMD	Implantable Medical Device
IC	Integrated Circuit
MRI	Magnetic Resonance Imaging
MPL	Micro Porous Layer
NWBFC	Nanowire-Based Biofuel Cell

NW	Nano-Wire
OCD	Obsessive Compulsive Disorder
PtVCC	Platinum Nanoparticles Supported On Vulcan Carbon Cloth
PDM	Pulse Delay Modulation
PEM	Polymer Electrolyte Membrane
QAM	Quadrature Amplitude Modulation
RF	Radio Frequency
RFID	Radio Frequency Identification
Redox	Reduction-Oxidation
SOIC	Small Outline Integrated Circuit
TX	Transmitter
TR	Transponder
WPT	Wireless Power Transfer

Contents

List of Tables

List of Figures

Acknowledgments

To my supervisor and colleagues: Dr Tony Vilches and the family, Dr Wenhui Song, Dr Dele Sanni and Dr Thomas Maltby: Thank you all for your support, friendship and laughter over these past seven years.

To my wonderful family and friends in London and in Angola: Kissanga Madalena, Miguel Paca, Sunguila J M Paca, Cassa Petronel, Paulina Kiloso, Sebastiao Emanuel, Maria Mbongo and The Messenger Choir family: Thank you all for everything you've added to my life over all these years.

To Dr Tony Vilches: Thank you for your decision for allowing me to join your PhD team and for my transfer to Brunel and to my oral defence, you have supported and guided me in this journey, your guidance and instructions have been invaluable to me - adding discernment, strength and joy to my life. You are an amazing person and you have been such a wonderful friend. I am so very thankful to have you in my life.

To Dr Wenhui Song: Thank you for your time, support and guidance, I have learned, grown and been inspired so much by you during this PhD.

To mam: This PhD is mostly dedicated to you, for all that you have missed and wished for, I hope that your joy is complete through what Lord Jesus has given me. I thank the Lord Jesus for giving me such wonderful and amazing mother, I love you!

I thank Lord Jesus for giving me the strength, joy and determination to learn and explore the challenges of research in electronics and Bio IMD elements.

Declaration

The research work presented in this thesis is the original work of the author conducted between June 2009 and May 2016. Parts researched externally have been suitably referenced.

Chapter 1

Introduction

Human body is the most complex, well-structured system mankind has ever known, and consequently, one third of most common cause of death and disabilities in the world are through its metabolism disorder (WHO, 2004). The ability to control, monitor, assist and improve patient's health is increasingly relying on advancement in technology, and subsequently significant appreciations of biological processes are taking place through breakthrough of these technologies (Bazaka, 2013 and Burleson, 2012), however the challenge of a sustainable power-source to drive bio-implants remains. The human body can provide sources of power for implantable devices by means of energy harvesting techniques. In spite of recent advances in various approaches using mechanical vibrations, body movements and thermoelectric forms of energy harvesting, there have been no promising results that can replace batteries for medical implants (Bettin, 2006; Bazaka, 2013; Burleson, 2012; Van, 2012; Olivo, 2011 and Rapoport, 2012). However, Implantable fuel cells that make use of naturally replenishable body fluids should also be considered as a source of power wherever continuous and sufficient power output, longevity, biocompatibility and integration into medical devices are important and challenging. To design intelligent implants with low power systems capable of long-term usage to reduce frequent surgical activities that are cumbersome to patients (Bazaka, 2013), is best achieved with a continuous energy harvesting power systems, to avoid replacing batteries eventually when powering IMDs over 10 years. Since designers of IMDs face enormous challenges to balance safety, reliability, complexity, power consumption, cost and design requirements to reduce the size and weight of these devices, thus, the need for device integration becomes vital (Burleson, 2012; McDonald, 2011 and Yakovlev, 2012). This study focused on key design features that enables latest medical devices technology that include microcontrollers, sensors, wireless products and fuel cell energy. The transition analogy to integrate the implantable circuit features into silicon does provide the keys to meet different aspects of this design. It is obvious that human body can also provide sufficient power by harnessing the energy harvested by devices such as vibrations and thermoelectric from body movements and body temperature respectively (Gollakota, 2011), however, currently they do not produce enough power to assist on continues recharging of the batteries of existing IMDs (Yakovlev, 2012).

It is well known that BMDs have been around for decades (McDonald, 2011), but in recent years, the progress on working capabilities of implantable biomedical systems that support advanced technological functionalities such as wireless communication system

for implantable means (Yakovlev, 2012), are new and recently driven by adaption of radio frequency identification (RFID) technology concept, that leads different implant devices to be used in many different parts of the body for various applications such as pacemakers, cardiac defibrillators, insulin pumps, and neurostimulators including drug delivery systems (Bazaka, 2013; Gollakota, 2011; Khan, 2014). As a result, by combining the wireless communication technologies with low-power biomedical sensors and body energy harvesting solutions, including the wireless networks for in-home monitoring and diagnosis of patients, this should give rise to improved system able to deliver timely treatment, leading to increasingly patients' improved medical outcomes and subsequently providing a better health care systems (Bazaka, 2013; Burleson, 2012 and Gollakota, 2011). However, GFC studies have shown promising capabilities to producing higher output power capable of driving implantable devices compared to other energy harvesting techniques, and the concept of harvesting human's body fluid to drive IMDs with consistent and reliable power solution for driving the low-power bio-sensing platform with accurate data sensing, data storage and data transmission has been accomplished.

1.1. Structure of thesis

This thesis is structured as follows: in chapter One, presented significant appreciations of biological processes taking place through technological breakthroughs, the current challenges in designing intelligent implants with low power systems capable of long-term usage to reduce frequent surgical activities that are cumbersome to patients. In chapter Two, current and relevant literature review of IMD interfaces for data communication and power are discussed, with emphasis on Implantable glucose fuel cells as the best possible energy harvesting technique for powering IMDs. Chapter Three presents a discussion of the initial experimental methodologies leading to low power smart microcontroller systems; a bio-sensing platform self-powered system using widely available components capable of being powered by the GFC, circuitry consisting of a designed microcontroller-transmitter systems without an oscillator. While Chapter Four discusses laboratory experimental results from the designed and developed self-powered bio-sensing platform with IGFC Power Management and Energy Storage system based on Quadrature amplitude modulation (QAM) radio frequency (RF) micro-transmitter (TX) systems that transmit sensory data to a RFM12B reader microcontroller interfaced to a PC. Chapter Five summarizes and concludes with suggestions for future work.

1.1.1. Aims

The aim of this study was to monitor, assist and improve patient's health state, by employing self-sustainable monitoring device to last the lifespan of the patient, to:

a) Reduce frequent cumbersome and painful surgical activities to patients
b) Reduce the costs involved with frequent implant or battery replacements.

1.1.2. Objectives

1. Improve the electronic processes and systems of transferring signals / data outside patient's body, and management of power source inside patient's body.
2. Design microcontroller based transmitter system to capture (patient's health state) data, and:
    a) Send the captured data wirelessly
    b) Provide accuracy performance in various conditions
    c) Develop control-circuits that have only essential hardware functions designs:
        i. with or without an oscillator
    d) Obtain low power design concepts
3. Improved energy harvesting device by selecting design and materials with higher output power compared to the existing devices.
4. Design and test power management systems that can provide efficient energy storage and energy distribution.
5. Consider bio-compatible materials that meet the implantable requirements
6. Design microcontroller based reader system to decode the transmitted data, by:
    a) Capturing data with or without further amplification
    b) Confirming performance accuracy of received data
    c) Confirming performance of effective data decoding mechanism
7. Confirm overall system performance using different/multiple analytical and data displaying tools for validation.

The interfaced bio-sensing platform presents a simple and cheap low-powered system using widely available components that can be powered by GFC system. Finally, this study's objective is to design IMD with key attributes required in the silicon technology for implementing implantable integrated circuit (IC) designs.

Chapter 2

Literature Review

2.1. Implantable Medical Devices (IMDs)

Any device purposely placed inside the body through surgical means and planned to remain in place after the medical procedure for at least a month is considered an implantable device, and this also include devices intended to replace body parts, however, temporary vascular access skin nor a wound closure intended to be removed after 7 – 30 days or more are not considered long-term implantable devices (MEDDEV, 2010). Consequently when a medical device is equipped with a source of electrical energy for diagnosis, prevention or monitoring and is totally or partially and surgically or medically placed inside the body; this is then referred to as an IMD (Peisino, 2013; Campi, 2014 and Joung, 2013). Irrespective of their intended use, most implantable systems comprise of two essential modules; an internal to the body, and another external device outside the body. The external device communicates with the internal device for mostly two-way data transfer, while some system designs incorporate also power transfer, (Bazaka, 2013). Furthermore, IMDs can be divided into two categories: Active; that use energy source for their function to monitor relevant parameters or signals in order to optimise treatments to the patient by delivering electrical signals or medicine to organs or tissues (Campi, 2014). Contrary to that are Passive implantable devices, which do not contain energy sources to monitor or provide treatments.

Since medical devices (MD) are man-made instruments aiming to replace, support, or enhance biological structures (Peisino, 2013), with this comes the challenge to retaining this support to the lifetime of the patient, as such, the main challenge to IMDs is the short lifespan of the batteries, which leads to undesirable surgery to replace the IMD battery; for that reason the durability of the whole IMD is determined by the battery lifespan (Cadei, 2014). In order to avoid such issues different solution including battery less IMDs through energy harvesting techniques are being studied, because human body is a rich source of energy that can be harvested kinetically (body movements parts), thermal (heat), breathing, or chemical reactions such as glucose oxidation from a fuel cell, (Bazaka, 2013; Cadei, 2014; Kerzenmacher, 2008; Olivo, 2011; Oncescu, 2011 and Schmidt, 2011), include inductive links for wireless power transmission to recharge the battery (Bazaka, 2013; Burleson, 2012; Yakovlev, 2012; Peisino, 2013; Campi, 2014; Kiani, 2012 and Hached, 2014). Another area of IMD trial researches involve the communication between IMD and the external controller including internet based network; sending and receiving status and performance commands to adjust operations leading to remote monitoring through data transfer between the devices (Meng, 2014).

Even though using implantable wireless devices reduce the frequency of routine follow-up visits, in turn reducing staff time and costs while improving the patient's life, this also can lead to new threats concerning security of IMDs, becoming vulnerable to hackers, yet this concern is less addressed on most IMD research papers, (Burleson, 2012), nonetheless this will not form part of this report. For the purpose of this perspective report, the focus will be on implantable devices with electrical features and function which do require electrical power to operate, hence comprising review of the current literature on IMD powering and data transmission research, to have a better understanding of the state of the art and the gaps on the active implantable devices (Peisino, 2013).

2.1.1. Different types of IMDs

Each country regulatory authorities categorise medical devices in different classes, based on their design complexity, use features and their likelihood to cause harm if misused (Khan, 2014). In EU, medical devices according to their application can be classified as for: monitoring, control (actuation/stimulation) and identification (MEDDEV 2010). Medical devices can be classified into various types; some external to the body (such as external insulin pumps) others internal to the body (such as implanted glucose sensors). Yet certain IMDs are capable of monitoring factors inside the body and provide definite treatment, this are called active IMD such as Pacemakers and neurostimulators, contrary to this are implant devices that do not contain any energy source to monitor or provide treatments, this are passive implants such as hip and breast prostheses, as shown in Table 2.1 (Peisino, 2013). Other classifications fall between wired and wireless IMDs for power or data transmissions or both, although the trend in the latest years has been to implant wireless medical devices only (Peisino, 2013). Whereas some IMDs are powered by batteries and others are battery-less, such as using energy harvesting solutions (Cadei, 2014). Furthermore, there are two categories of medical devices operations: in-vitro (within the glass) and in-vivo (within the living) processes; and the in-vitro processes for medical devices presents the most challenges in terms of power consumption (Sagan, 2007).

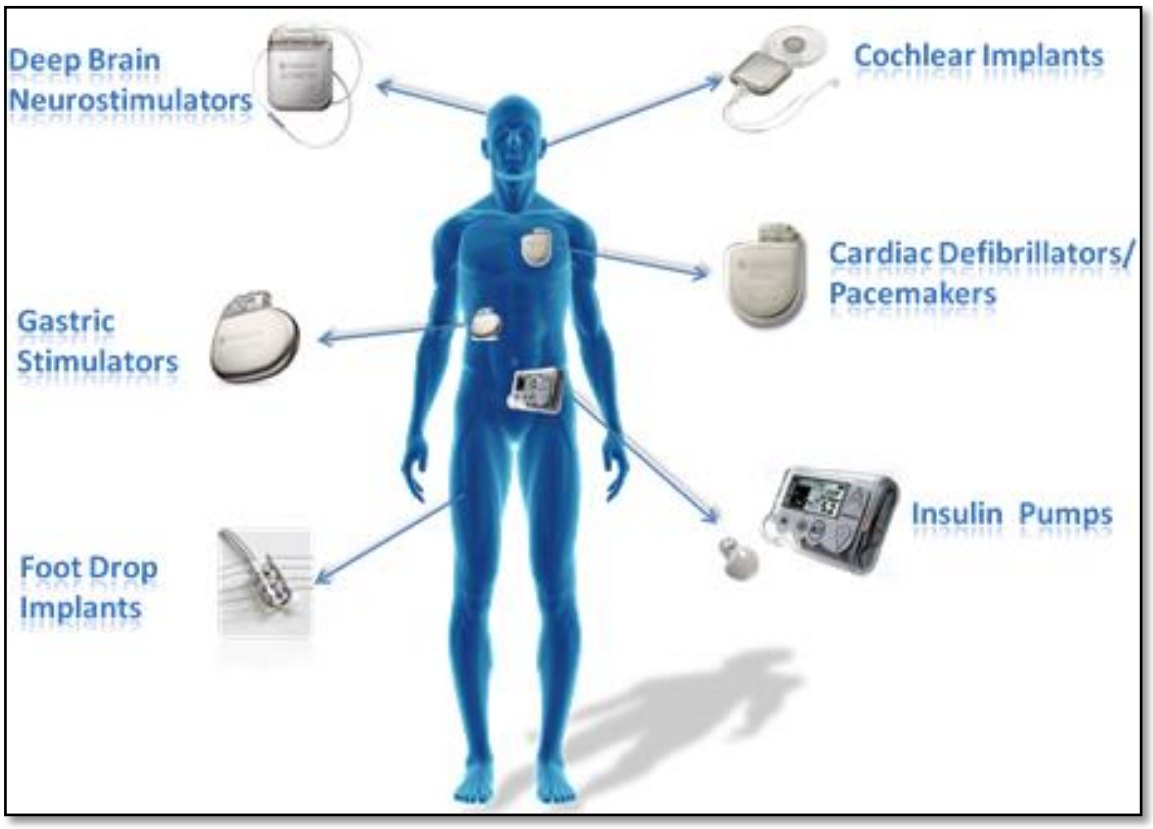

Figure 2.1. Wireless IMD applications (Gollakota, 2011)

Figure 2.1 illustrates varied applications of wireless IMDs, is in fact covering the entire body (Gollakota, 2011). Further classifications of MDs including some examples of internal and active variations of IMDs are presented in Table 2.1.

Table 2.1. Classification of External and Internal (Implantable) Medical Devices

Medical Devices		
External	**Internal (Implantable)**	
	Passive	**Active**
Glucose monitor	Artificial eye lens	Artificial heart
Dialysis machine	Limb prosthesis	Pacemaker
Heart-lung machine	Brest implant	Ventricular assist devices
Insulin pump	Heart valve	Defibrillators
Nebuliser	Stent	Bladder and Diaphragm stimulators
Artificial limb	Screws/pins/plates/rods	Drug pump
In-the-ear aids	Knee replacements	Muscle /neurological stimulators
Orthopaedic footwear	Hip replacement Impl.	Visual prosthesis
Hearing aid inserts	Spinal implants	Cardioverter defibrillators
Artificial eyes	Intervertebral spacers	Gastric implants
Maxillofacial prosthesis	Cervical implants	Glucose monitoring implants
Ophthalmic	Joint replacements	Deep brain Neurostimulators
Dental appliances	Shoulder implants	Cochlear implants

Table 2.1 further presents classification of MDs, including some examples of IMDs (internal and active), (Burleson, 2012; Khan, 2014; Campi, 2014; Cadei, 2014; National patient Safety Agency, 2008 and GOV.UK, 2013). In addition, currently IMDs are being used in many different parts of the body for various applications such as deep brain; nerve and bone stimulators being implanted in patients worldwide to treat sleeping disorders, pain management, Parkinson's disease, epilepsy, bladder control, gastrointestinal disorders, numerous autoimmune diseases and psychological disorders such as obsessive compulsive disorder (OCD). Particular implantable systems can now provide precise dosage and interval delivery of drugs to effectively treat patient's conditions while minimising side effects (Bazaka, 2013; McDonald, 2011 and Yakovlev, 2012). Nevertheless, Table 2.1 also show that there are more internal, IMDs than external medical devices used to monitor and improve patients life, with the tendency to better patient's life, at the same time providing less visible aiding tools as possible, without the necessity for the patient to control or interact with the device, leading to an autonomous monitoring systems, that may enable the patient to forget that they are artificially being assisted.

2.1.2. IMDs power supply and consumptions

There is significant increase in technology advancement of hardware electronics including wireless communication and sensors, but very little progression has been achieved with portable power supply, including battery capacity and performance. Nevertheless, the new advanced sensors and communication devices in contrast are occasionally more power hungry, requiring medical implant devices to have a reliable source of power for long term operation. And many independent solution approaches that investigate optimum means of supplying power to IMDs have not yet satisfied the complex design and functionality of self-reliant IMDs despite the fact there are encouraging investigation involving implantable fuel cells solutions promising autonomous power sources (Reid, 2005; Cleland, 2005; Werner, 2003 and Bloom, 2011).

For over 30 years, low-power implantable devices have been powered using non-rechargeable lithium batteries that have a lifespan of 5 to10 years (Bartona, 2004 and Cadei, 2014) for low-power drain devices such as pacemakers, but can only operate for up to a year at power-densities above 45μW cm^{-3}; the bench mark power required to be

produced by energy harvesting devices, the alternative power sources for the long-term operation of the IMDs currently being developed.

The current power supply of most IMDs is usually provided by a battery that governs the durability and performance of the entire implantable system. (Cadei, 2014). Meanwhile, the advances in existing power supply technologies are expected to increase durability and reliability of IMDs and lead to innovative technologies, such as the Wireless Power Transfer (WPT) system based on magnetic resonant coupling between two coils, whose secondary is located inside the human body and connected to a rechargeable battery system of an active IMD (AIMD), is considered an innovative technique (Campi, 2014), yet this is quickly being side-lined because of its cumbersomeness involving coupling between transmissions and receiving coils, because new technologies are promising complete independent systems with no external to the body devices involved.

In addition, improvements are required to design IMDs with reduced need of reenergising the implants from outside the body, by adopting energy harvesting solutions; because the living body produces substantial amount of energy to power medical implants. (Peisino, 2013). The most common energy harvesters from human body motion exploiting kinetic energy are electromagnetic, electrostatic or piezoelectric generators, but lately GFCs are the most researched type of energy harvesting solutions for implantable devices, and current technological materials favours GFCs as a better energy convertor solution with promising performances better than thermal or kinetic (vibration) energy convertors combined.

While, theoretically vibration energy convertors should be the ultimate energy harvesting solution for IMDs, because this energy environment is not in direct contact with the vibration converter device just like the wireless power transfer system is based on magnetic resonant coupling between two coils, whereas, the vibration energy source is self-sufficient and should guaranty a lifetime supply more than a fuel cell, because chemical reactions on fuel cell materials will eventually degrade its performance more quicker over time. Therefore vibration (kinetic) energy converter, similar technology used on VeriChip are capable of working beyond the existing low-power technologies (Meng, 2014); since VeriChip's energy harvesting system produces very little power, but its electronic components (technology) is sufficiently low-power beyond the most research experiments.

Other implantable energy harvesting devices are the most possible energy supply systems desirable for developing autonomous IMDs that do not require any external power input, by adapting the design concept involving abiotic, enzymatic or microbial fuel cells, as well as thermal and vibrational energy convertors. (Oncescu, 2011). Implantable fuel cells that use glucose as a reactant are almost certainly the most studied biofuel cells, due to the high convenience of glucose in body fluids (Olivo, 2011), and generate power through glucose oxidation (Oncescu, 2011; Rapoport, 2012 and Pan, 2011), whereas, kinetic and thermoelectric energy harvesters for powering IMDs are based on electromagnetic, electrostatic and piezoelectric conversion (Cadei, 2014).

Table 2.2. Power consumptions of different IMDs

Device	**Pacemaker**	**Cochlear**	**Muscle stimulator**	**Drug pump**	**Neuro-Stimulator**	**Molecular biosensor**
Power Consumption	8 – 100 μW	145 μW	1.3 mW	400 μW	50 μW	48 μW

Table 2.2 shows the power density required from the power source to supply IMDs; representing the power consumption expected from devices containing microprocessor and sensors (Peisino, 2013). And the pacemaker presents the lowest power consumption at 8μW.

Autonomous power supply is a major challenge for IMDs, therefore wireless recharge of local power storage from an external unit is easier. Two main strategies have been claimed essentially to provide lifetime and unlimited supply by using magnetic induction and ultrasonic energies for recharging implant batteries (Yakovlev, 2012 and Schmidt, 2011). Therefore power management is critical in the development of IMDs where some devices could incorporate other types of charge storage devices including super capacitors and rechargeable batteries (McDonald, 2011). For that reason the design challenges for battery less IMDs is the low-power availability, which in turn demands a circuit design with ultra-low power input on-chip controller, including data transceiver and the auxiliary circuitries, and may include the use of rechargeable batteries, to achieve the required lifetime implant monitoring capabilities with no planned replacements (Yakovlev, 2012).

Crucial requirement towards an ideal IMD involves a long-term implantation with no planned replacements. Future IMDs are required to ensure at least ten years of maintenance-free implant life (Peisino, 2013). To realise this, an autonomous power supply based implant such as an abiotically catalysed GFCs, with its biocompatibility and functionality in a body environment are of highest importance to achieve the required lifespan, therefore the implantable energy harvester lifespan must be greater than that of the implanted medical device or at least similar (Cadei, 2014).

2.1.3. IMDs Communication systems

The communications and operation frequency of many existing IMDs occurs in low-MHz range, including the known 13.56MHz industrial, scientific and medical (ISM) band. And the disadvantage of this frequency band is the difficulties in designing effective high data rate transceivers, consequently acquiring large receive antennas, while design of smaller antennas to achieve optimal power and data transfer efficiency is essential (Yakovlev, 2012).

A near-field communication with low-complexity design that promises a low power consumption for inductively powered IMD applications is based on carrier-less modulation technique; Pulse Delay Modulation (PDM), which takes advantage of the undesired power carrier interference on the wireless data link (due to the proximity of power and data coils) to deliver the data (Kiani, 2012), while exploitation of carrier for power and data transfer is achieved using ultrasonic (mechanical) waves (Peisino, 2013).

An ideal IMD communication design requires delivering higher data transfer rate and reliability, with data accuracy, appropriate data security, and ultimately low power consumption (Yakovlev, 2012 and Bazaka, 2013). The IMDs communications are therefore stirring towards autonomous monitoring; where device status and performance monitored with a short-range communication between an external reader and the implanted device to, send commands to adjust operation, but ultimately, the IMDs remote monitoring technique enables the transfer of data between devices using internet based network (Meng, 2014).

2.1.4. IMDs Materials, Safety and reliability

The first concern when dealing with implantable devices are the toxicity and biocompatibility problems about the material being used, where different parts of the implantable device must be fully sealed in a biocompatible packaging material such as titanium. (Vaddirajua, 2010 and Cadei, 2014) while other safety concerns does involve power malfunction including the battery-less devices powered by radio frequency (RF) link, where the excessive electromagnetic energy emitted or backscattered by the device during wireless communication or power transfer exposed to tissue, can potentially destabilise accurate hardware device functioning, leading to temporary or permanent device malfunction or damage to the tissue (Bazaka, 2013), or ultimately software malfunction since currently there are no standard for validating, verifying and testing these software for IMDs, and makes this vulnerable to hackers, especially IMDs with remote monitoring technique that enables data transfer between devices using internet protocol (Gollakota, 2011).

The challenges to IMDs are the effective composite materials for biocompatible packaging that promises long-term implant usage; and mainly metals such as polymers and ceramics or glass packaging (specially where wireless communication with an external reader unit is required), are used to protect and separate the contact between the body tissue and the electronic materials strictly non-biocompatible materials that should remain inside the body, and prevent it from causing further damage. For many medical implants, titanium, platinum and glass materials like Pyrex and Borofloat are the material of choices due to their high biocompatibility mechanical properties. That is why for years the cardiac pacemakers have been packaged into fused titanium covers. (Hogg, 2014 and Bazaka, 2013) claims that successful on-organ monitoring using IMDs is imminent with the use of multiple biocompatible materials to fabricate IMDs that includes titanium metal, polymers, ceramics that should improve degradation and provide long term implants.

2.1.5. IMDs design complexity

Implantable power sources including implantable energy harvesting devices are usually required to be limited by size of typically about $1cm^3$ (Cadei, 2014), because smaller size

systems usually denotes low power consumption, and the total weight and size of an IMD is totally dependent of how power sources and the remaining components are encapsulated, whereas battery-less implants such as inductive (or near field) and electromagnetic (or far field) link are battery-less systems frequently used in remote powering, this are known to reduce device size by harvesting energy immediately from the person's body to directly power the IMD. Although initially fuel cell falls also under the category of energy harvesting device, but because their design are significantly configured similar to batteries, therefore fuel cell contribute to the overall weight and size of the IMD the same way as a single-use (non-rechargeable) or rechargeable batteries does (Bazaka, 2013).

Inductive links have been used extensively for IMDs such as auditory and visual prostheses Radio frequency identification (RFID) applications also utilize inductive links to not only power up the ultra-low power RFID tags, most of which cannot have batteries due to their size, weight, and lifetime limitations, but also interrogate the tags and read their stored information (Gollakota, 2011 and Kiani, 2012). Applying optimum size-reduction and low power consumption in order to achieve long-term, the IMDs are not necessarily needed to be powered externally using wireless systems such as inductive links, but this can be achieved using fuel cell as a continues source of energy already produced by the hosting body, and this eliminates the need for any other external device, but makes the IMD more autonomous, although there are not examples yet of a fuel cell that guaranteed a working device life of ten years in a standard implant system (Peisino, 2013).

2.1.6. IMDs experiments

All IMDs reviewed on this study have not been tested in the same manner; most tests were carried out in-vitro rather than in vivo test. The in-vivo tests presents the most challenging in terms of power supply and management, biocompatibility and communication procedures, while in-vitro tests mostly validate the energy transfer and the communication between the control units and the Transponder (TR) as well as the user interfaces on IMDs, as a result the assessment of IMDs in real conditions (ideal tests) are achieved by in-vivo tests on the patient or animal (Peisino, 2013).

A successful in vivo tests involving an implantable thermal energy harvesting device was implanted on a pig and this produced output power up to approximately 0.1W/cm^2 (Peisino, 2013). While another in vivo experiments involving the same thermal energy harvesting device, was performed with a rabbit, and this produced an output voltage about 5mV, and could obtain output voltage increases up to 25 mV with higher temperature difference between the inner and outer sides of the rabbit body (Cadei, 2014).

In addition, a biologic battery extracting electrochemical energy gradient within the inner ear has been tested in vivo as an ultra-low power energy harvesting device integrated with a wireless sensor for monitoring the ear electrochemical gradient. With the same biologic battery device when implanted in a guinea pig this generated minimum of 1.12nW for up to 5hrs, and was powerful enough to transmit wireless information of the electrochemical potential using a 2.4 GHz radio (Bazaka, 2013). The majority of implantable fuel cell devices have been tested in-vitro generating power through glucose oxidation, producing between 3.4μW cm^{-2} up to 180μW cm^{-2} steady-state peak power (Bazaka, 2013).

2.2. Implantable Glucose Fuel Cells (IGFCs)

This review work presents a significant overview of implantable bio fuel cells (IBFCs), in particular the IGFC, thus extracting the full potential of practical techniques required to achieve the necessary improvements that promises a long lifespan powering of IMDs (Olivo, 2011; Bartona, 2004 and Wang, 2007).

The basic idea of fuel cell is; an electrochemical device that generates current through the reaction of two chemical types flowing into it. And IGFCs are capable of harvesting energy directly from body fluids, which has considerable advantage in the field of implantable monitoring sensors (Olivo, 2011) also known as IMDs, since these low-powered medical devices have capable applications needed to improve patients' lives, IMDs such as; Pacemakers, hearing aids, transdermal drug delivery (Kerzenmacher, 2008 and Halámková, 2012), all require long-time battery life, a requirement that IGFCs are claimed should be able to accomplish well (Cinquin, 2010 and Oncescu, 2011). Essentially, IGFC could overcome many problems relating to IMDs, because it uses body fluid to harvest its energy, as a result, utilising the chemical reaction of oxygen in

glucose from the blood to produce enough energy to run a low-power IMDs with a long lifespan (Cinquin, 2010).

Human body can certainly provide sources of power to assist its own IMDs by means of energy harvesting techniques. However, even with currently available experiments carried out using vibrations, body movements and thermoelectric forms of energy harvesting techniques, so far there have been no valuable results that could replace batteries on IMDs using these techniques (Cinquin, 2010). Consequently IGFC presents a potential option for replacement of batteries in implanted medical devices, as IGFCs are superior to mechanical and thermal energy harvesting systems in terms of continuous and reliable power generation (Kloke, 2011).

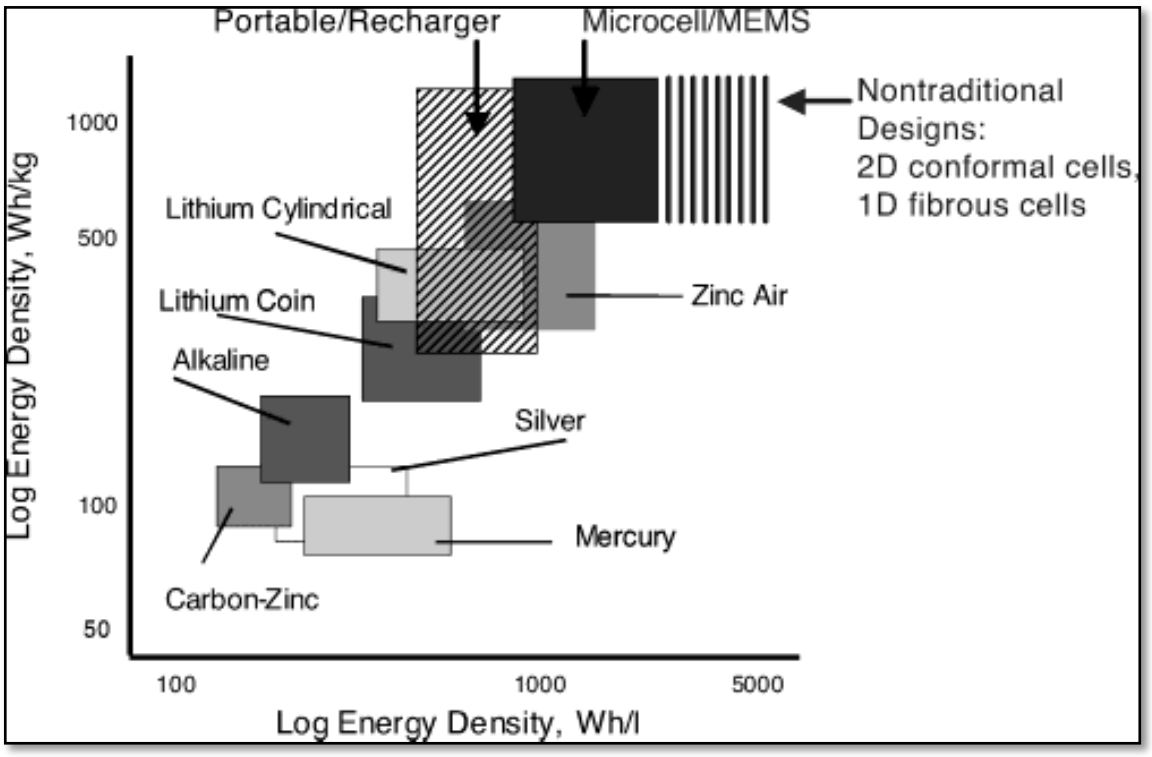

Figure 2.2. Conceptual product definitions of BFCs as they are compared in their specific energy and energy density to the existing primary battery technologies (Bartona, 2004).

The illustration by (Bartona, 2004), Figure 2.2 compares the energy fields of three potential materials including conventional battery technologies and fuel cells. The energy performance numbers of fuel cell materials (carbon-zinc, alkaline or silver) are lower compared to reportable/rechargeable batteries or micro-electro-mechanical (MEMS) systems based technologies, as a result, the advantages on adopting fuel cell

technology will require outweighing the disadvantages it presents relative to conventional technologies. Further analyses carried presents the key technology directions, identifying the required energy density of BFCs depends on product definitions, such as portable, reserve power or micro-system power application, that ultimately results into a micro-miniature power source for independent power-on-chip or micro-fabrication techniques in an enclosed structure.

A definite record of searches were performed including key wards such as BFCs, Energy harvesting, GFC, Implantable BFC. And all searched results were refined to those only that were considered implantable techniques. Furthermore, the search was regulated to IGFCs, which produced more than 30 references. But more than 30 cited full papers were read for this review, from which it was possible to obtain the main findings to produce a full review. All other papers and areas of research citing IMDs (already covered on previous section), body movement vibration and thermoelectric forms of energy harvesting techniques, will not be discussed in this section.

2.2.1. History of IGFCs

Research in the field of IGFCs dates back to the early sixties, with the first abiotic GFCs developed in 1964 Early efforts in producing IBFCs were driven to replace the existing batteries with short life-time that were made of zinc/mercury oxide, since the battery implants that were used to power cardiac pacemakers required frequent replacement (Kerzenmacher, 2008). The power output of the first implantable fuel cells in early 1960s was in the range of 30-70$\mu W/cm^2$ for 5h in a dog and 2$\mu W/cm^2$ for 5 months (Kerzenmacher, 2008). In the 1970s the range of 50μW was obtained, and claimed to be sufficient to supply a cardiac pacemaker (Stetten, 2006). Although IGFCs were tested in animals, such as dogs, rats and rabbits, for more than 150 days, however, they were not fully tested for their biocompatibility.

2.2.2. Problem formulation & findings

IGFCs can be described as a micro-power source operating in living organisms, where in medical applications, a patient own blood's glucose is broken down, and the oxygen is

oxidised in the process, and energy is harvested through this process to power the IMD (Halámková, 2012).

The results obtained from the performed search have produced a series of topics currently being studied, methods of which have more or less produced applicable techniques that have successfully improved IBFCs as a long-term powering source (Stetten, 2006; Cinquin, 2010), (Oncescu, 2011).

2.2.3. Types of BFCs

There are different types of fuels that have been used as electrolysis for BFCs; such as glucose, hydrogen, methanol, ethanol and higher alcohols in conventional direct fuel cells for portable devices (Bartona, 2004 and Ivanov, 2010). For implantable purposes, Glucose is used as main reactant, and BFCs are probably up-to-date the most explored energy conversion devices, due to the high availability of glucose into the body fluids (Olivo, 2011). This has resulted in an in-depth study of GFC techniques, which involves either catalyst by enzymes, microorganisms or abiotic (Kloke, 2011), as further defined in Table 2.3.

Table 2.3. Different types of GFCs

References	GFC Types	Declarations
(Kloke, 2011) (Stetten, 2006) (Bartona, 2004)	**Enzymatic fuel cells**	▪ High power densities compared to other concepts. ▪ Allows a simple, one-compartment design. ▪ Lacks longevity and amenability to steam sterilization required for long-term medical implant.
(Kloke, 2011) (Stetten, 2006)	**Microbial fuel cells**	▪ Self-regenerating capability, ▪ Allows for long-term application, ▪ Not implantable due to infective or immunogenic nature of microorganisms.
(Kloke, 2011) (Sharma, 2009) (Stetten, 2006)	**Abiotic fuel cell**	▪ The only known concept that meets all the demands of long-term medical implants. ▪ Has the advantage of longevity, amenability to sterilization, and biocompatibility. ▪ Typical catalysts are made of simple metals or carbon, and currently silicon nano-particles and platinum catalysts are under study. ▪ However, exhibit low power density compared to other two concepts.

The three practices shown in Table 2.3 have different satisfactory designs for GFCs, where each individual concept present some strengths or weakness compared to the other, except the abiotic fuel cell (AFC) that has the combination strength of the other two, despite having low power density. Though enzymatically and abiotically catalysed fuel cells are the most commonly used for IMDs (Olivo, 2011), nevertheless, abiotic fuel cell are the indispensable design method for implantable fuel cells aiming to improve the power density, by reducing the drop of power density caused by oxygen mass transferring to the cathode (Kloke, 2011; Stetten, 2006 and Ivanov, 2010), by increasing the cathode to anode area proportion (Pan, 2011; Bartona, 2004 and Ivanov, 2010), and by maintaining chemical stability in the presence of active species that attack key electrode components, that leads to build-up of fungal laccase species (Bartona, 2004).

2.2.4. GFC's operational principles

GFC operates by generating electricity from a process involving the transfer of electrons from glucose (sugar) to oxygen, where the anode electrode from the GFC performs glucose oxidation and the cathode electrode performs oxygen reduction. And when the electrons flow between the electrodes, they produce an electric current (Stetten, 2006 andHalámková, 2012), a micro-scale power source process that can be used to power a circuit (Kerzenmacher, 2008). The electro-chemical reaction processes that occur inside GFCs are illustrated in Figures 2.3.

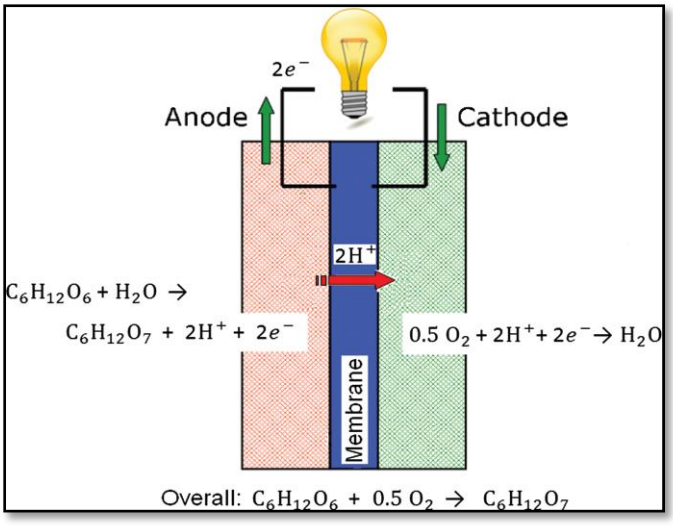

Figure 2.3. Typical chemical reaction of BFCs capable of lighting a bulb, (Kerzenmacher, 2008; Stetten, 2006; and Olivo, 2011)

Figures 2.3 illustrate characterises a typical chemical reaction process of a direct GFCs. In an acidic environment, charge exchange takes place by the diffusion of protons, in an alkaline environment by hydroxyl (Stetten, 2006 and Olivo, 2011). This same illustration is summarised and simplified as such; glucose is predominantly oxidised by a two electron transfer reaction to gluconic acid (Kloke, 2011).

Since IBFCs oxidises sugars (glucose - $C_6H_{12}O_6$) to generate electricity as a result, the only by products of the electrochemical reactions would be water (H_2O) and gluconic acid ($C_6H_{12}O_7$) or carbon dioxide (CO_2). And the electrons obtained by means of oxidation are used to generate power (Stetten, 2006 and Olivo, 2011), example of lighting a bulb shown in Figure 2.3.

Agreeably, IGFCs provide new approaches for self-powered implantable nanotechnology devices, thus harvesting electricity from their environment to power implantable biomedical devices (IBMDs). This demonstrates great design advantages over other existing conventional methods, as a result; further key advantages and disadvantages of IGFCs are shown in the Table 2.4.

Table 2.4. Advantages and disadvantages of GBFC

Disadvantages of IBFCs	Advantages of IGFC
▪ Inefficient output power. ▪ No breakthrough on life-time (over 5 years) device powering yet. ▪ The associated presence of glucose and oxygen and the lack of glucose selective inorganic catalyst. ▪ Current is either limited by the availability of oxygen at the cathode or glucose at the anode. ▪ The separator membrane between the electrodes also causes degradation.	▪ Can be simplified and integrated into any arbitrary shaped customary fabrication. ▪ Reduced overall thickness or size for implant ▪ Be coated directly on the surface of medical implants. ▪ Continuous output power ▪ Longevity ▪ Amenability to sterilization and ▪ Biocompatibility.

Table 2.4 illustrates the disadvantages naturally placed in other of importance. The existing low power density of IGFC is a critical disadvantage followed by the lifespan realisation as an implanted power source device. Other associated disadvantages

involving bio-catalytic function, electron transfer, and substrate interactions are expected to improve as the technology matures, and can be outweighed by the advantages of using GFCs as implantable devices compared to batteries, from the fact that fuel is supplied to the cell, rather than being embedded within it (Bartona, 2004). Also (Bartona, 2004) states that the main advantage of IGFCs is the inherent bio-catalytic property that cannot be duplicated by conventional technology. Among these key properties are (1) activity at low temperature and near-neutral pH, (2) chemical selectivity, and (3) potentially low-cost production using fermentation and bio-separation technologies. In comparison to other conventional fuel cells, the advantages of using IGFCs, (Ivanov, 2010) concludes that; the use of a simple fuel cell design with lower cost of main fuel cell components and extensive usage of biocatalysts is expected to lower the cost of production.

2.2.5. Applications of IGFCs

Application specific of IMDs has always been the driving force for the development of successful power sources and the main possible applications for IGFCs, leading towards implantable sources with micro-scale cells, capable of being implanted in human or animal tissue or in blood vessels (Bartona, 2004). In general, a number of IMDs might benefit from these implantable power sources, and the most obvious is the cardiac pacemaker (Kerzenmacher, 2008; Bartona, 2004 and Halámková, 2012), a device that has been in use for more than 40 years and is currently powered by lithium-iodine battery with a lifetime exceeding 10 years (Bartona, 2004). As mentioned previously in the introduction, other applications include artificial hearing aids, vision and the use of sensors for monitoring of diseases will also benefit from IGFCs (Kerzenmacher, 2008; Kloke, 2011; Bartona, 2004; Cinquin, 2010, and Halámková, 2012). Should stability, lifespan, and power density of micro-scale implantable power sources easily be achieved when dealing with medical IBFCs problems, applications of IGFCs is expected to grow as new technologies are established and energy demands expand (Bartona, 2004 and (Ivanov, 2010).

Table 2.5. Review of different biofuel cell, electrode catalysts, their construction and performances

Anode - O_2 (reduction)	Cathode Oxidation	Separator or Membrane	Fabrication Method	Fuel Source	Fuel Type	Power Output	Experiment Duration	Reference Papers
Microbial fuel cells								
Activated Carbon Cloth	Carbon Paper with Pt	Air and Carbon Paper		In vitro		73.3mWm^{-2} (0.55V)	2 months	(Han, 2010)
Carbon cloth with ammonia	Carbon paper with Pt	None		In vitro		11.7mWm^{-2} (0.16V)	2 months	(Dong, 2013)
Enzymatic fuel Cells								
GOX Graphite	POP-Graphite	None	Mechanical. Confined	Rats	Glucose /O_2	2µW cm^{-2} (0.13V)	3 months	(Hareland, 2013)
Glucose Oxidase	Laccase	Nafion Nano-wire (NPNW)		In vitro	Glucose /O_2	30µW cm^{-2} (0.23V)		(Pan, 2010)
MW Carbon Nano-tubes	BP Laccase	MWCNT carbon	Chemical vapour deposition	In vitro	Glucose /O_2	(0.88V)		(Hussein, 2011)
Abiotic fuel Cells								
Raney Platinum	Raney Platinum	Hydro-phobic	Alloying partner	In vitro	Glucose /O_2	2.2µW cm^{-2} (0.5V)		(Kloke, 2011)
Platinum Thin-film	Graphi-ne	Polypropylene based porous	Evaporation induced	In vitro	Glucose /O_2	5µW cm^{-2} (0.26V)		(Golla-kota, 2011)
Carbon	Carbon	Polymer (Hydrogel)	Doctor blade-gluing	In vitro	Glucose /O_2	20µW cm^{-2} (0.26V)	11 Days	(Stetten, 2006)
Raney Platinum	Raney Platinum	Porous (Supor-450)	Diffusion & Photo-lithog.	In vitro	Glucose /O_2	4.4µWcm^{-2} (0.5V)		(Kerzen-macher, 2011)
Platinum nickel	Pt/Carbon paper	AAO membrane		In vitro	Glucose /O_2	2µW cm^{-2} (0.35V)	4 Hours	(Bartona, 2004)
Carbon, Pt-bismuth	Activate carbon	Polyethersulfone filter	Doctor blade Tech.	In vitro	Glucose /O_2	3µW cm^{-2} (0.38V)	240 Days (8 months)	(Kerzen-macher, 2008)
Raney Platinum	Platinmaluminu.	Hydrophobic	Alloying partner	In vitro	Glucose /O_2	(0.38V)		(Kerzen-macher, 2010)
Raney Platinum	Platinmaluminu.	Hydrophobic	Alloying partner	In vitro	Glucose /O_2	(0.38V)		(Kerzen-macher, 2010)

2.2.6. Evaluation of IGFCs

Research studies show efforts that have been made that are driving the development of devices that make use of ambient body energy (harvesting) to power IMDs, and GFCs are underlined to be better than any other existing energy harvesting technologies in use today for IMDs, but currently only a few of these reviewed papers can satisfy this declaration. The comparison carried out to highlight the achievements obtained so far relating to IGFCs is shown in the Table 2.5.

2.2.6.1. IGFCs proprieties

a. Fuels

The most common and natural energy for biofuel cells is glucose fluid due to its high abundance and an important source of energy for a variety of living organisms. The main fuel to the respective three types of fuel cells (enzymes, microorganisms and abiotic) described in Table 2.4 is the glucose fluid, which is consequently broken into oxygen in oxidation and reduction reactions, as illustrated previously, and now listed in Table 2.5.

b. ***Oxidants***

The most widely employed oxidant in GFCs is oxygen and there are only few reports of other compounds. The respective half-cell reactions and catalysts used for the bio-electrochemical reductions are also listed in Table 2.5. Oxygen is the typical oxidant in conventional fuel cells, where mostly is used in the form of pure gas or air.

c. Catalysts

Glucose catalysts vary between microbial, enzymatic and abiotic fuel cells. The main catalyst that are responsible for glucose oxidation and reduction reactions, are illustrated in Table 2.5, where the abiotic catalyst materials that are widely employed in the area of biofuel cells, are also employed in biosensors designs.

2.2.6.2. Evaluation of Implantable Bio-Fuel Cells (IBFCs)

A literature review of the field highlights countless efforts to drive the development of devices that make use of ambient body energy. Bio-fuel cells are highlighted as more appealing than any other existing energy harvesting technologies in use today, but few of

these efforts are proven satisfactory. A comparison has been put together to highlight some of the achievements obtained so far relating to IBFCs, shown in Table 2.5.

From Table 2.5 we established that the use of microbial fuel cells provides the highest power density 73.3mWm^{-2}, or 733μWcm^{-2} (Bartona, 2004) and 117μWcm^{-2} (Bartona, 2004), compared to enzymatic and abiotic concepts. However microbial fuel cells power generation has a shorter life span compared to the other two design concepts.

Most of the catalysts used by enzymatic fuel cells are made of glucose oxidase (GOX) and laccase oxidase with gold electrodes for both anode and cathode terminals. The enzymatic catalysts enables higher power densities compared to abiotic concept designs, where the highest enzymatically catalysed fuel cells (Mousavi, 2011), generated power density up to 30 μWcm^{-2} at 0.23 V, with the use of gold as main electrode material for both anode and cathode terminals. The highest result in the table for abiotic fuel cells can be found using carbon for both anode and cathode, providing a power density of 20μWcm^{-2} at 0.26V (Oncescu, 2011). This experimental work matches the highest power density abiotic design concept published in Table 2.5, however provides better output voltage >0.4 V.

Non-enzymatic glucose fuel cells are appealing since they may overcome insufficient long-term stability and reproducibility due to the nature of the enzymes. The catalysts of abiotic fuel cells were mostly made of platinum or its alloy materials, Table 2.5 shows that platinum and its alloy based abiotic types (Hussein, 2011), including this paper, have a promising long lifetime albeit with a limited power density of just 20μWcm^{-2}. However, noble metal and alloy-based fuel cells face different challenges of the low sensitivity, selectivity and poor resistance to the poisoning of chloride ions and intermediates that originate from glucose oxidation. Carbon supported metal catalysts show the most durability compared to the other two types, with stability for > 8 months or 240 days (Kerzenmacher, 2010) using platinum–bismuth alloy supported by activated carbon as catalysts.

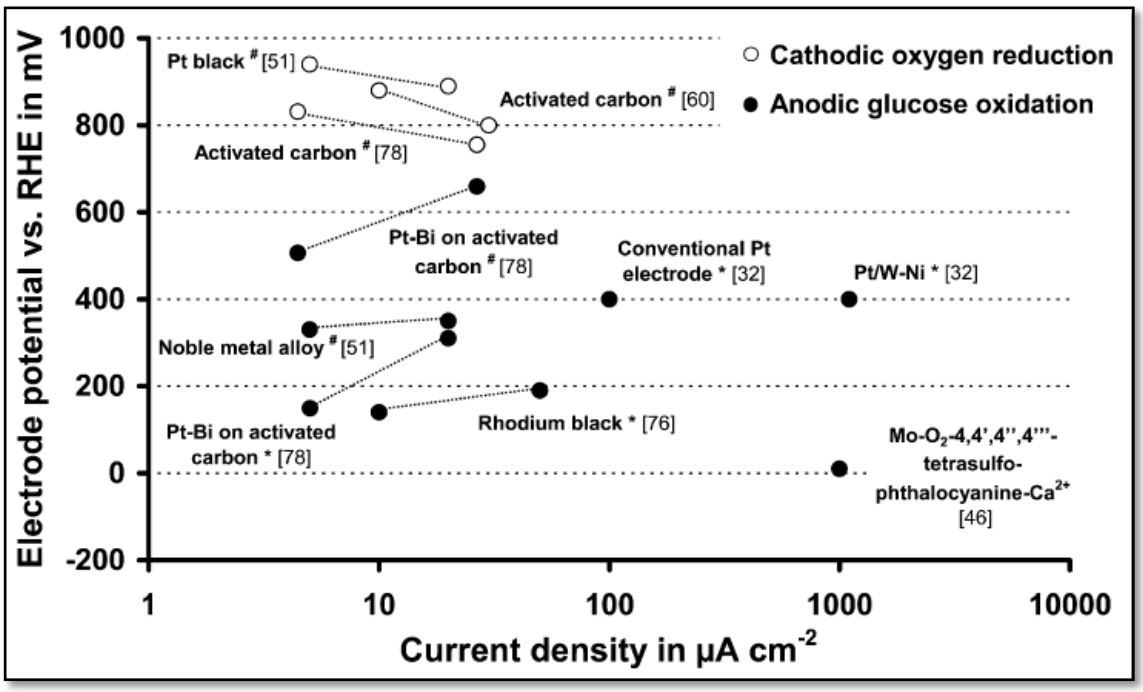

Figure 2.4. Current density-potential plot of different electrode materials in neutral buffer containing glucose. Legend: "": in deaerated solution; "#": electrode part of a complete fuel cell in aerated solution (Kerzenmacher, 2008).*

Figure 2.4 highlights the difference in current density to potential performance plots between electrode materials used for GFCs. Platinum electrode is therefore favoured as a selective catalyst showing the highest performance materials for glucose oxidation in comparison to other noble materials such as palladium, gold, and silver. Platinum presents 400mV more positive potential, and currents above 100µW. While activated carbon (oxygen reduction) also has high potential values >800mV, but lower currents than platinum, but the combination of both material can directly translates to higher voltage, currents and performance for GFCs (Kerzenmacher, 2008). And the catalyst materials for oxygen reduction and glucose oxidation can be summarised as follow:

a. Abiotic catalytic materials such as activated carbon and platinum have the advantage to not being sensitive towards glucose compared to silver, but their oxygen reduction onset potential are also greatly greater than silver (300mV), and more negative compared to platinum, which directly translates to lower fuel cell voltage and performance, and thus activated carbon is preferred than silver as it displays a better oxygen reduction performance than silver (Kerzenmacher, 2008).

b. In the other hand, the noble metals and alloys that are highly active for glucose oxidation are: platinum–ruthenium, rhodium, and iridium alloys. And the most

special type of alloy used for IGFCs shown in Table 2.5, is the Raney-platinum catalyst.

c. The enzymatic catalytic material capable of glucose oxidation is the glucose oxidase (EC 1.1.3.4, GOx) is the most widely employed in the area of biosensors and biofuel cells. Another enzyme that has been widely used in biofuel cell applications is glucose dehydrogenase, the typical enzyme used for oxygen reduction using plant and fungal laccase (Ivanov, 2010).

d. The only advantage microbial fuel cells have over enzymatic or abiotic fuel cells, is the long lifespan ability to convert the chemical energy of glucose into electrical energy through microorganism's reaction.

e. Membranes separator and insulators working principle and components of the conventional polymer electrolyte membrane (PEM) for fuel cells presented in Table 2.5 are best illustrated in previous Figure 2.3, but these membranes are also believed to contribute to the fuel cell loss of performance overtime (Ivanov, 2010).

Following previous report of platinum catalysts as the best possible catalytic material with the highest performance, consequently both Table 2.5 and Figure 2.3 present most of the electrode materials required to design all three types of fuel cells, nevertheless therefore, other existing catalytic materials not yet covered such as carbon fibre, carbon nanotube, including noble metals and alloys that are highly active for glucose oxidation, among these are platinum-ruthenium alloys, rhodium, palladium and iridium. Also platinum-bismuth alloy on activated carbon, raney-platinum, platinum-tungsten containing nickel, rhodium black, platinum-gold and platinum-gold alloys, and this demonstrate that platinum is the most alloyed metal for GFC fabrication, and these alloys exhibited current densities three, five, seven even nine times higher compared to a conventional platinum or platinum black electrodes, while carbon nanotubes with metallic nanoparticles have also shown an increase in performance of GFCs, achieving power densities of $760\mu Wcm^{-2}$ (Kerzenmacher, 2008).

2.2.6.3. Design and fabrication method of IGFCs

Common problem with designing IGFCs is avoiding the continuous presence of glucose and oxygen on both cathode and anode electrodes simultaneously, and also the lack of glucose selective inorganic catalyst. For this purpose there has been significant effort on development of electrodes materials (Bartona, 2004 and Bartona, 2004) and designs (Stetten, 2006) to bypass the oxygen intervention on the anode. Thus the most popular design so far has been the sandwich type assembly of electrodes (Stetten, 2006).

Nevertheless, out of the three types of GFCs concepts mentioned in Tables 2.3 and 2.5, the Abiotic or direct GFC is the only known concept that meets all the demands of long-term medical implants with the advantage of longevity, amenability to sterilization, and biocompatibility, and its typical catalysts are made of simple metals or carbon, as shown in Table 2.5, which includes other materials that are currently under study. An abiotic GFC despite having low power density compared to other two concepts, have shown promising results required to provide power to implants used in treatment of life-long diseases. As a result three different papers have been singled out; (Kloke, 2011; Stetten, 2006 and Pan, 2010), based on their simple and clear study on GFCs, these papers have shown outstanding and significant contributions to the understanding and improvements on the techniques and construction of IGFCs studies, and as a consequence a great deal of attention has been drawn particularly from these three papers to expand on their materials and methods of fabrication that defines an ideal GFC design.

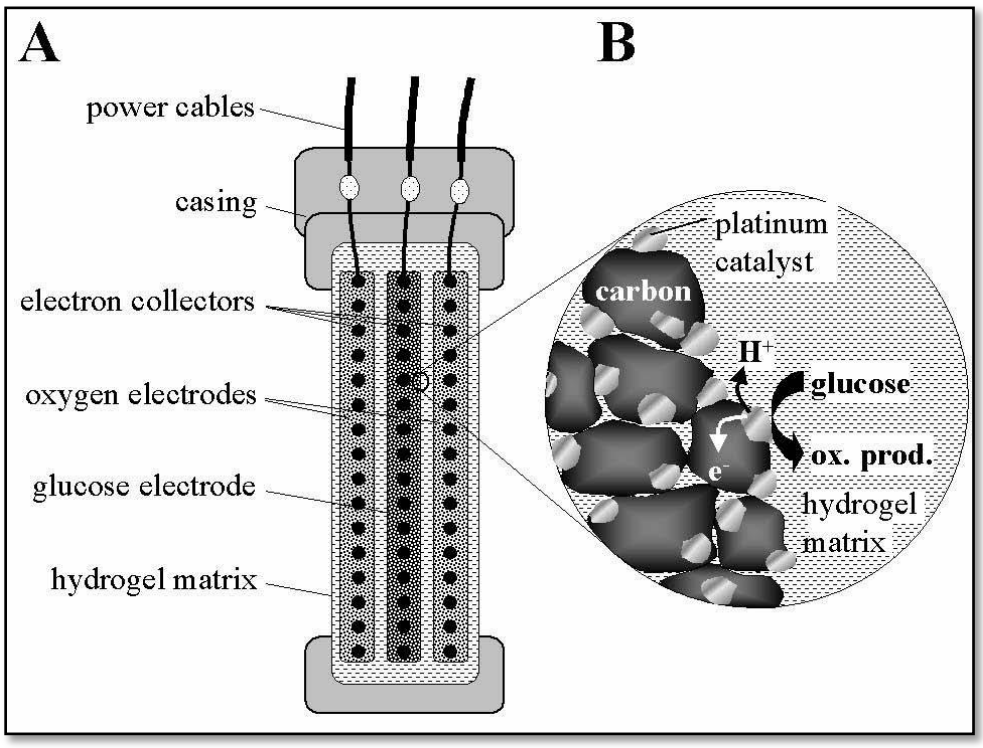

Figure 2.5. (A) Representation of a sandwich type electrode assembly fuel cell. (B) Close-up illustration of the interface between surrounding materials (Stetten, 2006).

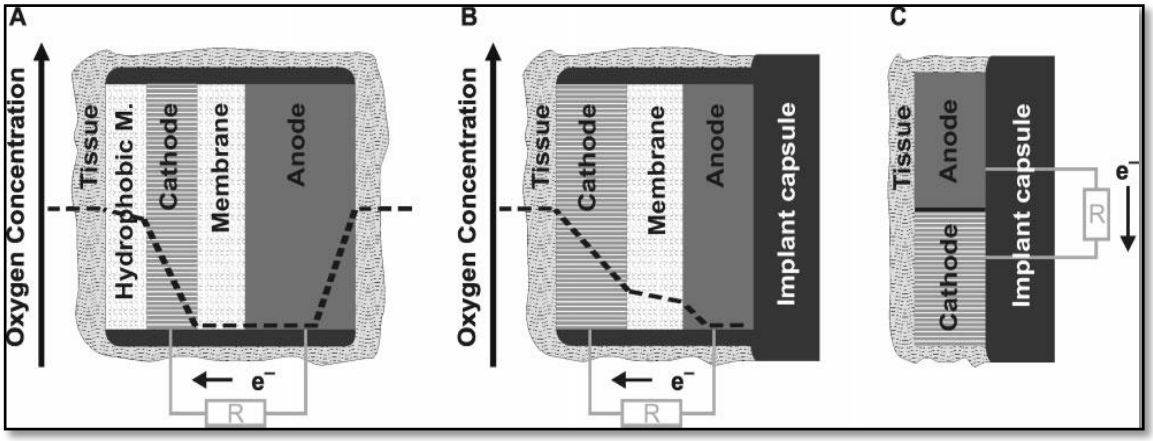

Figure 2.6. GFC designs: (A and B) Sandwich assembly design and (C) A single layer design (Kloke, 2011).

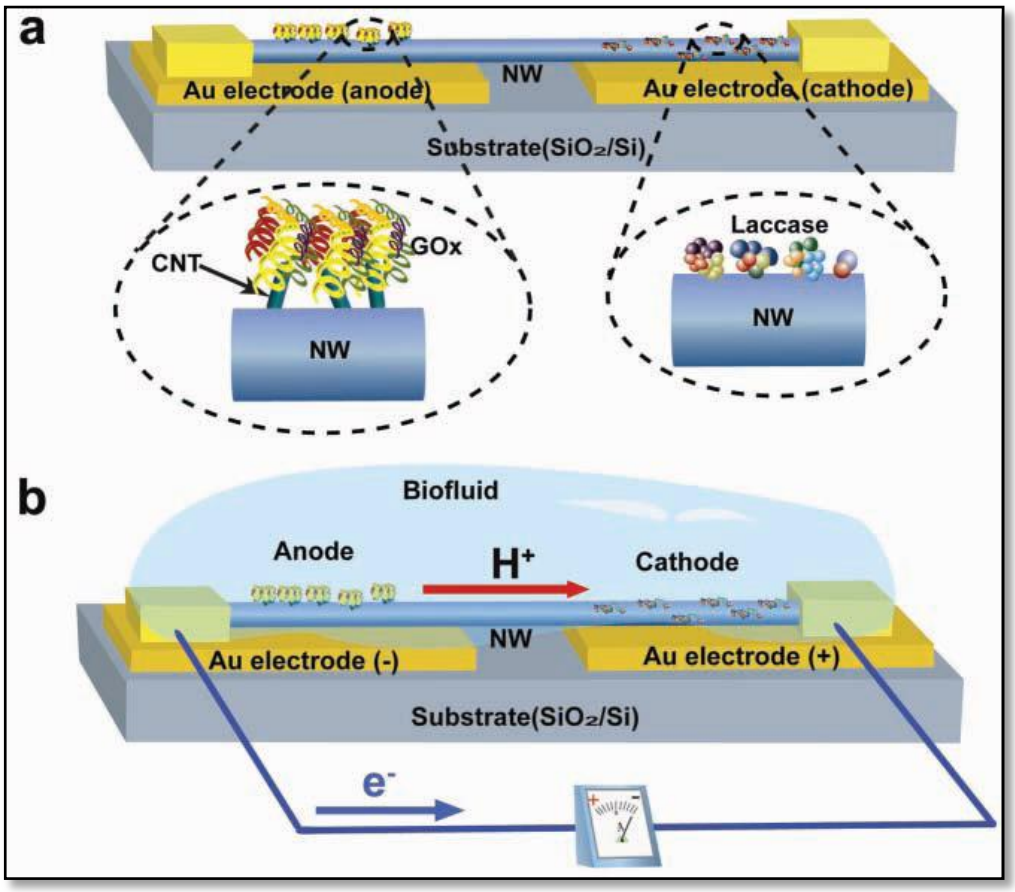

Figure 2.7. (a) A Nanowire-Based BFC (NBFC) with glucose oxide (GOx) and laccase used as catalysts in the anode and cathode region, respectively. (b) The (NBFC) is immersed into a biofuel solution for a direct single layer fuel cell design (Pan, 2010)

The first three techniques used in Figure 2.5 (Stetten, 2006), and Figure 2.6 (a and b) (Kloke, 2011), have similarities in operational concept of micro-fabrication and electrical performance of enzyme-less direct GFC, and the three use sandwich design type of electrodes assembly, but (Kloke, 2011) additionally presents a different designs involving a single layer GFC design Figure 2.6 (c). Both (Kloke, 2011) and (Stetten, 2006) concepts are abiotic, direct GFC techniques, while (Pan, 2010) GFC in Figure 2.7 is an enzymatic process. But all three GFC commonly harvest the chemical energy of glucose from body fluids, which contains both oxygen and glucose reactants (Stetten, 2006 and Kloke, 2011).

Significantly the work presented in (Stetten, 2006), includes the experimental results illustrating credible works with full evidences supporting arguments on main material used and the breakdown of the writing. But the process goes a step further with (Kloke, 2011). Figure 2.6 (c), by describing the construction and integration of the fuel cell into implant capsules by using a novel single layer fuel cell design; the only abiotic fuel cell

design that clearly deals with this concept. However, an enzymatic technique that shows full potential in this field of GFCs is the Nanowire-Based Biofuel cell (NWBFC) (Pan, 2008 and Pan, 2010). It's an improved technique that is ideal for self-powered devices. The Nano-wire (NW) technique uses a substrate of any kind that is connected tightly to anode and cathode. It uses glucose oxide and lactase as catalysts bound on the wire in the anode and cathode region respectively, and the two chemical reactions that occur, creating a corresponding chemical potential drop along the NW, which drives the flow of protons in the NW and electrons through the external load (Pan, 2010).

From above design concepts, Figure 2.7 has not only shown a different direction of fabricating a GFCs but has also enhanced an understanding on full practical potential requirement to achieving the improvements that guaranties a lifespan powering of implantable devices. This is also simplified by materials used and the method arranged on the nano-wire surface, which enables the flow of protons and electrons to produce the power needed to drive an implants. And other great compensation is related to membrane-less technique and the fact that it uses the same bio-fluid (containing both oxygen and glucose) on anode and cathode regions, a method that is difficult and is known to reduce the device's output performance, as shown in Table 2.6.

Table 2.6. A summary of materials and methods of fabrications for the 3 techniques

Reference	Electrodes	Membranes	Declarations
A single layer BFC (Kloke, 2011)	**Anode:** Platinum foils, and electrodeposited thick layer of zinc. **Cathode:** Platinum and aluminium successively evaporated onto a silicon substrate with titanium as adhesion layer. Aluminium as sacrificial alloy partner was removed after leaving behind a rough Pt-Al catalyst.	**None** A single layer fuel cell design, where anode and cathode are placed side by side on the same impermeable surface. This concept requires an anode that shows sufficient tolerance towards the presence of oxygen in physiological concentrations.	Although this method show strong performance degradation, but Raney-platinum film anodes exhibit high oxygen tolerance, a good thing. The presented strategy enabled a significantly faster product desorption and lower sensitivity towards interfering substances.
Sandwich type Assembly BFC (Stetten, 2006)	Consist of activated carbon coating a noble metal screen that collects the electrons. The activated carbon at the glucose electrode contains an additional 10% of platinum. An epoxy resin frame is used to electrically insulate the wire connections, and to protect the anaerobic glucose electrode against oxygen breakthrough. (PVA-PAA) matrix occupies the inter-electrode space of the fuel cell, and is also used as binder for the activated carbon particles.	Membranes with a thickness of 30µm were cast from PVA-PAA solution. The electrodes are manufactured by a doctor blade technique. The catalyst ink consists of activated carbon saturated with PVA-PAA solution. After drying, membranes and electrodes are assembled by wet gluing	By rearranging the presented 3-electrode sandwich setup with a 2-electrode blind-end concept this microfluidic cell can even be implemented as an external coating of implants. The presented concept of a direct GFC is well compatible with the technical and important legislative demands regarding implantable power sources for long-term medical implants.
Nanowire-Based BFC (Pan, 2010)	GOx and laccase are used as catalysts in the anode and cathode region, respectively, where Gold electrodes are used at both ends. The NBFC is immersed into a biofuel solution; two chemical reactions occur in the anode and cathode regions, creating a corresponding chemical potential drop along the NW, which drives the flow of protons in the NW and electrons through the external load.	A proton conductive polymer nanowire is used for transporting protons, which lies flat on a substrate (of any kind) as electrolyte and is affixed to two electrodes at both ends. The key component as proton-conductive NW used is the Nafion Poly (vinyl-pyrrolidone), obtained via electro-spinning.	The NBFC can be directly integrated with a single NW-based Nano-sensor for building a self-powered chemical- or bio-sensor, which typically requires an operation power as low as a few Nano-watts if one excludes the RF unit. A self-powered Nano sensor formed with NBFC.

2.2.6.4. Dimensions and fluid flow rates

The apparent objective of implantable fuel cells research is still for in vivo applications where the glucose in use is without limit from the flow of blood to provide a long-term power to IMDs (Kerzenmacher, 2008). As a result, fluid flow is an important matter in microfluidics on which can depend on both conditions of heat and mass transfer including; flow conditions, fluid properties and channel geometries. Given the small dimensions (microscale) of the channels involved for fluid flow in fuel cells materials, the flow regime has as typically straight flow and is ruled by low ratio of momentum forces to viscous forces, this type of flow favours the control and modelling of bio-chemical reactions while providing high surface area to volume ratio (Rapoport, 2012; Marques, 2011 and Kjeanga, 2009). Overall, fuel cells incorporating microfluidic fuel cell setups, have been designed with flow rates of 0.1 mL min^{-1} to 0.5 mL min^{-1} of fluid flows, with pressure driven and regulated tests using pumps (Guerra-Balcázara, 2012). But GFCs are best to be implanted just under patient's skin, as a result most experiments involving GFCs are carried out at zero pressure regulation fluid flow tests with no pumps, evaluating the ability of the cell working in extended times with no continuous injection of fuel, as a result these tests establish the ability of the fuel cell to work well without an external fuel pump, establishing similar environment of blood flow rate. Hence the fuel cell power density is higher at low fuel flow (zero flow rates) and decreases with the increasing fuel flow rates (Cuevas-Muñiz, 2012) .

Dimension wise, implantable fuel cells devices are usually required to be limited by size of typically $1cm^3$. Although initially fuel cell falls also under the category of energy harvesting device, but because of their design do significantly configuration similar to batteries, fuel cell therefore contribute to the overall weight and size of the device the same way as a single-use (non-rechargeable) or rechargeable batteries. As a result, smaller size fuel cells usually denotes low power density, and the total weight and size of an implantable fuel cell capable of driving an implant device requiring to be obtained from a stuck of multiple fuel cells arranged in parallel, harvesting the instantaneously energy from the person's body glucose fluid (Cadei, 2014 and Bazaka, 2013). There are also challenging issues in relation to integrating implantable fuel cell and the IMDs, include involving electrical arrangement, packaging and voltage matching, especially when multi-cell stacks are desirable to produce the conventional 1-5V output voltages (Bartona, 2004).

2.2.7. Electrochemical tests of IGFC suitable materials

The testing of GFC in various in-vitro experiments involves the electrochemical test setups to characterise the fuel cell and its individual electrode components and catalytic materials. Typical fuel cell components include (reference and counter) electrodes configured in a cell container together with the holder, normally using cyclic voltammetry (CV) test method (Stetten, 2006).

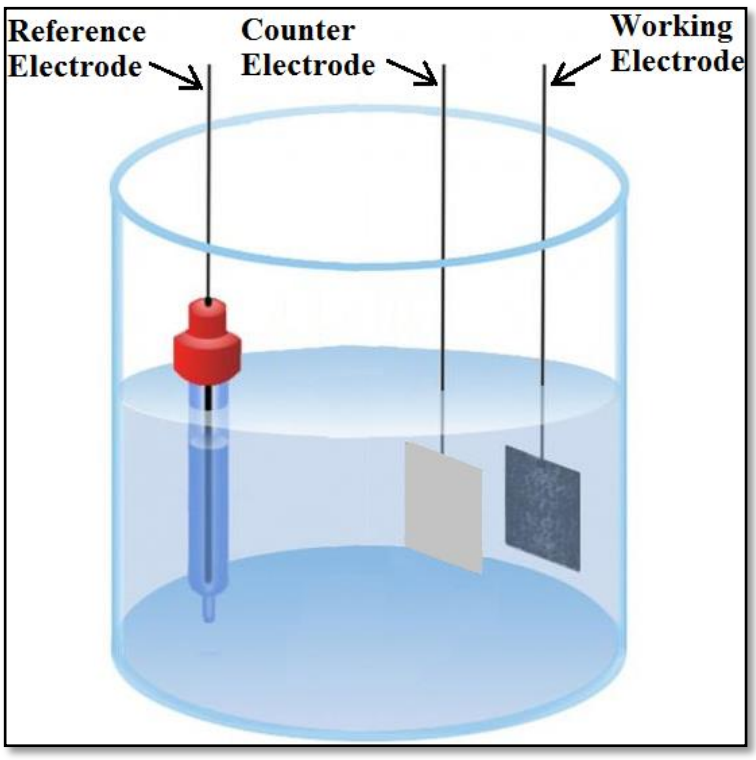

Figure 2.8. Three-electrode setup for CV test measurement of electrode potentials

The above CV test setup in Figure 2.8 is generally used to strictly study the electrochemical properties of an analyte in solution, and is often the first experiment performed in electrochemical studies. CV test is obtained by applying a linear potential sweep (that is, a potential that increases or decreases linearly with time) to the working electrode. As the potential is swept back and forth past the formal potential, Eo, of an analyte, a current flows through the electrode that either oxidizes or reduces the analyte. The magnitude of this current is proportional to the concentration of the analyte in solution, which allows cyclic voltammetry to be used in an analytical determination of concentration. A cell setup for electro-analytical measurements for cyclic voltammetry

always consists of three electrodes and an electrolyte: (KIETMA, 2013 and Marusak, 2007).

1. Working electrode (e.g. carbon fibre or Platinum wire)
2. Counter electrode (e.g. Platinum, Gold or Carbon fibre/cloth)
3. Reference electrode (e.g. Calomel electrode or an equivalent)

Glucose solution is the electrolyte needed in the CV setup to provide the electrical conductivity between the first two electrodes involved (Rapoport, 2012).

2.2.8. GFC Design Technology and Materials Background

Considerable laboratory experiment tests had evaluated variety of different GFC materials and fabrication techniques with the aim to obtain suitable cathode electrode as oxygen reduction catalyst in the presence of glucose and optimum anode material for glucose oxidation in the presence of oxygen (Justin, 2004).

The challenge to designing an ideal IGFC has been acknowledged to being limited by lack of cheap and desirable material able of provide appropriate catalytic proprieties required to extract the existing energy from glucose electrolyte, capable for high performance.

Table 2.7. Selection of material innovations

Non-metallic (Electrodes)	Metallic (Electrodes)	Metallic Alloy (Electrodes)	Material Combination (Electrodes)
▪ Carbon paper ▪ Carbon fibre ▪ Graphite ▪ graphene ▪ Carbon nano-fibres ▪ Carbon nanotubes ▪ Activ. Carbon ▪ Carbon cloth	▪ Nickel ▪ Gallium ▪ Silver ▪ Platinum ▪ Titanium ▪ Stainless still ▪ Iridium-Black ▪ Bismuth	▪ Gold-Silver ▪ Titanium-Gallium ▪ Platinum-Gallium ▪ Titanium-gallium ▪ Gallium-Silver ▪ Pt-Gold	▪ Carbon fibre and platinum ▪ Carbon fibre and gallium ▪ Carbon fibre and titanium gallium ▪ Platinum and Gallium ▪ Platinum and Titanium-Gallium ▪ Iridium black and Bismuth ▪ Platinum on vulcan carbon cloth

In the laboratory, a small number of common electrode materials listed in Table 2.7, were tested to validate the material technological requirements stated in Table 2.8.

Table 2.8. GFC material technological requirement

Catalytic Materials (Electrodes)	Electrolytes (Glucose solution)
▪ Sufficient porosity, ▪ High surface areas, ▪ Good electronic and ▪ ionic conductivity, ▪ Good electrochemical activity to ▪ Promote redaction oxidation reactions.	▪ High ionic conductivity, ▪ Negligible electronic conductivity, ▪ Chemical stability with electrodes, ▪ Impermeability to gases, ▪ Sufficient stability with minimum thickness.

The laboratory experiments involved combining different raw materials to form new compounds with improved catalytic performance. Most material combinations listed in the Table 2.7 showed performance improvements listed in requirements of Table 2.8, compared to their pure single states. Nevertheless, laboratory experiments required an unprecedented number of test arrangements to obtain an optimum electrode material combination that time and resources could not permit.

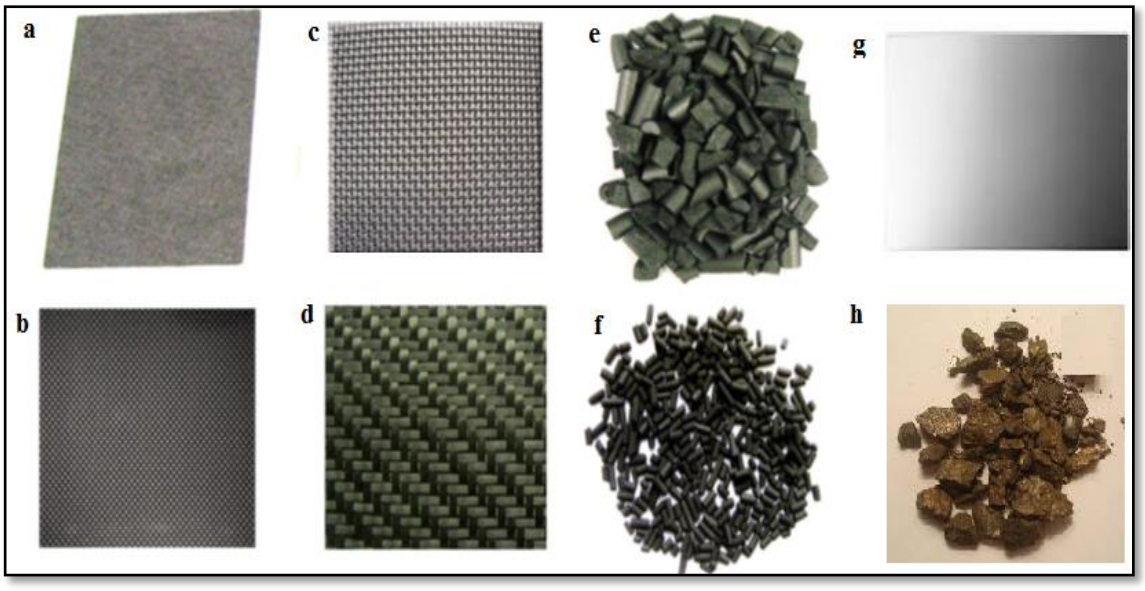

Figure 2.9. Pictures of typical electrode materials tested for DGFC: (a) carbon paper, (b) carbon cloth, (c) stainless steel mesh, (d) carbon mesh, (e) granular graphite, (f) granular activated carbon, (g) Platinum and (h) Iridium.

Figure 2.9 show the pictures of few raw electrode materials from Table 2.7; such as carbon cloth, platinum and other noble metals. These electrode materials from Table 2.7

were selected based on their application range capabilities, including materials of carbon embedded with metal nanoparticles such as platinum, which are known to greatly improve the active surface area of reactions (Wei, 2011), as confirmed by platinum nanoparticles supported on vulcan carbon cloth (PtVCC) in this project, and presented as the most flexible and porous catalyst electrode that have produced higher power densities compared to any listed material in Table 2.7, of which most electrodes presented unsatisfactory catalytic performance at their raw state.

This work laboratory tests confirmed that smooth surface metals as non-corrosive materials, mostly anode electrodes, such as stainless steel and platinum metals don't have good catalytic capabilities and fail to achieve higher power densities compared to corrosive metals such as silver or also non-corrosive materials such as carbon. Although most metal materials are more conductive than carbon materials, but only platinum, stainless steel and titanium have been approved as suitable metals for implantable fuel cells, while most other metals are less appropriate as fuel cell catalyst because of their high corrosion flaw.

2.2.9. Electrode Material Combinations, Coating and Alloying

This study laboratory experiment involving surface treatments were conducted on some electrode materials to improve performance via addition surface coating involving mainly carbon materials with different metal particles aiming to improve power generation through the development and creation of different cathode compositions. Also anode electrodes were separately coated with different structures of carbon fibres, carbon nanotubes, carbon black, carbons nanostructures, platinum or gold nanoparticles, including modification using chitosan residues in order to enhance electrode conductivity and electron transfer capabilities. Furthermore laboratory experiments of metal alloying fabrications were conducted, which at the time presented negligible gain to electrode performances. Yet again, cumbersome limitations were encountered from obtaining the best electrode combination of materials because this again required vast period of experimental time and resources.

Materials combination between carbon fibre or carbon cloth and different metals were straight forward, easy to implements and test. This experimental method showed quick

response of promising results to power improvement than any other method in the laboratory test.

2.2.10. Cathode materials for IGFCs

Fuel cell performances are currently being limited by the cathode, because cathodes are made of catalytic materials such as platinum film for oxygen reduction. Cathode selection therefore presents the most challenge in designing an efficient fuel cell, which mostly results only on large material area enough that can provide efficient current collection to achieve high power density, causing the design to become large and unpractical for IMDs.

Using electrochemical methods, such as CV test and electrochemical impedance spectroscopy, these revealed that off the shelf materials such as PtVCC can work as a good cathode or anode, capable of facilitating the electron transfer from glucose solution that results in improved and increased power density, with large surface area leading to designs of small enough GFCs capable of powering IMDs.

2.2.11. Electrode Selection for IGFCs

Electrode selection has been the ultimate challenge in manufacturing IGFC using cost-effective technologies. A variety of carbon and metal material have been explored in developing anodes and cathodes materials, and several electrode modification methods have been tempered in attempt to improve power density, however, power generation and electrode cost so far have not reached the levels for commercial use suitable of replacing batteries. Current options on cost-efficient electrode using of the shelf catalytic materials and configurations such as platinum on Vulcan carbon cloth are expected to be capable of overcoming current challenges and offer superior IGFC designs with optimum power densities.

2.3. PtVCC material technology

PtVCC has been fabricated with gas diffusion layers (GDL) arrangement; a porous structure made by weaving carbon fibres into a carbon cloth, which also provides an electrically conductive pathway for current collection. produced with a Micro Porous layer (MPL) and hydrophobic treatment (PTFE), Nafion post coating to help with the contact to the membrane and with liquid management and provide a smooth layer with sufficiently surface area for catalyst and good interface with the membrane. This GDL material is generally made with hydrophobic coatings (Nafion post coat) and penetrability properties. This GDL has been specially designed to help get the solution away from the catalyst layer while it's still in vapour form and not allow it to form to liquid until it is well clear of the catalyst sites, which helps maintain fuel cell's performance high (FuelCellsEtc).

PtVCC is a low-cost electrode material that utilises a woven carbon cloth substrate and a 40% Platinum on Vulcan Carbon support catalyst (Fuel Cell Store) This electrode is designed for applications suitable for electrochemical systems needing low amounts of platinum to support the catalytic reaction. As a result PtVCC electrode is perfect catalyst for GFC applications where custom sizes and loadings, including improved solution management and connection to the membrane are required to achieve higher output power densities.

There are several choices of PtVCC materials that have been developed with different physical proprieties of materials compositions. Detailed arrangement of PtVCC not easily seen by the naked eye, which has been optimised for diverse operating parameters and physical properties, features that include:

- 0.3 mg/cm² 40% Platinum on Vulcan (40% on Carbon Cloth) on gas diffusion layer (GDL) material
- Nafion post coat for improved solution management and adhesion to the membrane
- Perfect for IGFCs where material compatibility is required.

Table 2.9. Catalyst Properties of PtVCC (Fuel Cell Store)

Catalyst Type	**40% Platinum on Vulcan (Carbon Cloth)**
Loading	0.3 mg/cm²
	Gas Diffusion Layer Properties
Material Type	Woven Carbon Fibre Cloth
Thickness	0.410 mm (410 microns)
Basic Weight (g/m²)	180
Air Permeability (s)	< 8
Electrical Resistivity (through plane)	< 13 mΩcm²
Tensile Strength	MD: >10 N/cm and XD: >5 N/cm
PTFE Treatment	30 wt%
Micro-porous Layer	Yes, on catalysed side

Table 2.9 presents the PtVCC material composition that has been developed with different physical proprieties. In addition to the physical developments, PtVCC has diffusive transportation that takes into account solution movements that are encouraged by in-plane compression dissimilarity between adjacent channels, through-plane flow made by mass source/sink due to electrochemical reactions, heat transfer like the heat pipe effect, two-phase flow, and electron transportation.

Table 2.10. Comparison of different gas diffusion layers

Gas Diffusion Layer (GDL)	Material Type	Thickness (um)	Density (g/ cm^3)	Basic Weight (g/m^2)	Air P Permeability (s)	Through Plane Resistance ($m\Omega cm^2$)	Tensile Strength (N/cm)	Flexural Modulus (MPa)	Porosity	PTFE Treated	MPL
Plain Carbon Cloth	Cloth	356	1.5	132	-	-	19.25	7.5	-	No	No
GDL-CT	Cloth	410	-	180	< 8	< 13	>10 MD & >5 XMD	-	-	Yes	Yes
AvCarb GDS3250 EP40	Paper	225	0.33	75	-	< 14	-	-	-	Yes	Yes

The comparison in Table 2.10 presents the proprieties of plain carbon cloth and GDL before they are combined to form the PtVCC electrode material with the following design and physical capabilities:

a. Deliver sufficient mechanical strength to clamp membrane electrode assembly from extension affected by water absorbance.
b. Assistance to eliminate water produced outside of the catalyst layer and stop saturation.
c. Deliver spread pathway from flow channels for solutions to reach the catalyst layer.
d. Hold some solution on surface for conductivity through the membrane.
e. Provide sufficient temperature transfer during cell operation helped by compression.

As a result, PtVCC material is conductive, corrosion resistant, non-ion leaching and allows easy solution flow through it to the proton exchange membrane (PEM), and our preferred PEM material is a thin Nafion. PtVCC is essentially an electrode with a design that facilitates diffusion of reactants across its catalytic material. The surface area and porosity of the PtVCC is made of gas diffusion layers (GDL) which allows the reactants to diffuse along the PtVCC active area. With the improved surface area that the GDL delivers, movement of current on this catalyst material involving PtVCC to the current collectors increases (Fuel Cell Store).

2.3.1. IGFC Fabrication Background

Theoretically, the fuel cell design reaction requires involvement of glucose (liquid) and electrodes (solids), and the reactions involved bring together electrons and ions to break down glucose (glucose oxidation) to form water, releasing 24 electrons for every glucose molecule (Alam, 2009).

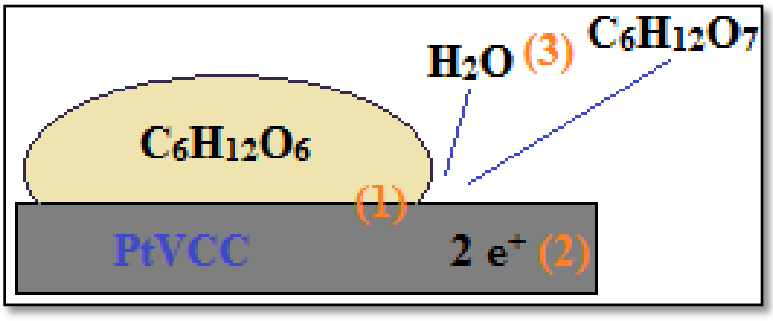

Figure 2.10 Direct fuel cell concept design based on PtVCC.

Figure 2.10 illustrate the three phase contact area between the (1) glucose ions coming together with (2) the electrode, and the produced electrons that are then transferred to (3) the by-products as a result from the reaction. Fuel cell design criticality is based very much in bringing the electrons, electrolyte and ions together to produce electricity. The experiments results demonstrate that glucose has a significant influence on PtVCC electrode behaviour as described further by these possible chemical reactions (1 - 3), were the catalysed glucose ($C_6H_{12}O_6$) in water produces gluconic acid ($C_6H_{12}O_7$), which usually goes through further oxidation, examples of which are shown below:

At the anode (negative): $C_6H_{12}O_6 + H_2O \Rightarrow C_6H_{12}O_7 + 2H^+ + 2_{e-}$ (1)

At the cathode (positive): $O_2 + 2H^+ + 2_{e-} \Rightarrow H_2O$ (2)

Overall reaction: $C_6H_{12}O_6 + O_2 \Rightarrow C_6H_{12}O_7$ (3)

Desirable requirements for constructing and designing ideal IGFCs:

- Large surface area, wherever the electrodes are in contact with the electrolyte.
- Having suitable catalyst material capable of increasing reaction rate.
- Small distance between the electrodes, so the electrolyte can facilitate the flow of ions and as a result the current flow.
- Efficient conduction of ions between anode and cathode by the electrolyte
- Improve the conductivity with electrode porous structure so that both the electrolyte from both sides can penetrate simultaneously.
- Connect the fuel cells in series to produce higher voltages.
- Facilitate powering and system integration into IMD.
- Potentially biocompatible materials that is amenable to established sterilization techniques.

2.3.2. Summary of an ideal IGFC

Based on IGFC findings, it has been established that the goal to uncover effective electrodes with combined catalytic performances and grand transference properties for a direct oxidation GFC system have been realised, and the subsequent observations are highlighted below:

a. As mentioned previously, one of the current and primary challenges in designing IGFCs is the ability to obtain a worthy catalyst that increases fuel cell output power density (Bartona, 2004).
b. Noble metals can be considered the most suitable catalysts because of their long-term stability and biocompatibility (Rapoport, 2012 and Wei, 2011). With improvements on future electrochemical technologies, a consideration to long lifespan operations and stability proposes the use of silver (Ag), gold (Au), Pd, Ni, and manganese oxide as main catalysis alongside Pt, as key component contributors to the optimum fuel cell designs (Wei, 2011).
c. Demonstrations show that using alkaline electrolyte instead of acidic electrolyte remarkably improves performance of fuel cells (Wei, 2011)
d. The most attractive electrode material for a potential IGFC is carbon; undisputedly cheap, plentiful and biocompatible.
e. In addition, affective IGFC designs are promising to one day fully accomplish the replacement of batteries in IMDs.

Throughout the evaluation process, significant findings of distinctive improvements are presented on different design choices, even though some need more practical in vivo tests to prove their significant reliability and performance, nevertheless they can be considered as decent starting point for designing and building an ideal IGFCs that meets the aims and objective of this review.

2.4. IMDs Summary - Successes and Challenges

Medical procedures have been transformed extremely by advances in medical device technologies. Hence, effective comparisons of these innovative medical devices have not been realistically examined and consequently have been largely lagging behind (AHRQ 2011). There are different types of IMD designs and functionalities, and their difference are continuously changing, such as becoming smaller yet efficiently low-powered implantable microsystems (Hached, 2014). However, the same challenges remain of requiring adequate energy for lifelong functionality, while supporting increasingly complex processing (Bazaka, 2013).

Currently the advancement on battery technologies has allowed for the development of long-term implantable devices with high reliability, multiple functions and improved

performances (Bazaka, 2013), together with the advancement of low power integrated circuit including power management systems, these have allowed for long term IMDs. (Bazaka, 2013) also claims that device with choice of external wireless powering has the potential of extending the life-time of the implant system, at the same time provide the long-term reliability needed to reduce the cost and time associated with the surgical implantation of these devices and the recovery of the patient. As the performance of the device is the most important factor in the design, hence (Joung, 2013) report on a number of successful IMDs in terms of achieving their set objectives.

Researches show most registered medical devices exist in the area of cardiac implants (Niederländer, 2013). Most of the established applications for medical devices focused on cardiac rhythm management (McDonald, 2011); as such the advancement of medical devices is well characterized by the successful treatment of heart anomalies using pacemakers, which can be considered one of the most successful IMDs in relation to the number of users implanted and their criticality. Since the beginning of the 20th century, the artificial pacemaker idea was already known (Peisino, 2013), and today its capable of serving patients at a life span of more than 10 years before it requires being replaced (Cadei, 2014), yet still very few other IMDs can achieve this lifespan. Whereas (Meng, 2014) presents IMD that is currently in clinical trials; Hemodynamic Monitor system (IHM), capable of monitoring pressure in the left atrium or ventricle in the body. While another successful IMD made of degradable implantable material was effectively implanted on mice, with a controlled degradation rate and products. This implant device has the potential of being used as an infection mitigation device (Tao, 2015). Otherwise an approved IMD; the VeriChip (PositiveID, Delray Beach, FL, USA), is capable of working beyond of RFID tag, and therefore provide monitoring capabilities such as temperatures and other features, since this is considered a lifetime implant with no planned replacements (Peisino, 2013).

Many published IMDs are prototypes or proof-of-concept components of what will eventually be a much larger system, and most of these studies have focus only on validating performance, usually in a perfect model environment not similar to the difficult implant environment. As a result, most of researched IMDs present either just monitoring or control of medication delivery, and power sources that involves either batteries or energy harvesting techniques such as GFC that promises to be implanted deeply anywhere in the body, and be able to generate power to monitor, sense and

transmit data whenever is required. However this review finds the published research studies of IMDs suffers from the lack of revealing the monitoring sensory technology of these IMDs as well as the self-powered capabilities incorporating power management system. Another underrepresented key area is potentially practical design and evaluation of factors that affect reasonable safety and security of wireless in IMDs (AHRQ, 2011).

Most of the existing published research studies on IMDs have not claimed to have produced successful monitoring of a particular disease, or present a complete design addressing the power consumption as well as the communication system, but most researches focused on one particular function but not a complete integrated design system; some focus are put on the IMD power source, on the encapsulation and implantation method, as well as on the communication with the external world, while others focus on active, implanted, long-term medical devices, but positively these existing designs present challenges that should guide the requirements to better IMDs design system (GOV.UK, 2013).

But in mean time, it can be acknowledged that most body energy harvesting to date are not ready yet to be used as a steady, reliable power source for IMDs (Peisino, 2013), but in the future this will become the only power source fit for IMDs. The 10 years battery life of existing IMDs could be exceeded by the development of new sources that could ensure life span over 10 years using IFC instead, as illustrated in table 2.11.

Table 2.11. Power performance and State of the art of technologies and materials for IMDs (Peisino, 2013)

Technology	**Batteries**	**Vibration/ Motion**	**Temperature**	**RF / Ultrasound**	**Light**	**Fuel Cell**
Power Supply	165 $\mu W/cm^2$	4 $\mu W/cm^2$	25 $\mu W/cm^2$	0.1 $\mu W/cm^2$	10 $\mu W/cm^2$	180 $\mu W/cm^2$
Solution Techniques	Rechargeable Solid state electrolyte	Energy harvesting	Energy transfer	Ultrasound Carrier type	Energy harvesting	Deep implant
Advantages	Reliable	Efficient energy transfer	Minimise damages Cheaper	Low power	Efficient energy transfer	On-site Continuous
Drawback	Size	Depth Receiver size Interference MRI	Requires small IMD size	Proximity		Not yet steady source
State of Development	Commercial imaging Research for IMDs	Commercial imaging Research for IMDs	Commercial	Commercial imaging Research for IMDs	Commercial	Research for IMDs Some commercial use

Tables 2.11 summarises the main features of possible IMDs power supply, involving primary energy sources and energy harvesting sources, where the development of an implantable glucose fuel cell (IGFC) generated power up to 180 μWcm^{-2}, the highest among all possible power supplies for IMD, including the primary battery, and the fuel cell is also the only device capable of being extremely implanted deeply inside the body without affecting its power generation. The down side specifically to GFCs is that it remains a research based outcomes, and a viable commercial out of the shelf is required (Bazaka, 2013). Although in the past the research into IGFCs showed promising results in vivo tests in 1970s, but it was short lived with the introduction of long lasting Li-Iodine batteries with lifespan of over 5 years, (Kerzenmacher, 2008 and Stetten, 2006). But now, with advances in technology, two decades later, a restoration process to IBFCs is looking promising to power future IMDs.

In spite of substantial innovations in the fabrication and application of IMDs and systems, modern implants have yet not overcome the most challenges of IMDs related to long-term reliability of the device (Bazaka, 2013), capable autonomous operation systems with active management requiring no human-in-the-loop, avoid sensors that consume more power than the entire IMD, and the need for prognostic capabilities in IMDs, to provide estimates of the remaining useful life of the implant or provide indication of performance anomalies that may need to be addressed before a problematic clinical situation arises (Hareland, 2013). So outstanding knowledge and design of prognostics is key for developing capabilities and approaches similar to other fields that are directly applicable, to provide prognostics opportunities that can be utilised in future medical devices.

Nevertheless, these research studies have presented aspiration to successfully designing miniaturised IMDs capable of operating autonomously on a long-term basis; a design device that is heavily focused on low power consumption due to the necessary balance needed between device longevity to reduce surgical replacement burden and small device sizes for comfort and cosmetic reasons (Hareland, 2013), at the same time integrating both sensing and actuating possibilities in a feedback closed loop with autonomous power supply, suitable housing material, and reliable data transmission capable of releasing a drug, and adjust its operation according to the sensor information (Peisino, 2013). In addition, an ideal IMDs should be completely autonomous where the patients should not perceive that their health is being monitored by a machine, combining both monitoring and treatment such that both modalities work together to achieve optimised

and personalised closed-loop treatment that is designed to meet the patient's need, and precisely deliver prognostic monitoring of health checks to adjust the medication accordingly, in turn excluding pain, costs of money and time to the patient.

A successful innovative design of IMDs involves the integration of state-of-the-art technologies including; low-power microcontrollers or microprocessors (CPU), sensors, memory storage, RF technology (wireless communications) products and power management systems. The overall system level requirements such as functionality, performance, size, weight, power, including the latest packaging technologies, biocompatibility, sterilisation, surgical procedure, and magnetic resonance imaging (MRI) compatibility, are always being considered for optimum IMD design (McDonald, 2011).

Chapter 3

Methods

3.1. GFC Based on PtVCC Electrode for Powering IMDs

This section reports on PtVCC based fuel cell experimental method and materials for harvesting energy from glucose solution, the favourable body fluid for powering IMDs.

3.1.1. Materials

0.3mg/cm² 40% PtVCC material were purchased from Fuel Cell Store, Texas (USA), while platinum film (0.01mm thickness), platinum mesh (0.1mm diameter/99.9), Nafion from Alfa, Potassium ferricyanide $K_3[Fe(CN)_6]$, Potassium chloride (KCl), D-(+)-Glucose (powder) and Phosphate buffered saline (PBS) solution were purchased from Sigma–Aldrich UK. LTC3105 DC-DC converter samples were obtained from Linear Technology. NCP1400A DC-DC converter samples were obtained from ON Semiconductor. All chemicals, components and electrode materials were used as received from the suppliers.

3.1.2. Morphology and composition of PtVCC electrode

Platinum and carbon materials are widely used as electrode materials for GFCs and sensors due to their known electro-catalytic effect in response to redox involving hydrogen or oxygen (Oncescu, 2011). As part of this effort, many different electrode materials including nickel, PtVCC, silver, platinum and other noble metals were tested in the laboratory and some of these are described in the previous sections. PtVCC were tested and compared and as a result of these tests, their excellent electron transfer and electrochemical catalytic activity for glucose oxidation reactions, including stability and good performance results, these were selected as best performers.

The morphology, structure and composition of PtVCC were examined using under a field emission scanning electron microscope (Zeiss Supra 35VP FE-SEM) in combination with Energy-dispersive X-ray spectroscopy (EDS), and Fourier Transform Infrared (FTIR) Spectroscopy experiments collected on Jasco FTIR-4200 equipment.

3.1.3. Electron transfer activity of PtVCC electrode

The electron transfer activity of the electrode was tested using cyclic voltammetry (CV) in electrolyte containing potassium ferricyanide K_3 [Fe (CN) $_6$] (4mM) together with potassium chloride (KCl) 0.1M in deionised water were prepared as a means of standard solution reduction-oxidation (redox) potential. A computer controlled potentiostat/galvanostat IM6 (Zahner-elektrik GmbH & Co. KG) was used. Each type of experiment was repeated three times with freshly prepared electrodes or solution for a better comparison with platinum sheet as control.

3.1.3.1. Characterisation of electro-catalytic propriety of PtVCC electrode in glucose solution

To confirm the electrochemical activity of PtVCC as a catalytic material for glucose fuel cells by recording the output voltages and currents, electrochemical measurements were performed using a computer controlled potentiostat/galvanostat (IM6). The test involved a concentration amount of glucose in a stable pH around 7.4 (glucose solution in PBS solution), resembling the mean normal blood glucose concentration in human body fluid which is roughly constant at 5mM.

The electrochemical cells test setup used in this work involved a saturated calomel electrode (Saturated KCl) and platinum electrode as reference and counter electrodes respectively and the working electrodes were made of either plain platinum sheet or PtVCC sheet.

All electrochemical measurements were performed with a computer controlled potentiostat / galvanostat (IM6), digital meter such as a Fluke meter and/or an Oscilloscope. All experiments and solutions in the cells were stirred during electrode testing, and conducted at room temperature first and then at 37°C.

3.1.4. GFC Design based on PtVCC

Considerable laboratory experiments were conducted investigating the optimum design techniques that allow glucose oxidation in the presence of oxygen, and oxygen reduction in the presence of glucose. The first common technique involved the sandwiched type (Stetten, 2006 and Alam, 2009), direct GFC concept with the electrodes separated by

nafion membrane. The second experimental technique was the single layer design (Kloke, 2011 and Alam, 2009), where the anode and cathode electrodes are placed side by side. The first two concepts do allow the presence of both glucose and oxygen at the cathode and anode. The third design was the depletion technique (Alam, 2009), involving placing the porous PtVCC at the cathode in front of the anode contained only platinum sheet, such that the oxygen gets reduced before getting to anode, permitting glucose oxidation to take place at low oxygen concentrations. The fourth design concept involved a combination of sandwich and depletion techniques to form a concentric design (Oncescu, 2012) where the anode is surrounded (and sandwiched) by the cathode, this increased the interface area between the electrodes and it helped increase glucose-oxygen separation when the layers were stacked.

The sandwich and depletion layer design techniques produced insignificant improvement on overall fuel cell power density compared to single and concentric designs, where the later designs required arrangement of large electrode volumes, while depletion and concentric design techniques presented the most complications in regards to fabrication and assembly process, and the single layer design present the most desirable because of simple fabrication method, reduced packaging thickness and easy integration to implantable devices, but single layer design also required large amount of electrodes, while sandwich concept produced excellent power output with small amount of electrode materials, which could easily be stacked to increase performance, as a result, provided an effective low cost design, easy of fabrication, assembly and integration process into low volume implantable devices.

The sandwich concept oxidation reduction reactions were significantly facilitated by highly pressing the material structures closely, providing ideal configurations for achieving high surface area catalytic capabilities, by using nafion as a membrane separator between the cathode and anode, and also by using PtVCC electrode on two sides, but at the cathode side there was platinum metal sheet, that also served as a current collector

3.1.4.1. GFC assembly and characterisation

The PtVCC (active anode) and platinum (cathode) electrodes were cut into pieces no larger than $1cm^2$, and the third, intermediate electrode (passive anode) is also made of

PtVCC cut into 1 by 2 cm piece, this was sandwiched between the two sheets of nafion membranes separating the active anode and the cathode electrodes, making a three-electrode based GFC configuration design. The electrode materials were wetted with methanol, washed thoroughly and left in deionized water for at least 5 minutes before being assembled as GFC.

The sandwich type GFC design, was mechanically assembled and confined by two polycarbonate frames and Silicone Rubber Gaskets separated by three electrodes and two nafion membranes; a sandwich configuration design that supports the presence of both glucose and oxygen at the cathode and anode areas (suitable design for low temperature and low power applications).

The sandwich concept's redox reactions were significantly facilitated by highly pressing the polycarbonate frames material structures closely, providing relatively ideal configurations for achieving high surface area catalytic capabilities by using nafion membrane electrolyte between the two anode electrodes and the cathode. The intermediate passive electrode provides further stability and increased current and voltage outputs.

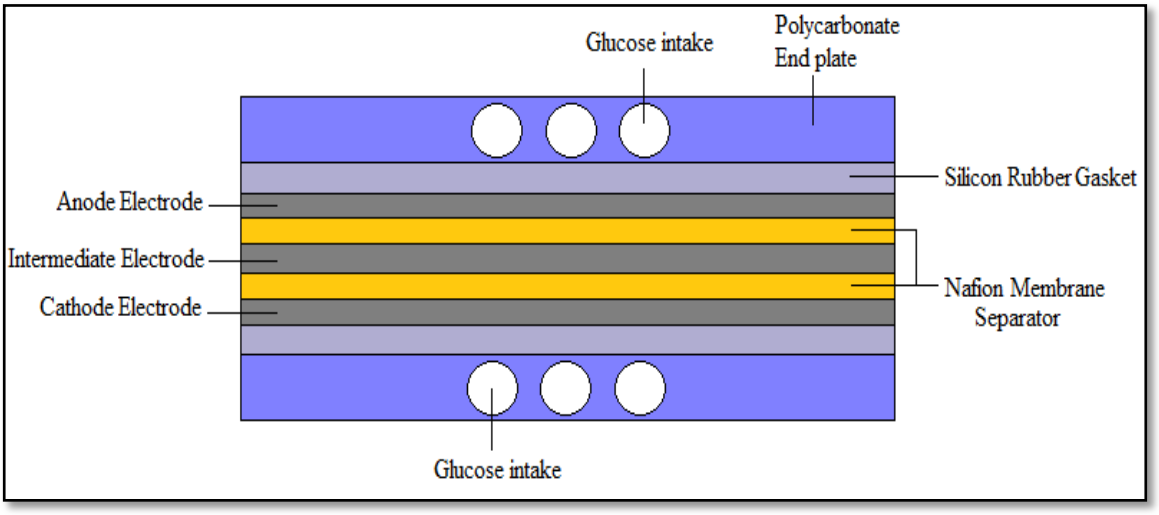

Figure 3.1. Basic components of a typical Sandwiched type design of a direct GFC based on PtVCC.

The Figure 3.1 shows GFC with delivery plates that are separated by the two electrodes and a nafion membrane which is sandwiched between them, presenting a sandwich design most suitable for low temperature and low power applications; a configuration

which supports the presence of both glucose and oxygen at the cathode and anode areas, with inconsequential drop of current.

We have considered rapid assembly fittings to which electrodes and membranes could be stacked between silicon rubber gaskets and thick polycarbonate frames and backings. The whole assembly is clamped together with nylon screws. Since the active anodes is comprised of PtVCC, which has a catalytic side, the cathode is comprised only of Pt sheet, while the intermediate passive anode electrode PtVCC is sandwiched between two nafion membrane electrolytes separating the active anode and cathode electrodes on each side. These materials were manually pressed together with silicon rubbers and polycarbonate frames, the final thickness of the fuel cell, including the contribution from the two active and passive anodes, cathode, nafion electrolyte, silicon rubber and polycarbonate was no greater than 10 mm. The electrodes could further be stacked together to obtain higher output currents. Polycarbonate frames and silicon rubber gaskets both provided mechanical support to the electrodes while damping the pressure effects due to the clamp.

3.2. Power Management and Energy Storage

In order to satisfy the applications of wireless IMDs, the implantable circuit development was expected to concentrate on small data transmission, efficient energy storage and power management. To reach the long-term, maintenance-free operations of IMDs powered by traditional battery, the self-powered IMD using GFC requires having an efficient power management system in order to be considered as an ideal candidate. Different techniques are available for attaining power from fuel cells. The IGFC requires the energy generation system to be combined with an energy management, storage and control, as a one complete solution.

3.2.1. Power Management Design Background

The power management system started first by capturing the energy harvested by the GFC, which is converted from chemical into electrical energy, and the potential is then boosted by a regulator circuit before storing it in a rechargeable battery to be used later, by releasing the needed amount to power the IMD. Therefore, a power level regulator

control circuit is used to intelligently manage a complex power distribution to the implant sensing system based on power needs and system operation. To maximise the usage of the energy harvested from a GFC, the power management systems provides a critical and highly efficiency energy conversion technique of optimum power usage, adapt to either constant impedance or variable impedance to match the impedance between the energy harvesting GFC and the IMD load. Following techniques were used to improve the performance of the GFC potential by incorporating the power management system basing on:

1. Optimisation for low average power in the system.
2. Used software timers and interrupts to isolate loads; all loads are switchable.
3. Quick processing with low power as an optimum choice.
4. Sending the data to be processed externally elsewhere.
5. Minimum wireless protocols and topology considered.
6. Powered each component of IMD system in sequence.
7. Considered minimise power consumption of individual devices.

To monitor factors such as glucose levels in the body, the IMD systems powered by GFC, harvesting the glucose energy to be restored in a rechargeable battery to ensure sufficient energy is available to power low-power, high-efficiency implantable circuit system, to transmit data wirelessly. To provide enough power to drive the IMD system for months if not years, the energy produced by the GFC utilising the existing and continues abundant glucose fluid in the body, is best stored in a rechargeable battery, and the power only used in short bursts when needed.

3.2.2. Direct GFC voltage boosting application

In order to satisfy the applications of a self-powered IMD using GFC, the glucose energy conversion technique is required to generate sufficient power to drive the medical device and sensors. However, all electronic components require working voltages higher than those delivered directly by the GFCs. And because the output voltages and currents of a GFC varies with time, as a result the voltage produced by the GFC needs to be stepped-up to drive any IMD.

The main problem with implantable GFCs, individual cells cannot effectively be connected in series like batteries to increase the overall output voltage, because the electrodes are in the same glucose solution, therefore when they are connected in series, this essentially shortens the anodes and the cathodes leading to a drop in cell voltage and current, providing a value that is lower than a single cell, <0.4 V. The only alternative is to connect the cells in parallel; this increases the current but keeps the output voltage equal to a single cell (0.4 V).

Since most electronic circuits require operating voltages high than the outputs obtainable from GFC, as a result, a requirement to boost the output voltage > 2 V is met by integrating a DC/DC converter circuit between the GFC output and the input to the IMDs, thus increasing the output voltage to the required operating range of IMDs.

Numerous reproducible experiment designs were carried out in order to obtain an increase in voltage and power outputs from GFC, and the working solution was obtained by connecting 3 fuel cells in parallel producing >0.4 V, and producing combining output current between 700μA and 1200μA. The output from the 3 GFC in parallel was directly connected to a booster; direct current to direct current (DC-DC) converter circuit that produced sufficient voltage > 4.0 V, enough to power an efficient IMD.

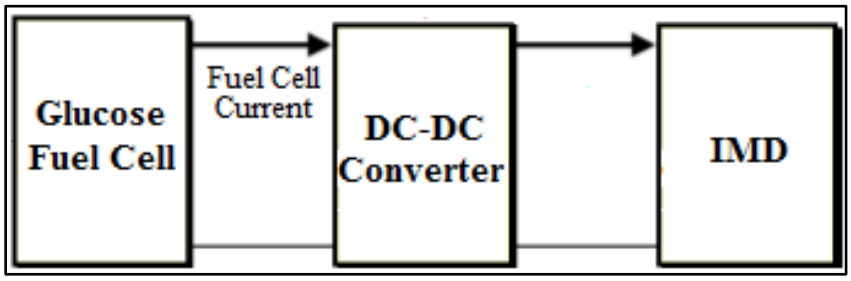

Figure 3.2. Basic block diagram of a glucose fuel cell connected to a boosting DC-DC converter before the IMD

Figure 3.2, shows a simplified block diagram connections comprising of a DGFC as the energy source, the intermediary DC-DC converter, and the IMD. Supplementary information is covered in sections to follow.

3.2.3. Architecture of the Power Supply and the Power Management System

Since the 0.4 V potential from the GFC could be increased >4 V, and maintained at this level by using a DC-DC converter. The switching regulator of DC-DC converter electronic circuit can be simplified as follow:

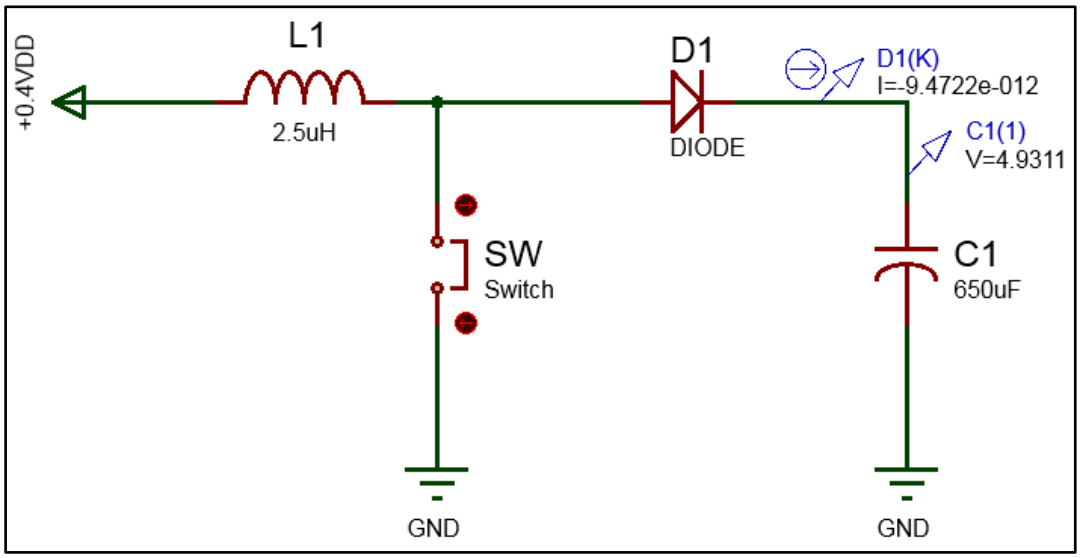

Figure 3.3. Basic configuration for boosting the output voltage, VDD: voltage in, C1(1): capacitor voltage. L1: inductor, D1: diode and C1: capacitor/battery, SW: switch

A simple step up of switching regulator configuration is shown in Figure 3.3, where V_{DD} is a constant input voltage source and C1 (1): capacitor voltage is the boosted output potential. The switching regulator works in steps, while the switch is open, the capacitor/battery is charged normally to the input potential, when is closed, the current flow through the inductor, and no potential flows through the diode, while also preventing the capacitor/battery to discharge. The potential at the capacitor will be rising with each charge and discharge cycle and this process is repeated continuously. Furthermore, the switch shown in the circuit can be replaced with a DC-DC converter circuit, as result the DC-DC converter circuit will perform automated and precision switching continuously. Whereas, capacitor C1 can also be replaced with a rechargeable battery to store the boosted potential generated from the circuit. With basic switching circuit shown Figure 3.3, if the input voltage changed, the output voltage will also change, but this can only be stabilised with additional circuit components or by adding a DC-DC converter to this circuit.

3.2.4. DC-DC converter setups

The DC-DC converters (LTC3105 and NCP1400A) setups were used as switching regulators (at frequency of 180 KHz), available for specific input and output voltage ranges, able to boosting input voltages as low as 0.225V- 0.5V to 5V output, to power the microcontroller, sensor and the transmitter systems which required a minimum stable potential of 2 V. The power management system includes the GFC, DC-DC converter or regulator and the rechargeable battery; the combination of these devices were used to increase and maintain potential at the desired maximum level of 4 V, to power the microcontroller system including the sensor and the transmitter circuit acquired to send the data to an external receiver.

3.3. Low power SMART microcontroller systems

The key to successfully implementing intelligent creations of IMDs to the real world of health monitoring, is by identifying and using key components needed for low-cost, easy to use control system with non-invasive universal sensor probes, with the goal to integrate these with intelligent wireless transceiver probes that can be implanted inside human's body to log real-time physical properties such as temperature, glucose level, high blood pressure and pH, wirelessly to an external system.

A series of experiments were carried out to test signal propagation and data transmission in a laboratory environment involving wireless data transmission (RF communication), wireless temperature monitoring tests. Instead of glucose sensors, in this experiment temperature sensors were used in the same configurations to measure temperature remotely. Eventually, the autonomous sensor systems will be comprised with not only a radio frequency (RF) temperature sensor monitoring probes, but also include a glucose sensor for measuring glucose levels changes within the human's body fluid. The initial experimental of autonomous sensor node design comprised of the following architecture: a sensing subsystem for data acquirement from the surrounding environment, a microcontroller-based processing subsystem for local data processing and storage, a wireless communication transceiver subsystem for transmission of sensed data, and a power supply unit providing sufficient energy to perform programmed tasks (Villafuerte, 2008; Gupta, 2014; Anastasi, 2009 and Chiara, 2009).

3.3.1. PIC microcontroller function tests

Initial experiments were carried out using a development kit shown in Appendix A; was designed and built in the Lab to test and programme different PIC microcontrollers, this served as an initial testing board which contained several inputs and outputs for the purpose of analysing various states and functions, such as microcontroller power consumption, ADC converter, Flash memory, software compatibility and interface to a PC using RS232 system.

The PIC microcontroller testing presented great advantage by being simple, reliable and cheap system to run with multiple tests configurations. Initially tests interfacing infrared transmission and detection system although were not useful for the implant solution in mind, but this method were found close enough to the RF communication system desired, as well as the use of serial data transmission, data coding and decoding, which are interchangeable from one technology to another, thus the same programming language used to transmit or receive data using infrared system needed only little modification to transmit the same IMD data wirelessly using an antenna.

3.3.2. PIC10F222 microcontroller based system

PIC10F222 microcontroller (Microchip 10F222 datasheet) was chosen for this work because it conveys in order of higher magnitude than its competitor type, with low-cost, high-performance, 8-bit fully-static Flash-based complementary metal-oxide semiconductor (CMOS) microcontroller, easy-to-use and integrate with other systems, reliably capable of running complex instruction codes, easy to remember instruction set reduces development time significantly. The PIC10F222 microcontroller is easily interfaced to different RF communication; transmission and detection systems, and easy-to-use of serial data transmission, data coding and decoding, including integration with implant monitoring sensors.

The PIC10F222 device is well known to fit in applications ranging from personal care appliances and security systems to low-power remote transmitters/receivers. The Flash technology makes customising application programs (transmitter codes, appliance settings, receiver frequencies, etc.) extremely fast and convenient. The small footprint packages, for through hole or surface mounting, make these microcontrollers well suited for applications with space limitations. This microcontroller technology is also equipped

with special features that reduce system cost and power requirements, including facilities such as programming language usage that transmit or read data requiring only little modification to transmit the same data wirelessly using an antenna (Microchip 10F222 datasheet).

Table 3.1. PIC10F222Microcontroller Proprieties (Microchip 10F222 Datasheet)

Parameter Name	**Value**
Program Memory Type	Flash
Program Memory	0.75 KB
CPU Speed	2 MIPS
RAM	23 Bytes
Timers	1 x 8-bit
Analogue to digital converter (ADC)	2 ch, 8-bit
Temperature Range	-40 to 125 ^{o}C
Operating Voltage Range	2 to 5.5 V
Pin Count	6
Cap Touch Channels	2

The information in Table 3.1 represent the microcontroller's proprieties, which were considered during the tests carried out in laboratory to confirm other in-built function states such as, power consumption capabilities, ADC converter, flash memory, software compatibility and the interface to a PC using RS232 system.

Knowing the power consumption of the microcontroller is crucial so the desired remote transmitters/receivers of the implant system can be emulated, which requires low power functionality. The manufacture's power consumption graph shown on Figure 3.4 gives an insight to choices of working power and frequency required to obtain an optimised low-consumption design.

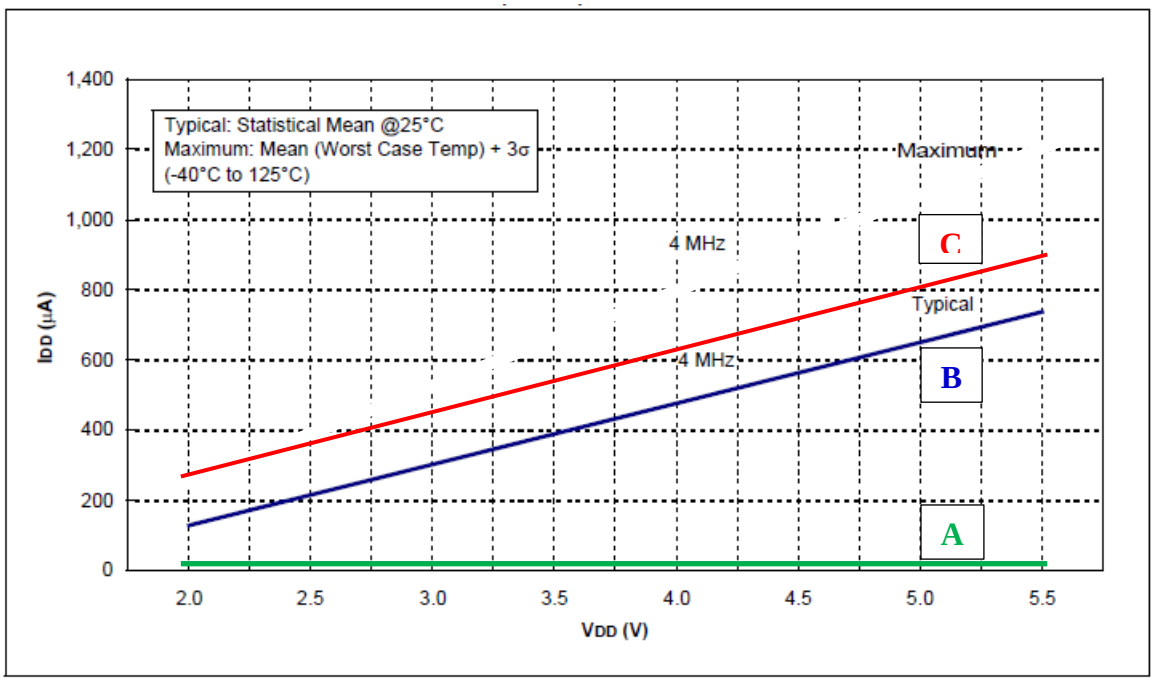

Figure 3.4. PIC10F222 Microcontroller Power Characteristics running; (A) at sleep mode, (B) at 400MHz, (C) at 800MHz (Microchip 10F222 datasheet)

The data provided from Figure 3.4 satisfies the use of this PIC10F222 microcontroller as a good candidate that emulates the desired autonomous bio-implant system. Plot (A) represents the microcontroller typical power consumption at sleep mode (all peripherals disabled), when running at lower voltage of 2V, it consumes only 0.1µA, and even at full 5V, it consumes only 1 µA. At plot (B) the microcontroller operation at low voltage 2 V and 400MHz, consumes low current of only 120 µA, while at 2 V and 800MHz, the current consumption increases to only 230 µA as shown by plot (C).

3.4. Clock-Less Pulsed RF transmitter

Further tests with PIC10F222 microcontroller device were carried out by experimenting with its low power consumption technology and communication methods that could be reassigned to a more improved design using CMOS technology, by isolating other function blocks contained in the microcontroller that are not being used during the experiments or will not be used on the final IMD system.

Therefore, this part of work focused with a view to creating a low speed wireless communication link for implant data retrieval and attempt to maximizing battery (fuel cell) life. A feature that all these systems have in common is that an RF carrier, at one of

the ISM band frequencies, is modulated in some way in order to transmit digital data to the reading device. However, the use of a carrier adds a significant power budget overhead to any design and should be avoided if at all possible in order to maximize implant battery life.

This investigation anticipated the use of a simple, low-data rate (Rabaey, 2002), carrier-less system consisting of a transient driven implanted microcontroller transmitter with monopole antenna and an external microcontroller system with antennas to initiate transmission and receive digital information over short distances (<10cm) (Belleville1, 2009; Belleville, 2009 and Colin, 2007), from an analogue sensor (eg. temperature sensor). This experiment analysed the signals involved and presents the hardware and software solution to the problem, involving low power, low cost hardware implementation consisting of a transmitter and receiver system to interface with a PC for monitoring purpose; this has been implemented as part of a solution to bio-implant power consumption by bypassing the use of an oscillator for data transition.

3.4.1. Clock-less microcontroller based system

The microcontroller based reader circuitry could consist of any number of low-power analogue sensors, but a single thermistor temperature sensor was chosen for this experiment;

Figure 4.6 shows the transmitter circuit consisting of thermistor sensor, which is connected to a built-in ADC of the EEPROM microcontroller (PIC10F222) and has a monopole antenna directly connected the one of microcontroller's output pin, while the transceiver block diagram contains another monopole antenna, a high gain pulse amplifier (Daly, 2007), phase-lock loop (PLL) circuit and a Microchip PIC16F1827 microcontroller connected to a monitoring PC by a 2 wire RS232 interface.

A PIC10F222 microcontroller is chosen to process and transmit sensory data as it has built-in ADC and 'sleep' power-saving topologies (Microchip 10F222 datasheet; Belleville1, 2009; Belleville, 2009 and Colin, 2007). The antenna used was simply an 18 mm long copper wire (1 mm diameter monopole) attached directly to one of the microcontroller I/O pins. No high frequency carrier wave was used, and no impedance matching or pulse shaping networks were used either, in order to achieve the simplest

functional prototype. Furthermore, no investigation into the bandwidth of the transmission produced was undertaken as, given the extremely low power levels involved, proportional to a switched 0V-2V transition on a TTL microcontroller pin, and the short distances targeted in this application, it is not considered important for this approach. The antenna length was arrived at through trial and error, by which the shortest length of wire that would trigger the pulse amplifier successfully at the distances chosen, 18mm, and another twice the length, for comparison purposes, were selected.

The microcontroller was programmed to produce a 1 kHz output signal for data transmission when powered from a 3V battery with an internal clock frequency of 31 kHz and the microcontroller's built-in comparator was used to detect the pre-amplified incoming pulses and convert them into numerical data, further detailed discussion to follow on the pulse amplifier section.

3.4.2. Propagation Simulations

3.4.2.1. Pulse-Excited Thin Wire Monopole Data Transmitter

Simulations using a commercial 3D Finite Difference Time Domain electromagnetic solver (Rouf, 2009) were carried out to investigate the propagation characteristics of the pulse signals in air. Two monopoles, each 18mm long by 1mm diameter, were placed within a virtual air-filled space connected to discrete ports 5mm from an electric ground beneath and surrounded on all other sides with a minimum 10 wavelengths of air at the simulation frequencies (Colin, 2007).

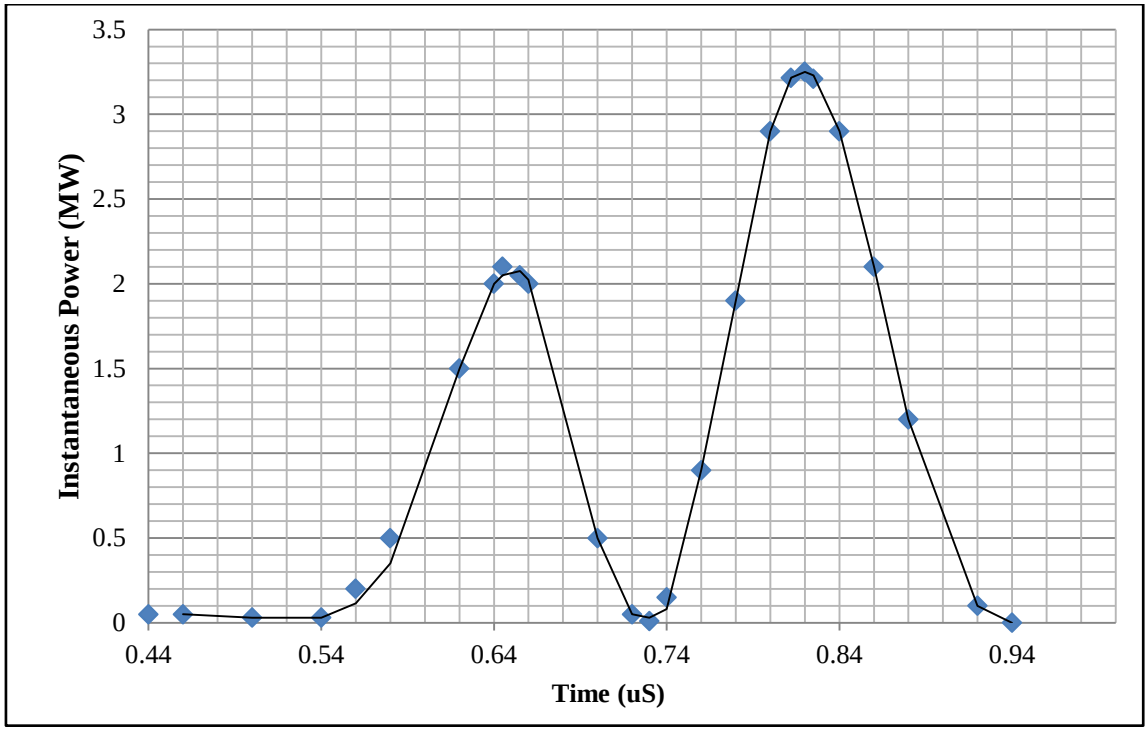

Figure 3.5. Simulated Pulse input power

The transmitting port was energized with a $1V_{Peak}$ Gaussian pulse with a duration of 253pS, containing a 10GHz bandwidth. It would have been more preferable to input a square pulse in order to emulate the step response of a TTL level signal but the simulation of such a wide bandwidth pulse was found to be far too system resource intensive for even our best computer and hence a 10GHz bandwidth was chosen as an approximation. Figure 3.5 shows the resultant power pulse obtained when the transmitting port's voltage and current data are multiplied together in a spread sheet. The pulse's energy ≈ 495fJ, obtained by simply integrating the data between t=0.54nS and t=0.94nS using the Trapezoidal Rule approximation. From this we can calculate that, when pulsing at 1000Hz, the total energy employed for the transmission ≈ 500fW.sec x 2 x 1000 = 1nW.sec.

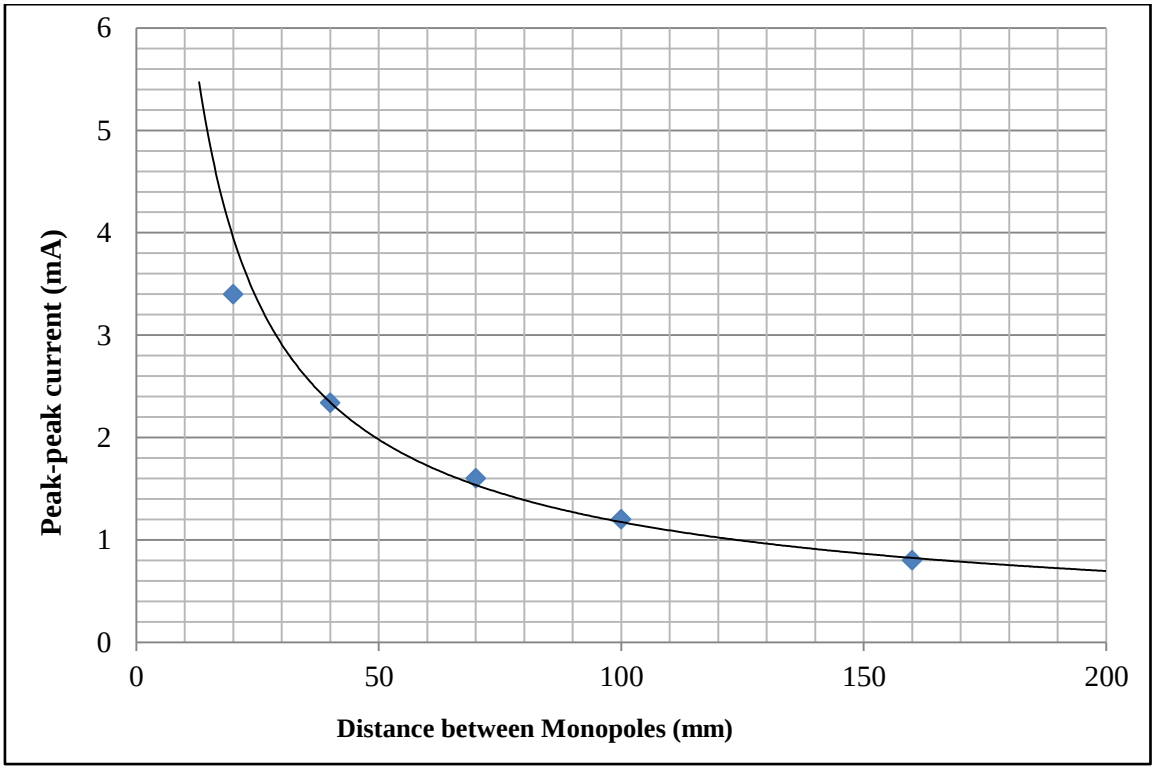

Figure 3.6. Peak-peak current (mA), induced in receiving monopole vs. separation distance

The distance between monopoles was steadily increased and simulated values for induced current in the receiving monopole were plotted on Figure 3.6, where can be noted that the maximum peak-to-peak current at 120mm ≈1mA and that the decay in amplitude with distance is predicted by a power trend line. The received pulses are, however, extremely short, with a maximum duration of a few nS, as denoted by Figure 3.7, which shows the current flowing in the transmitting monopole and that induced in the receiving monopole when at a 10cm distance.

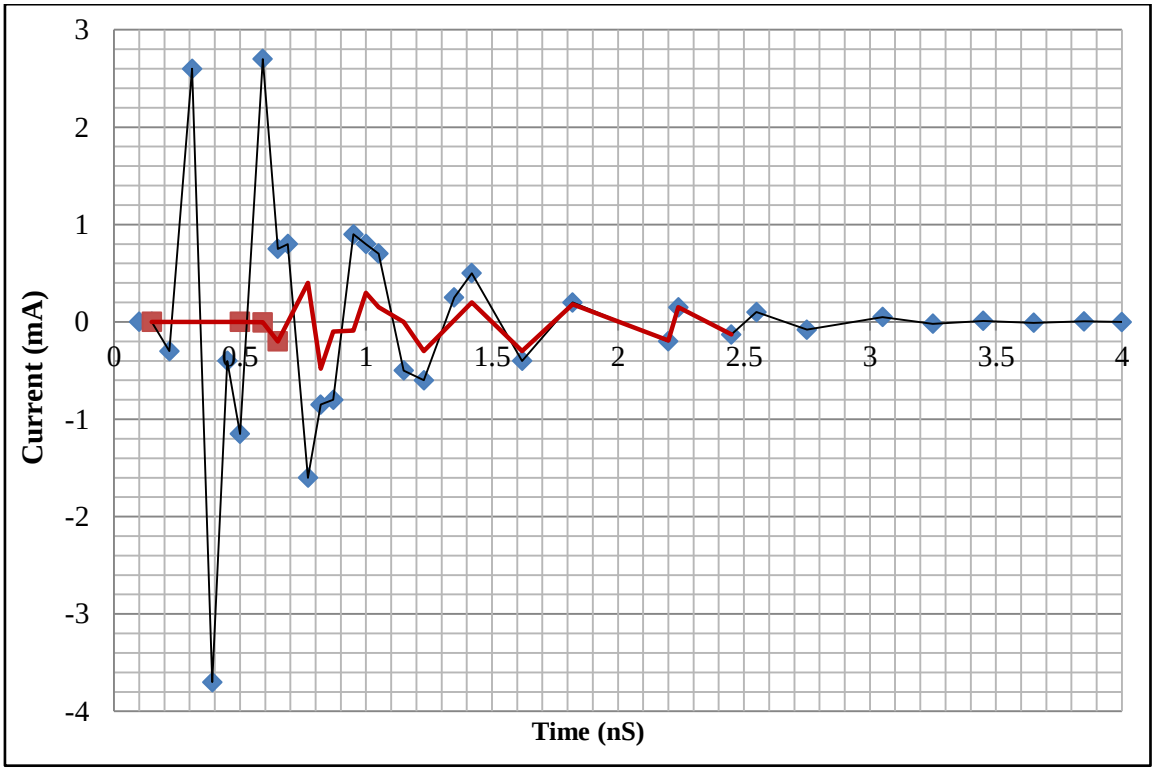

Figure 3.7. Simulated transmitter and receiver monopole current pulses

From the graph of Figure 3.7, it can be seen that the signal time period is 0.4nS which equates to a frequency of $1/0.4x10^{-9}$= 2.5GHz. Also, the received current pulse at this distance is 0.5mA peak and lasts just 4nS. It follows that in order to detect and buffer this signal to a level where it can be used as a suitable input for a PLL circuit (~$0.5V_{Peak}$), a high performance pulse amplifier capable of a minimum trans-impedance voltage gain of 0.5/0.0005=1000x or 60dB is required. In practice, in order to maximize reception range, a much higher gain is desirable. With this in mind, the following section describes our proposed prototype design and operation in detail.

3.4.2.2. Pulse Amplifier

To make a worthy the retrieval of data from the temperature sensor to the outside world where it can be read, communication means such as RF is the most simple and low cost method for data retrieval. As a simple solution, a step impulse amplifier was designed for the purpose of amplifying the signal transmitted from the implant to the outside world. The investigation gave out analytical results of possible required distance, power requirements for an optimum reading of data with accuracy. The criteria used in selecting the best configuration related to this pulse amplifier design is clearly based on

results obtained from previous section with simulated transmitter and receiver monopole current pulses, and from simulated bandwidth and impulse responses, hence the circuitry involved warrants further explanation.

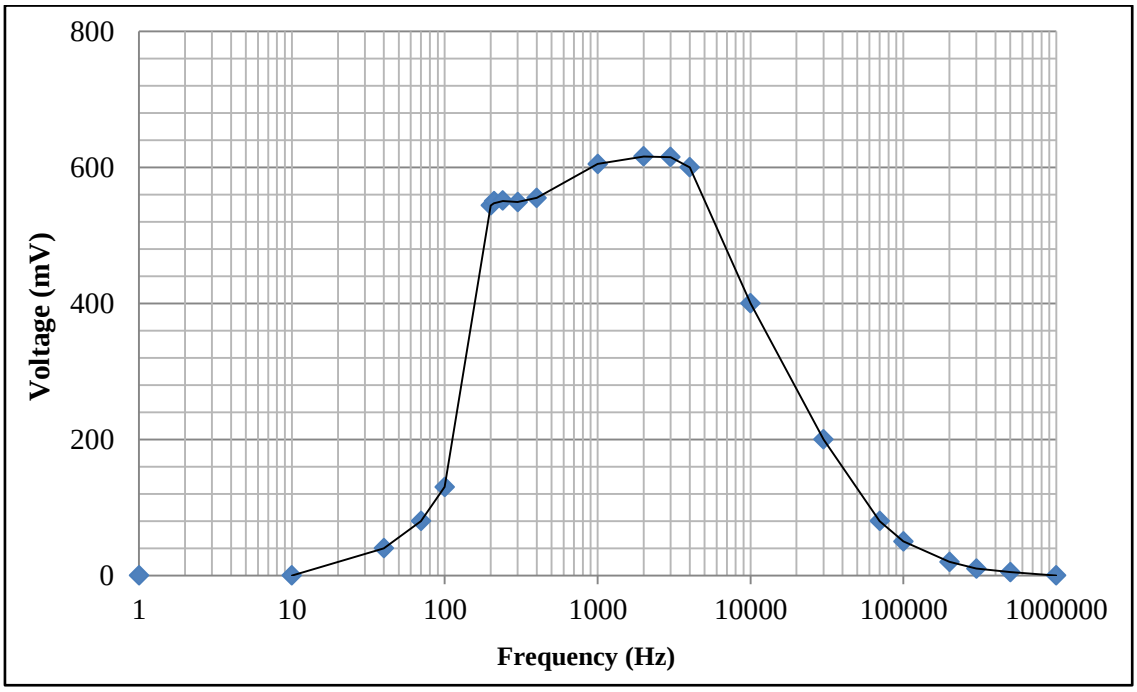

Figure 3.8. The simulated bandwidth in PPICE of the pulse amplifier - obtained before designing the amplifier.

The response of the circuit to a simulated bandwidth of the pulse amplifier is shown in Figure 3.8. Only the positive half of the coupled pulse is amplified by the circuit due to the chosen biasing arrangement and this is so that only one transient is amplified per square-wave cycle input. This simulation shows a voltage gain of 6/50µA = 120000 ≈101dB and a 10 kHz bandwidth centred around 1 kHz. Although the amplifier's slew rate is excellent (~8V/µS), its settling time (~60µS) is quite significant due to the large value drain loads employed resulting in high RC discharge times constants and the all NMOS topology used. However this is of no great consequence to this application as the output is merely required to edge-trigger a following stage. The maximum pulse repetition rate will also be low enough (~1 mS) for this to not create problems.

The new built amplifier's gain is a multiplication of the individual gains of each stage. At the output of the first stage, the signal is out of phase and therefore the output of the second stage is the result of another inverse of the input signal which in return makes the output to the second stage to be in phase with the input signal of the first stage of the two transistor amplifier (Q1 and Q2). Meanwhile the phase input signal on the main input to

the impulse amplifier (from stage one of Q3 transistor) to the output of the second stage M1, the signal remains in phase. A feedback current is taken from the output of Q2 to feed the input of Q1 for DC bias stability.

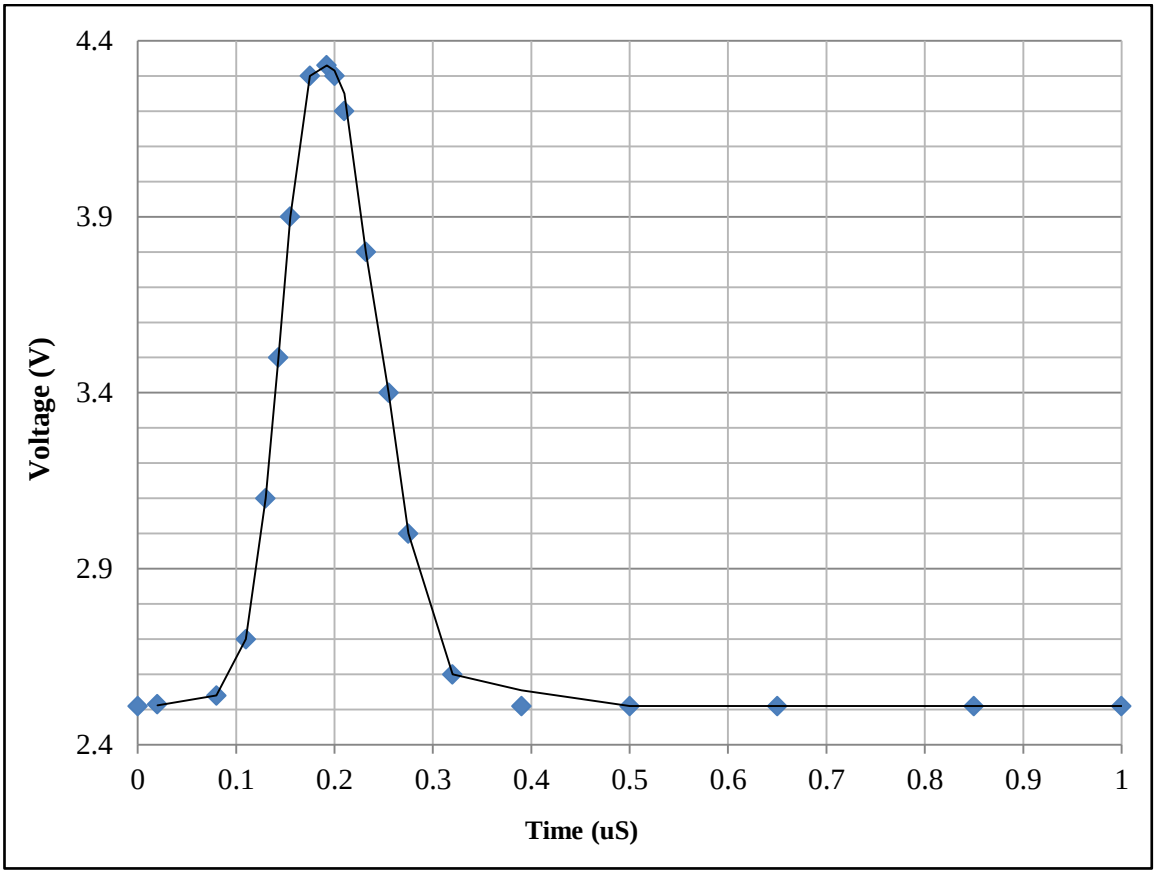

Figure 3.9. OrCad Cadence; simulated pulse amplifier response to an input pulse that is 0.1uS wide and 4.4V peak.

The graph of Figures 3.9 shows the Spice simulation of the amplifier's response with an output step voltage of 4.3V pick at time of 0.2uS, an equivalent pulse is shown in Appendix B3.

The pulse amplifier is clearly the most crucial part of the entire system, as without it, it would be impossible to retrieve the tiny pulses produced by the implant's antenna and

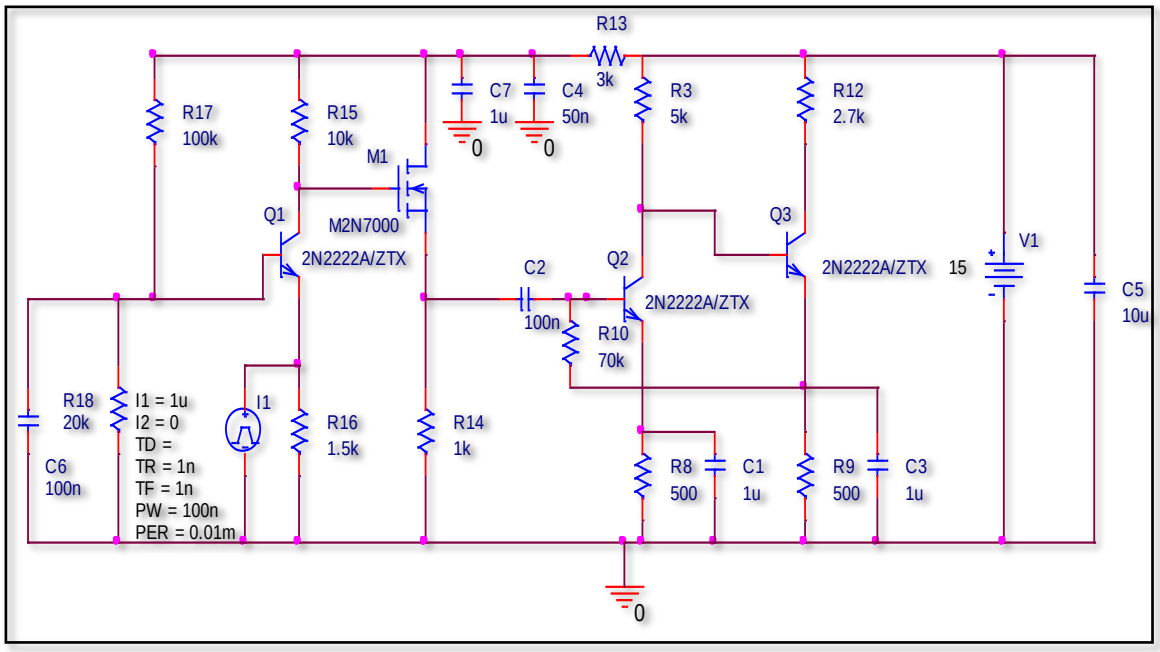

Figure 3.10. Pulse Amplifier schematic: C(1-7): capacitors, I1: input signal, M1: MOSFET transistor, R(1-17): Resistor, Q(1-3): BJT transistors, V1: voltage supply and (0): ground.

Figure 3.10 is a schematic diagram of the design employed here. Three 2N2222 and one NMOS FET 2N7000 discrete devices were chosen for their availability and especially for the relatively large forward trans-conductance of NMOS FET 2N7000. These are directly coupled so that bias levels at each stage are set by the voltage at the final common source stage's load (R13). Q1 is configured as a common-base amplifier (grounded base through a capacitor) giving a low input impedance (r_e) and a high output impedance (R_C), useful as a trans-impedance amplifier; that takes an input current and produces a related output voltage. The current is supplied by the antenna when influenced by an electric field. The output resistance here is very low and equal to (r_e//R_E). At this first stage the amplifier is a non-inverting amplifier, and thus the output of this first stage is in phase with the input signal and its gain is given by (4), where *gm* is the input resistance and *RC* is the output resistance at the collector:

$$AV = g_m R_c = \frac{R_c}{r_e} \qquad (4)$$

The following stage 2 is an NMOS FET 2N7000, as common source follower amplifiers with very high (> 1MΩ) input resistance and inverted phase output with voltage gains given by (5):

$$AV = \frac{-g_m R_L r_{ds}}{R_L + R_{ds} + R_s(1 + g_m r_{ds})} \qquad (5)$$

The last two stages is a Dual BJT amplifier with negative current feedback. With more gain required than that obtained from the previews stage, a three-stage circuit was designed with the last stage implementing a Dual BJT amplifier. Great care was taken to avoid using a coupling capacitor as this limits the low-frequency response of the amplifier, therefore ensuring that the quiescent output voltage of one stage Q2 represents the correct biasing voltage for the next input Q3. The voltage of stage 3 from a Dual-BJT amplifier is given by (6); where the overall gain is equal to the gain of stage 1.

$$A = A_{1^{st}} \qquad (6)$$

The difficulties encountered on designing amplifier to suit the required design was that the amplifier had been producing less gain than expected as well as less perfect DC bias, with small variations. Stability with no oscillation at any point was another concern during the amplifier design. Using the antenna with 1V input, and the aerials put at 1 to 2 cm apart, it was possible to obtain 2mV or 1mV respectively.

When the amplifier was altered with full negative feedback for all AC signals, the gains got allot less than before but the DC bias was perfected as a result of the change. It was still giving 2V at a distance of 1cm apart and 1V at a distance of 2cm apart, and from that point further modification were needed to add more amplification. Furthermore, the Spice simulation in Appendix B3, showed a 15V output for a 1uA input pulse. This was the similar and final design that was laid out with real physical electronic components that later built and tested successfully. It appears that the decay in signal strength is logarithmic and that the amplifier has a gain of somewhere between 5 and 7.5 thousand times, given by (7 - 11).

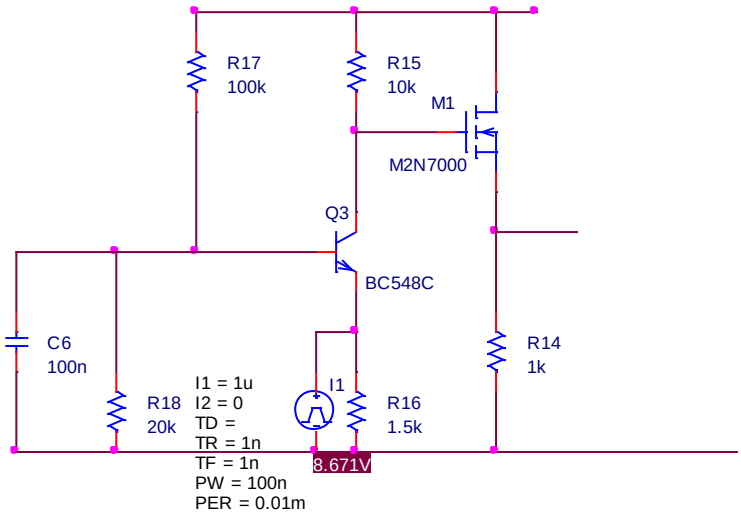

$$V_B = \left(\frac{R_2 V_s}{R_1 + R_2}\right) = \left(\frac{20 \times 8.6}{120}\right) = 1.43V; \tag{7}$$

$$I_2 = \left(\frac{V_B}{R_2}\right) = \left(\frac{1.43V}{20k\Omega}\right) = 71.5uA \Rightarrow I_1 = \left(\frac{V_S - V_B}{R_1}\right) = \left(\frac{8.6V - 1.43V}{100k\Omega}\right) = 72uA \tag{8}$$

$$\Rightarrow V_E = V_B - 0.7V \Rightarrow V_E = 1.43 - 0.7 = 0.73V$$

$$\Rightarrow I_E = \left(\frac{0.73V}{1.5k\Omega}\right) \Rightarrow I_E = 0.486mA = I_C \tag{9}$$

$$\Rightarrow V_R = R_C \times I_C \Rightarrow 500uA \times 10k\Omega = 5 \qquad \Rightarrow V_C = V_{S2} - V_R \Rightarrow 8.6 - 5 = 3.5V$$

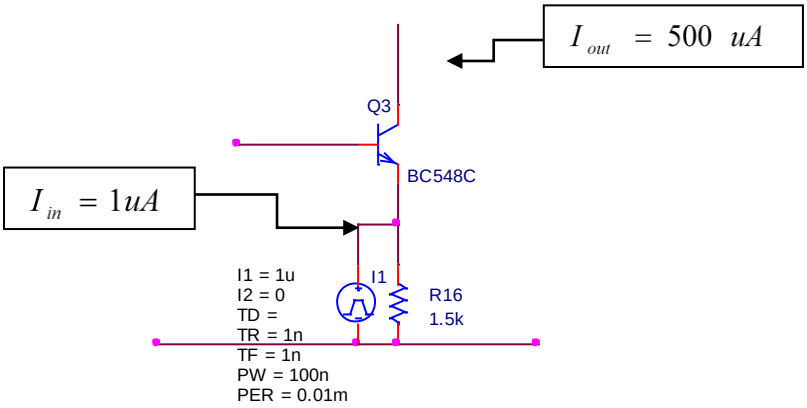

$$I_{in} = 1uA; \; I_{out} = 500uA \; \text{and} \; R_c = 10K\Omega \Rightarrow V_R = 8.7V \tag{10}$$

$$Gain = \left(\frac{I_{out}}{I_{in}}\right) = \left(\frac{500uA}{1uA}\right) \Rightarrow 500. \tag{11}$$

If $Gain = \left(\frac{I_C R_C}{I_E r_{in}}\right) \Rightarrow \left(\frac{V_R}{V_{in}}\right) = \left(\frac{5V}{0.486mA \times r_{in}}\right) \Rightarrow r_{in} = \left(\frac{5V}{0.486mA \times 500}\right) \Rightarrow r_{in} = 20\Omega$

$\Rightarrow V_{in} = I_{in} \times R_E \Rightarrow V_{in} = 1uA \times 1.5k\Omega \Rightarrow V_{in} = 1.5mV.$ This gives Volt output of $V_{out} = 3.5V$

The first stage (Q3) of this impulse amplifier, was designed so that the emitter terminal of the transistor in this circuit serves as the input, the collector the output, and the base as common by using a large capacitor C6, Figure 3.10, this design method because of its input capacitance does not suffer from the Miller effect, which degrades the bandwidth of the common-emitter configuration, and because of the relatively high isolation between the input and output, this high isolation means that there is little feedback from the output back to the input, leading to high stability (Rouf, 2009).

3.4.2.3. System Operation

Having built the implant-microcontroller or transmitter microcontroller based system, and then a programming code was developed to transmit a byte from the receiver-microcontroller circuit using a single wire monopole antenna to transmit data to trigger the transmitter-microcontroller. With the written code for the receiver to reject any pulses that arrive with a time difference more than 10% of 1mS. This circuit configuration as a transceiver selecting analogue input from the comparator's Vref as low as able, to detect data signal from the on the transmitting antenna placed 1cm or more away. A Part of the written code of the circuit that detects an incoming signal has been enclosed in the Appendix D.

The microcontroller will initially turn off all unneeded built-in functions and enable external interrupts from the I/O pin connected to the monopole and from its Watchdog timer. It will then go into a low power 'sleep' mode. When woken periodically by the Watchdog timer, it will sample the sensor (eg. Temperature sensor), using the built-in ADC and store the sampled value in the internal EEPROM before returning to 'sleep'. The Reader can request a data dump from the implant microcontroller at any time by transmitting a large pulse when positioned close to the implant's antenna. The voltage coupled to the microcontroller pin will wake the device from sleep and it will execute a serial dump of the entire EEPROM's contents.

In order to transmit the data, the I/O pin connected to the antenna is reconfigured in software to act as an output and the data is transmitted one byte (8 bits) at a time by using

a digit plus a delay value of 4mS per cycle added to it and a pre-set inter-byte gap of silence of 4mS, Table 3.2.

Table 3.2. Transmission speed per byte

Data	Interval	Digit (0)	Digit (1)	Digit (2)	Digit (3)	----	Digit (9)
Time Delay	4ms	4ms	9ms	14ms	19ms		49ms
Speed	-----	125B/s	77B/s	56B/s	43B/s		19 B/s

Table 3.2 show the transmission delay varies from 4ms to 49 ms, depending on the number sent and to this is added 4 mS time delay to separate the bytes. Sending the lowest number is done with a minimum time of 4ms plus a delay interval of 4ms, which gives a transmission speed of 125 cps, whilst sending number 9 reduces transmission speed to 19 cps. Another calculation, limiting transmission to the use of 0s and 1s only, results in time delays of 4 ms and 9 ms respectively and a maximum transmission speed of 77 cps.

The process of reading the data, from the Clock-Less Pulsed RF based transmitter microcontroller transmitter and reader microcontroller transceiver systems interfaced to a PC, could be presented in four stages; first: Capturing the input data from the sensor (eg. temperature) to the implant microcontroller and then transmit; second: Amplification of the transmitted signal received by the pulse amplifier within the external system, third: Data decoding of the amplified signal with the external microcontroller which locks onto the amplified pulses and counts their respective lengths in order to recover the data values sent; and fourth: Output decoded data and display on a PC with a Visual Basic client. In other words, the received values are sent by RS232 to a PC for further processing before display on a moving timeline graph.

3.4.3. Clock-less pulsed RF transmitter implant experiments

The pulse amplifier designed and simulated in PSPICE presented on previous section, and the associated electronics were assembled on PCB in the Lab as shown in Figure 3.11 and in Appendix B.

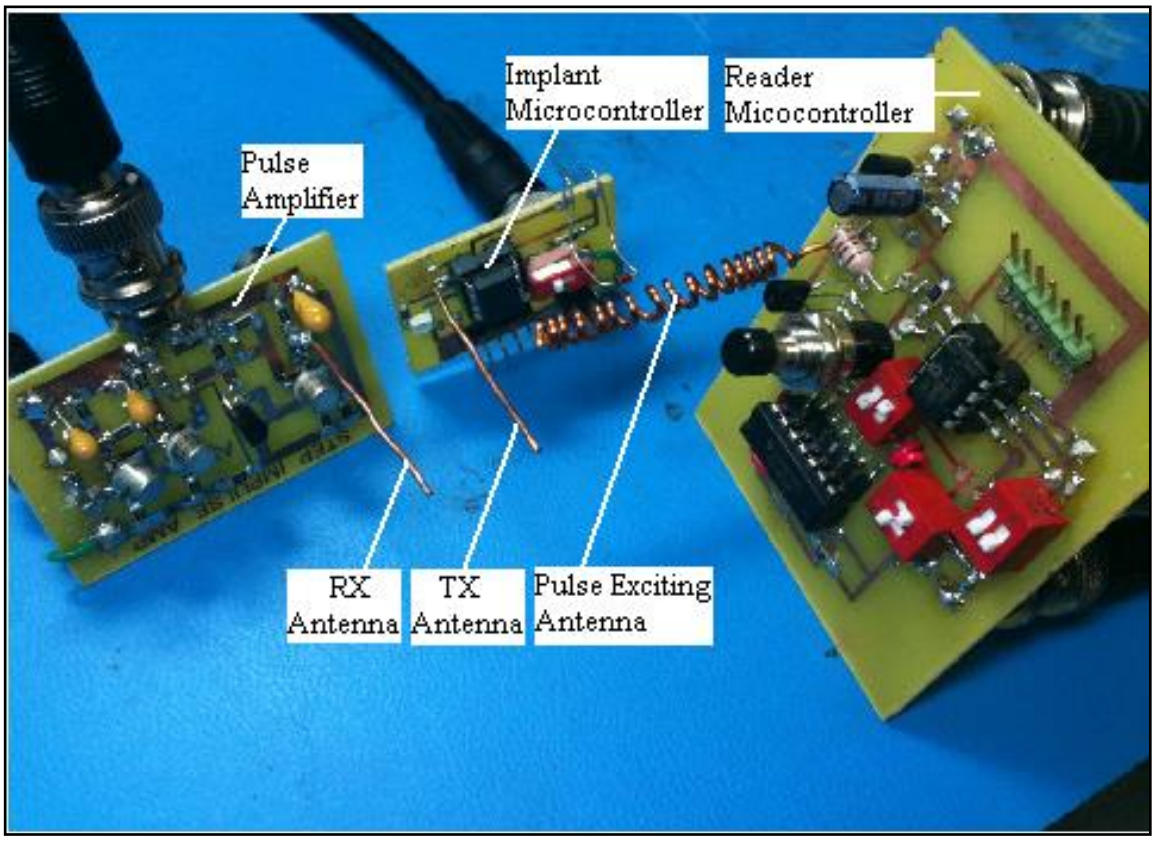

Figure 3.11. Photograph of the implant transmitter prototype.

The transmission experiment relating to distance were carried out using a 2V supply for the implantable microcontroller circuit and antennas with 18mm and then 32mm lengths placed from 1.5 to 2.5 cm apart, sandwiching a lump of fresh pork gristle to emulate human skin and fat. It can be noted in Figure 3.12, show the longer antenna contributes an extra 0.5 mV of signal over the lengths measured, which translates into an overall distance increase of +2cm, shown in Figure 3.13, when compared with the 18 mm antenna. The gain of the system is obtained by dividing the amplitudes in Figure 3.13 by those in Figure 3.12 and this agrees quite well with simulated gains of around 5000x (e.g. at 2cm, $A_V = 2.5/0.0005 = 5000$).

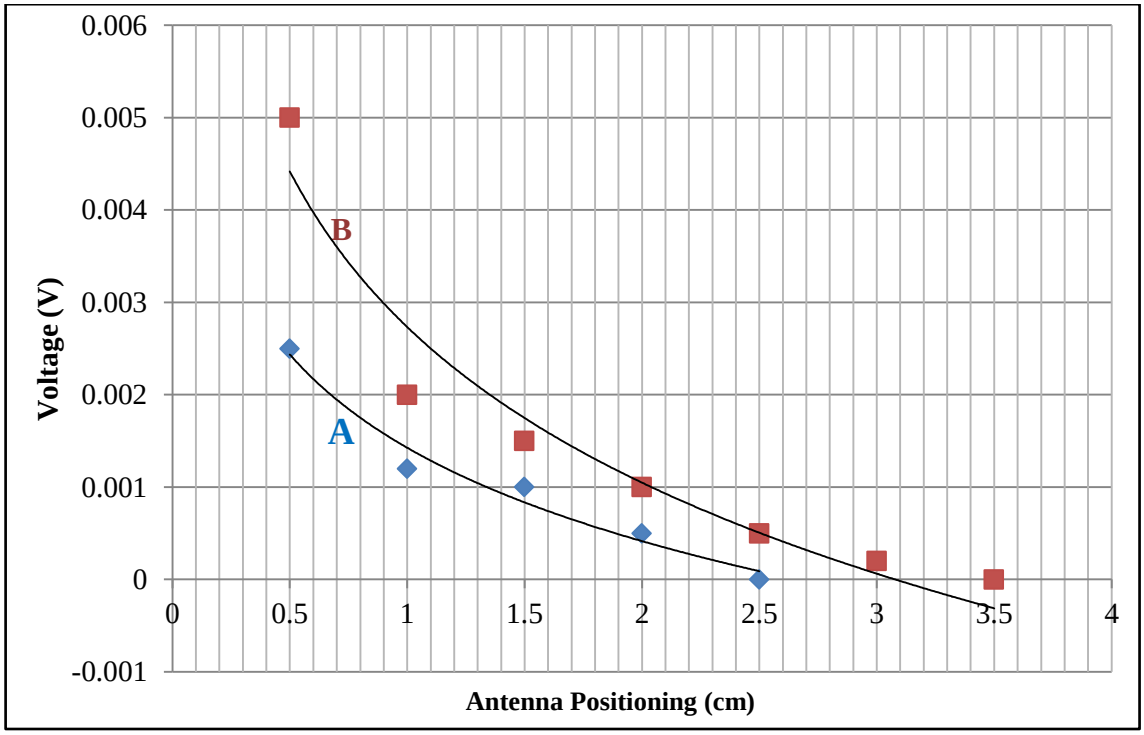

Figure 3.12. Single-wire induced in receiving monopole vs. separation distance over unamplified peak voltage with; (A) 18 mm wire length and (B) 32 mm wire length.

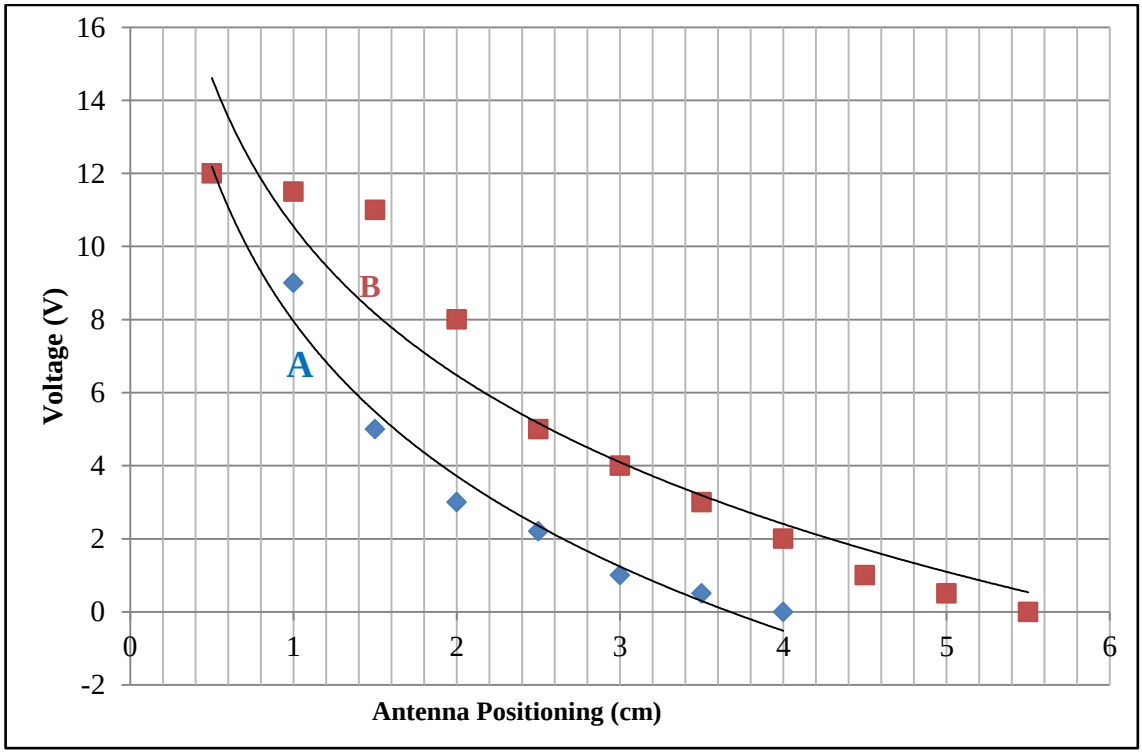

Figure 3.13. Single-wire induced in receiving monopole vs. separation distance over amplified peak voltage with; (A) 18 mm wire length and (B) 32 mm wire length.

Table 3.3. Power consumption at two different frequencies (power/byte)

Clock Speed	Voltage in (v)	Current (mA)	Power(mW)	Distance (cm)
8MHz	4	1.5	6	3.5
8MHz	2	0.635	1.27	1.5
31KHz	2	0.208	0.42	1.5
31KHz	1.9	0.17	0.32	1.5
31KHz	1.85	0.165	0.31	1.5

Table 3.3 lists power consumption values at various microcontroller clock frequencies employed during testing, and this shows that at 8 MHz, with a 2V supply, the circuit consumes 1.27 mW dropping to just 420 µW when clocked at 31 kHz. A second experiment was carried out, keeping the supply at 2V whilst clocking at 31 kHz, to test data transmission. The amplifier supply was set to 12.66V which resulted in a current consumption of 8 mA in the receiver circuit (~100 mW) and 18 mm TX and RX antennas were placed 1.5 cm apart for the test. A series of numbers were transmitted successfully over the link and details of the times taken are shown previously in Table 3.2. The setup performed well, with no error, until the supply voltage was dropped to 1.7 V and data corruption began to take place due to the microcontroller being powered below its recommended minimum voltage supply (2V). Furthermore, the effect of keeping the antenna's distance the same but changing the angels of the antennas does not affect the response.

3.4.3.1. Simulation of temperature sensor system

With satisfactory amplifier design, the transmitter microcontroller circuit using PIC10F222 with a temperature sensor was setup to carry out temperature readings for system's validations. An antenna was connected to the input pin that goes to the built-in comparator, to be used for both analogue input (when listening) and digital output (when transmitting). A MCP9700 thermistor (temperature sensor) was connected to the PIC10F222's ADC, to read ambient temperatures.

The working power consumption of the microcontroller was crucial to emulate the implant solution desired to obtaining low power functionality, therefore this experiment gave an insight to choices of programming codes as well as internal functions required to

be set for optimum low power design. The power consumption measurements results of the PIC10F222 are shown in Table 3.4 and the corresponding figure 3.14. Pico-ammeter and logic analysers were used to monitor the circuit performance and the gathering of data.

Table 3.4: Microcontroller (PIC10F222) Power Characteristics.

Clock Frequency (KHz)	Current Consumption - mA (@ 2V INPUT)
8000	0.422
4000	0.26
2000	0.19
1000	0.15
500	0.13
250	0.12
125	0.12
31	0.011

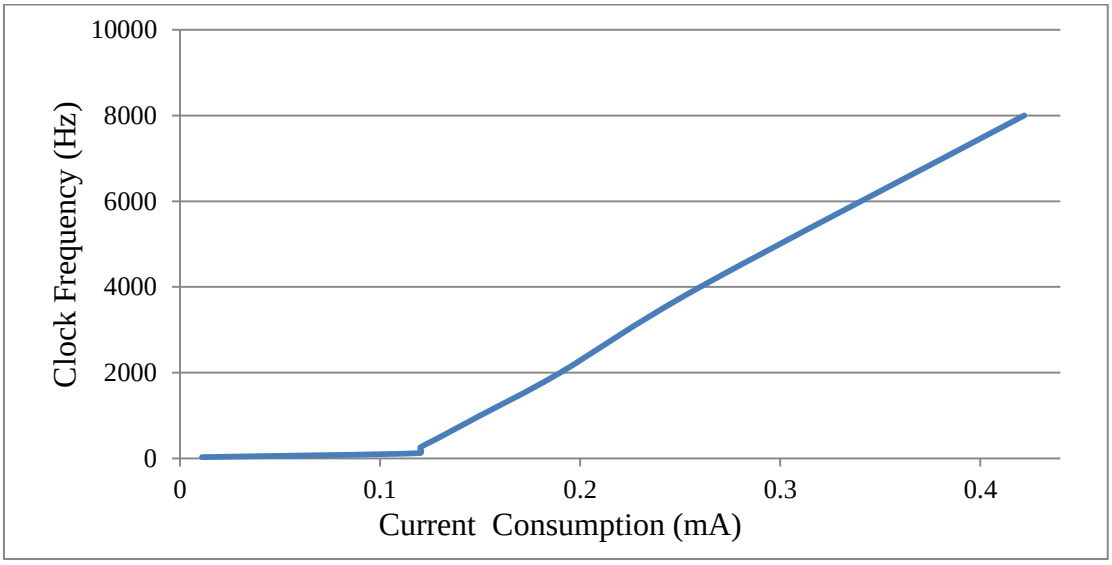

Figure 3.14. Microcontroller (PIC10F222) current consumption

With the data obtained during this experiment, the graphical data above satisfies the use of the PIC microcontroller and makes it a good candidate to emulate the desired bio-implant functions to be built. The PIC microcontroller has a technology that can provide low power consumption, a method that can and will be reassigned to a more improved device by using CMOS technology, while eliminating other function blocks contained in the microcontroller that are usually not used during on the final system.

The receiver microcontroller was also built using PIC16F819, in which the amplifier was connected to its internal comparator, in addition was a FET transistor, resonator (LC

tank) and an extra antenna connected to the same reader microcontroller, and was used to transmit a strong pulse (over 50V) to wake the implant microcontroller. The resonator was built and modified several times in such a way to be possible to drive a 40 KHz at 50% duty cycle (rather than 250 KHz at 90% duty cycle) to wake the implant microcontroller. And a third pin was configured so that the reader microcontroller can perform RS232 output to a PC.

The temperature sensor used was the MCP9700 thermistor connected to the implant microcontroller. The temperature test results are tabulated and graphed on Figure 3.15.

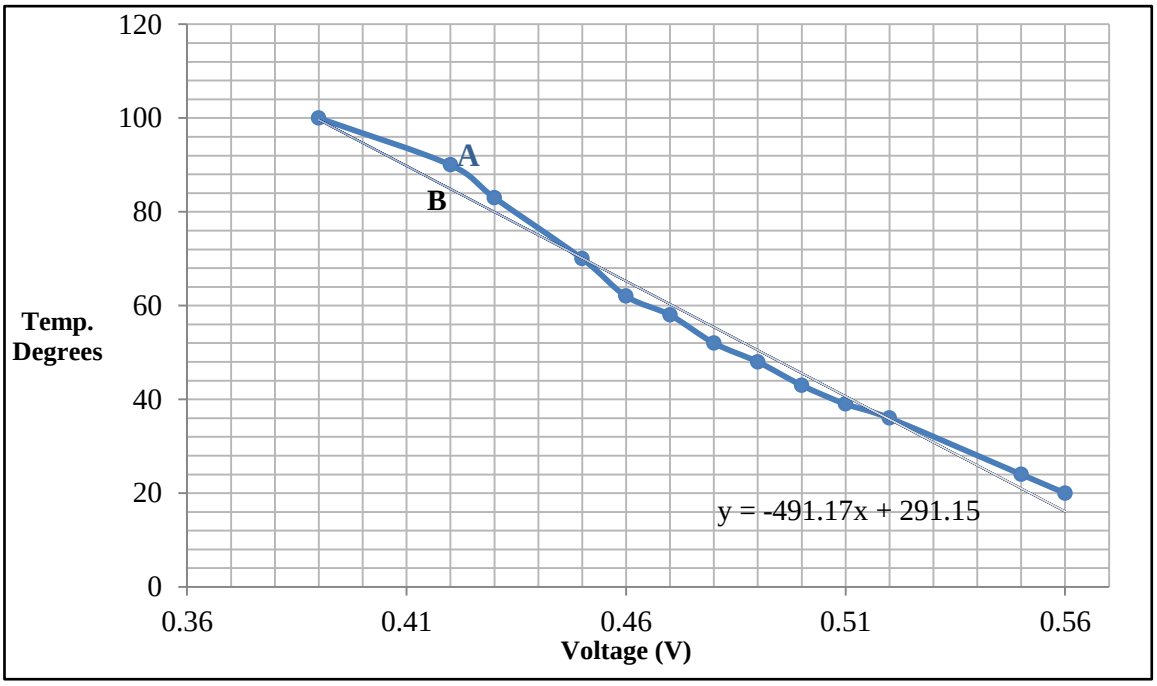

Figure 3.15. MCP9700 Thermistor (Sensor) average temperature responses vs voltage responses; (A) Actual sensor readings (at 5x resolution), (B) linear temperature description.

The transmitter presented is simple, low power, carrier free and cheap to implement using widely available components. It is capable of transmitting digital information at low voltage (2 V) over short distances (< 5 cm) with a power consumption of < 0.5 mW with a maximum speed of 125 cps. The antenna used can be as short as 18 mm in length and is easily integrated into an implant. Subcutaneous operation is safe due to the negligible power of the pulses created. Potential applications would include a variety of embedded solutions for general purpose monitoring, where software modifications could be made to support additional protocols and improve patient data privacy.

Chapter 4

Results and Discussions

4.1. GFC Design Results and Discussion

4.1.1. Morphology and composition of PtVCC

To confirm the morphology and composition comprising the PtVCC catalytic electrode, sample surface analysis and characterisation tests were carried out using electron scanning microscopy (SEM) in combination with Energy-dispersive X-ray spectroscopy (EDS) shown in Figures 4.1, 4.2 and 4.3; these results are part of my work from using the SEM machine.

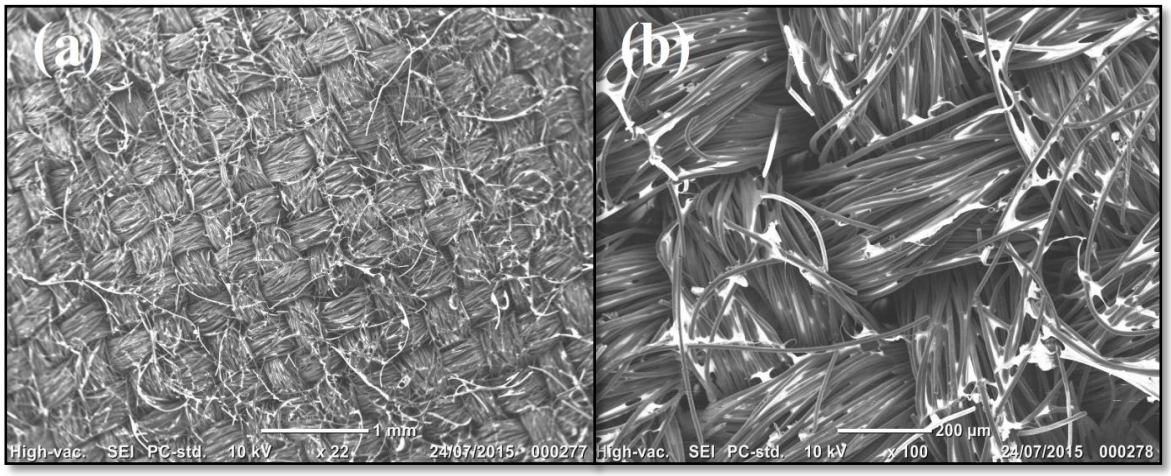

Figure 4.1. SEM images of the 0.3 mg/cm² 40% PtVCC Electrode, images zoomed at (a) 1mm, (b) 200µm.

There are several choices of PtVCC materials that have been developed with different physical proprieties of materials compositions. Figure 4.1 illustrate the detailed arrangement of PtVCC not easily seen by the naked eye, which has been optimised for diverse operating parameters and physical properties, features include:

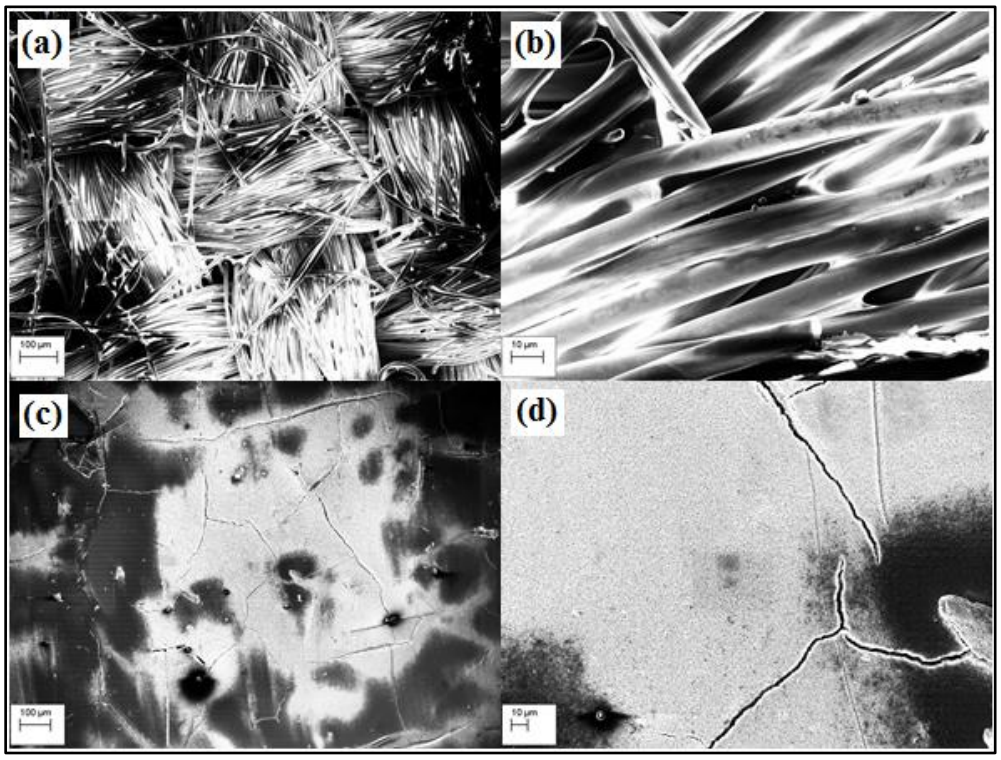

Figure 4.2. SEM/EDS images of the 0.3 mg/cm² 40% PtVCC electrode, (a) non-catalytic side (100µm scale), (b) non- catalytic side (10µm scale), (c) catalytic side (100µm scale), (d) catalytic side (10µm scale)

The SEM images of Figure 4.2 presents the different morphology seen between the two sides of the PtVCC electrode (a, and b) shows one side of PtVCC electrode consisting of woven carbon fibre cloth at different magnification respectively. The other side of the same electrode in (b, and c), are coated with platinum nanoparticles stabilised by Nafion, further supporting information by SEM/EDS are shown in Figure 4.2 (a), (b), (c) and Table 4.1, while FTIR information are obtained from (d) and shown in Table 4.2.

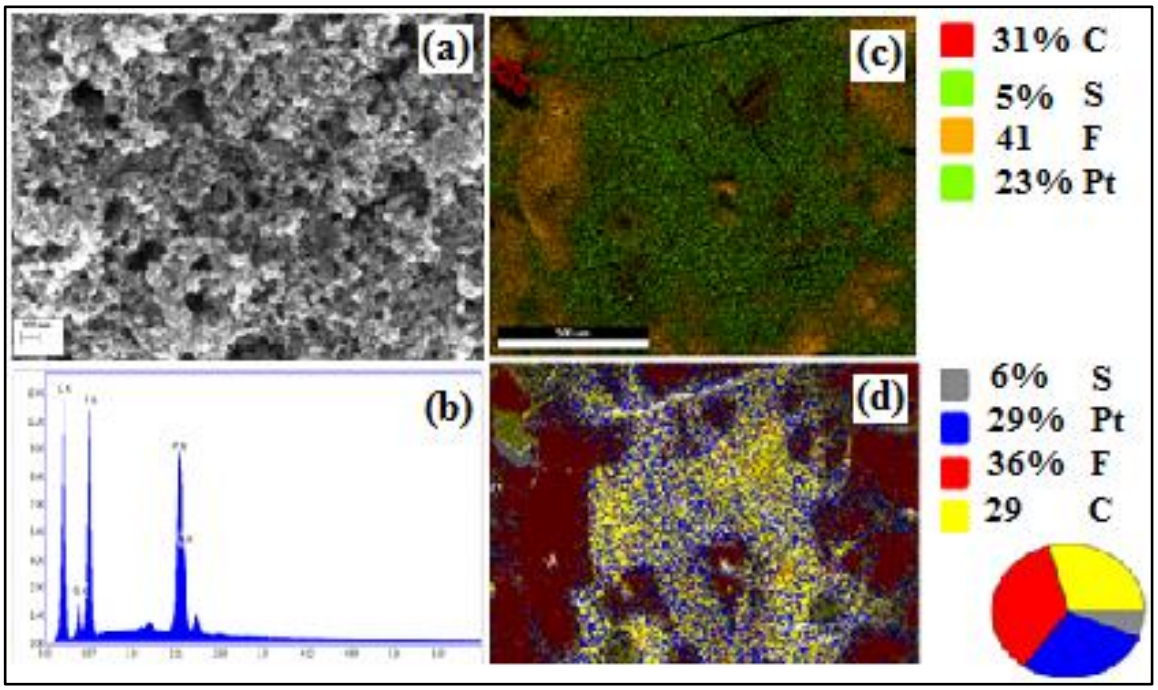

Figure 4.3. A close-up SEM/EDS image of 0.3 mg/cm² 40% Pt-VCC electrode on catalytic side (a): visible Pt nanoparticles (200nm scale), (b): spectrum of PtVCC elements detection and analysis containing high volumes of C, F, S, and Pt presence, (c): elements overlay with C (31% red), Pt (23% Green), F (41% Orange) and S (5% light green), (d): elements mapping with C (29% yellow), Pt (29% blue), F (36% red) and S (6% grey)

Figure 4.3 (b) shows a typical spectrum of a large amount of carbon, fluoride and platinum elements, with small trace of sulphur peaks at a local surface area of PtVCC. The corresponding quantitative results from the spectrum graph are shown in Table 4.1.

Table 4.1. EDS weigh % of possible constituents present on PtVCC electrode surface.

Element	Weight %	Atomic %	Net Intensity	Error %	K-Ratio
C	35.87	66.33	545.00	7.30	0.2248
S	3.94	5.47	66.20	9.71	0.0174
F	20.24	23.66	521.30	7.47	0.1102
Pt	39.96	4.55	468.10	4.52	0.3041

Figure 4.3 (b) and Table 4.1, are the results of SEM/EDS analysis of PtVCC electrode, with no other constituents present on the graph other than the PtVCC elements being detected on EDS analysis, and thus the weight and ratio % reflected only the expected PtVCC element.

Further EDS 2-D mapping results are shown on Figure 4.3 (c), overplaying the four elements, clearly distinguishing between platinum nanoparticles distribution on PtVCC catalysed surface. Figure 4.3 (d) shows the EDS mapping spectrum of detected elements on PtVCC, especially Pt in abundant quantity around 29%, the same quantity as the carbon elements. Since this catalytic side is coated with Nafion ($C_7HF_{13}O_5S.\ C_2F_4$), as a result, large amounts of fluoride elements are present, circa 36%, while the remaining 6% are sulphur elements.

Figures 4.3 (c and d) samples were captured from the same location, the difference in percentage between their elements are due to the fact that mapping percentage results were taken after long periods of sampling, which provided a more representative result over time.

Further tests were carried out to highlight the presence of sulphur element (S) expected in nafion layer (Pan, 2008), embedded within catalytic side of PtVCC electrode, by carrying out FTIR spectroscopy of nafion. More than 15 consistent spectra measurements were collected on Jasco FTIR-4200 equipment.

The assignment of the infrared (IR) absorption bands in Table 4.2 of IR spectra and analysis of peak corresponding to the presence of nafion on PtVCC catalytic side, were based on the already published data (Liang, 2004). PtVCC electrodes were pressured equally in all FTIR measurements to avoid the differences that may be caused by the pressure and penetrating depth.

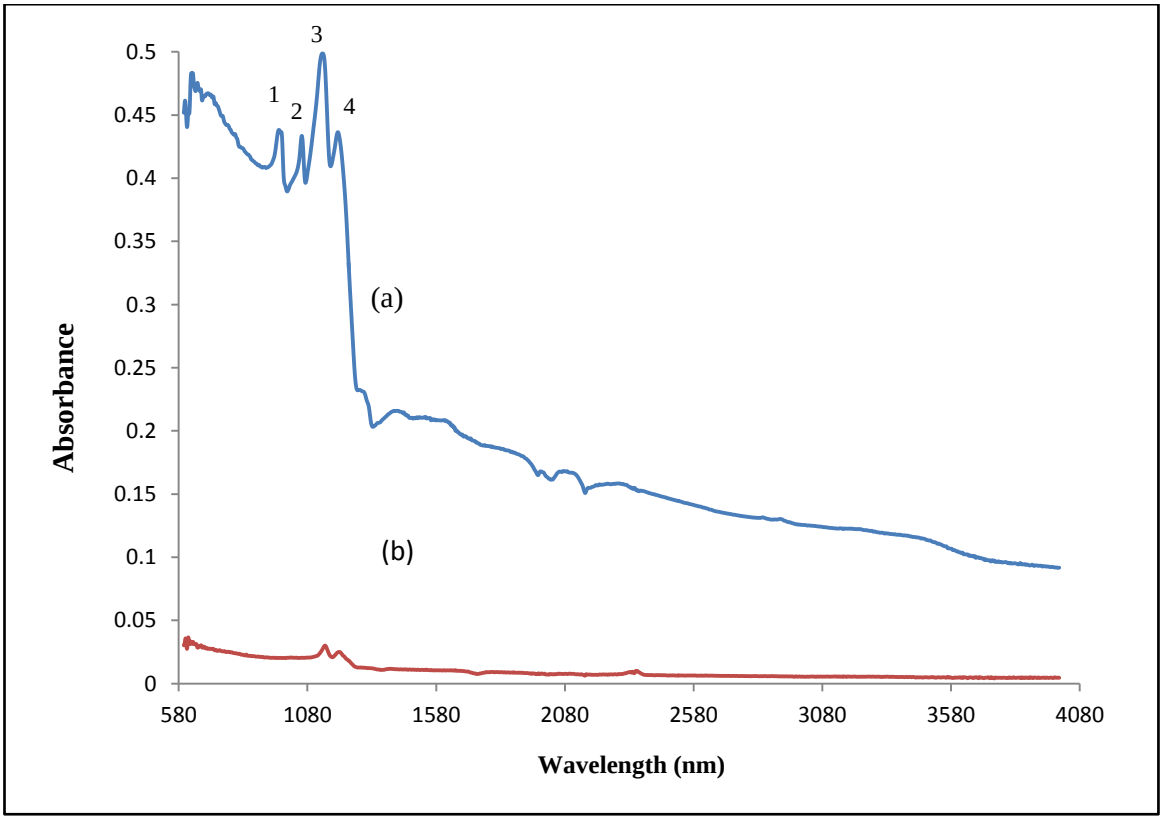

Figure 4.4. Infrared spectra of PtVCC electrode on (a): catalytic side containing peaks of nafion elements, (b): non-catalytic side and non-nafion presence

Table 4.2. Particular nafion infrared absorption bands

CF_2	CF_2	S–O	C–F	C–O–C	
~1200	~1100	~1060	~980	~960	(Liang, 2004)
1200	1138	1055	970	970	This Work

The absorption peaks on catalytic side of PtVCC electrode in Figure 4.4 (a); peaks 1, 2, 3 and 4 are 970, 1055, 1138 and 1200 respectively, corresponds to vibration absorption of typical chemical bonds; F-C-F, S-O, C-F and C-O-C in Table 4.2, agreement with those in Nafion ($C_7HF_{13}O_5S\cdot C_2F_4$) membrane. While Figure 4.4 (b) of non-catalytic, non-nafion side PtVCC, shows a response with negligible peak amplitudes around 1148 and 1204, which can be equated to small presence of CF_2, that may be produced by the pressure and penetrating depth on the carbon cloth. In combination to both EDS and FTIR analysis, it is therefore confirmed that Nafion is applied as binder for stabilising the Pt nanoparticles. Nafion has been demonstrated as binder for improving adhesion between Pt nanoparticles and the carbon cloth, as well as enhancing the proton

conductivity at the interface between Pt nanoparticles and Nafion membrane electrolyte (Khan, 2010; Cunci, 2014 and Chlistunoff , 2014).

4.1.2. Electrochemical tests results of Pt and PtVCC electrode materials

Initially, cyclic voltammetry (CV) test measurement of plain platinum sheet and PtVCC materials were carried out to study the electrochemical signal transduction ability of these electrodes 4mM Potassium ferricyanide $K_3[Fe(CN)_6]$/KCl and 5mM glucose PBS (pH 7.4) solutions discretely. Similarly, Current vs. Potential tests (I/E measurements) were made using dynamic scans where data is registered in steps equivalent to the actual resolution on a wide variety of scales from a range of -0.8 V to 0.8 V.

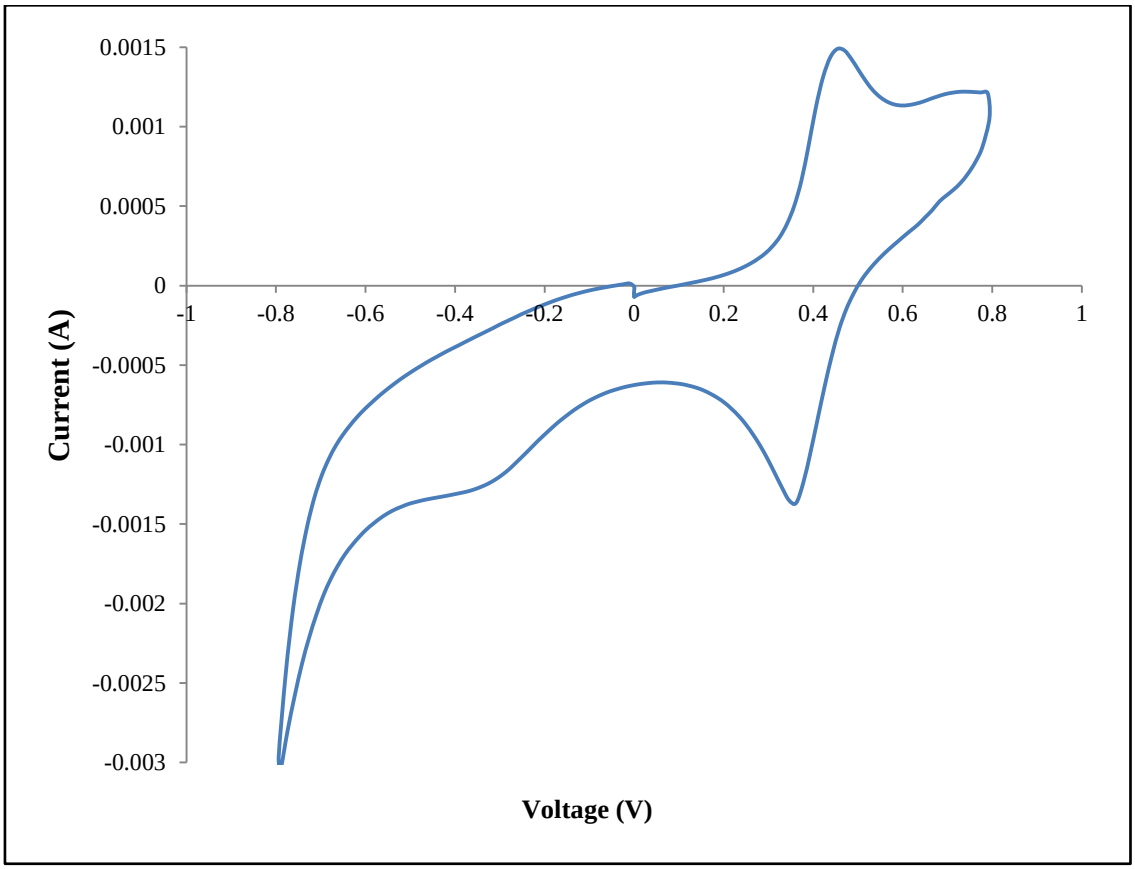

Figure 4.5. Cyclic voltammetry responses of platinum sheet electrodes obtained from 4mM potassium ferricyanide in 0.1 KCl with a scan rate of 50 mV/s

The graph in Figure 4.5 shows the expected peaks of a redox reaction from plain platinum electrode, where i_{pc} and i_{pa} cathodic and anodic current peaks of a reversible reaction, respectively, are displayed.

4.1.2.1. CV tests of Pt and PtVCC in potassium ferricyanide solution

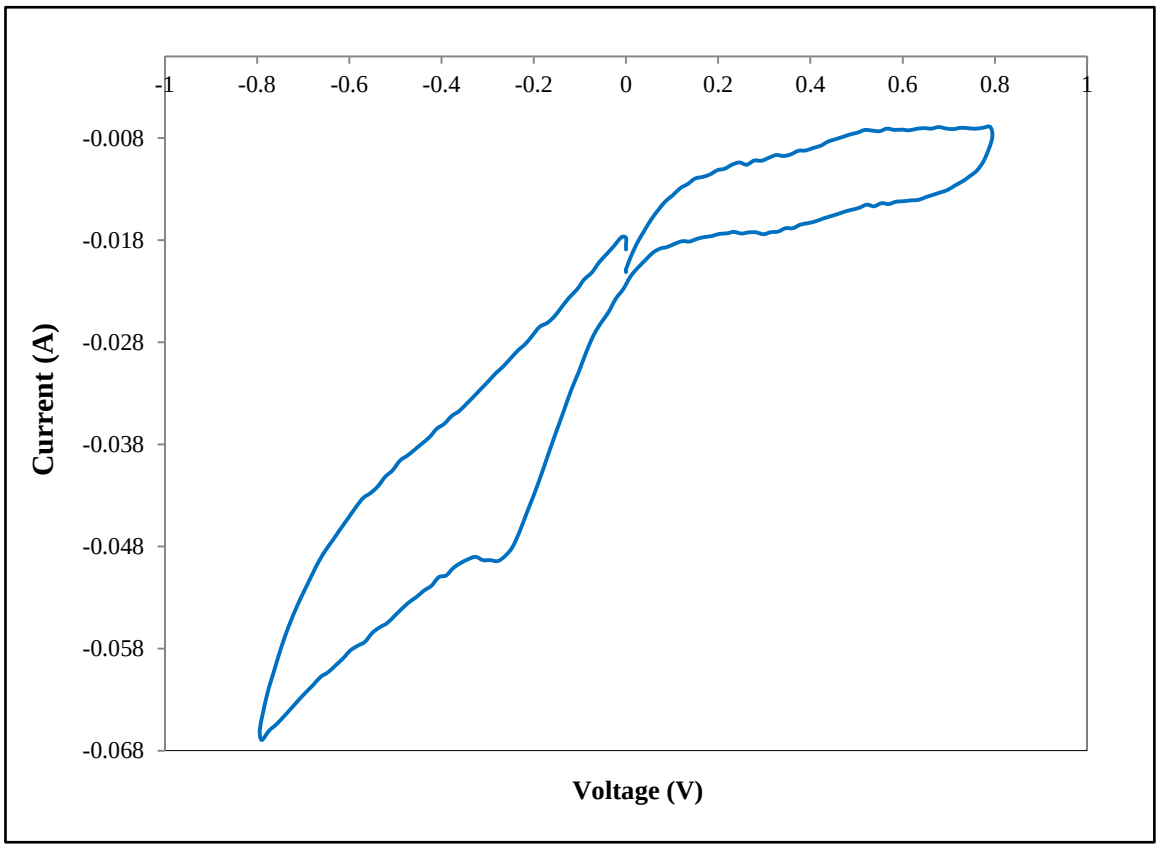

Figure 4.6. Cyclic voltammetry responses of PtVCC electrodes obtained from 4mM potassium ferricyanide in 0.1 KCl with a scan rate of 50mV/s

Figure 4.6, based on a PtVCC electrode, shows very minor cathodic current peaks with a more visible anodic current peak of a marginal redox reaction in Potassium ferricyanide $K_3[Fe(CN)_6]$ solution.

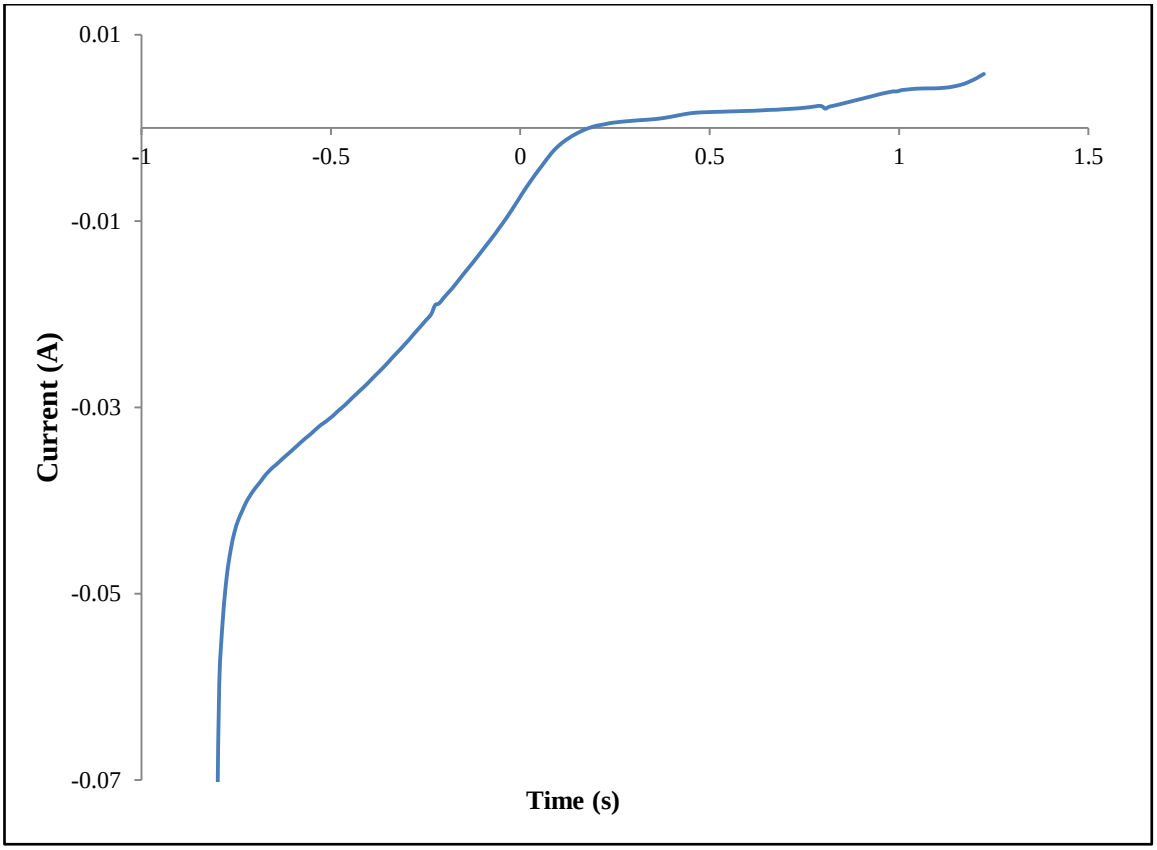

Figure 4.7. Current vs. Potential tests (I/E) - responses obtained from 4mM potassium ferricyanide in 0.1 KCl of PtVCC

The curve shown in Figure 4.7 is the result of PtVCC electrodes tested in potassium ferricyanide solution. The applied voltage ranging from -0.8 V to +0.8 V produced a positive current response of more than 2.3 mA. The maximum current value was obtained when the positive potential reached 0.8 V, whereas the current at negative polarity, where the potentials reached close to -0.8 V, was < -74 mA, hence PtVCC provides better electron conductivity than plain platinum electrode or other plain metals tested in this solution.

4.1.2.2. CV test of Pt and PtVCC in glucose solution

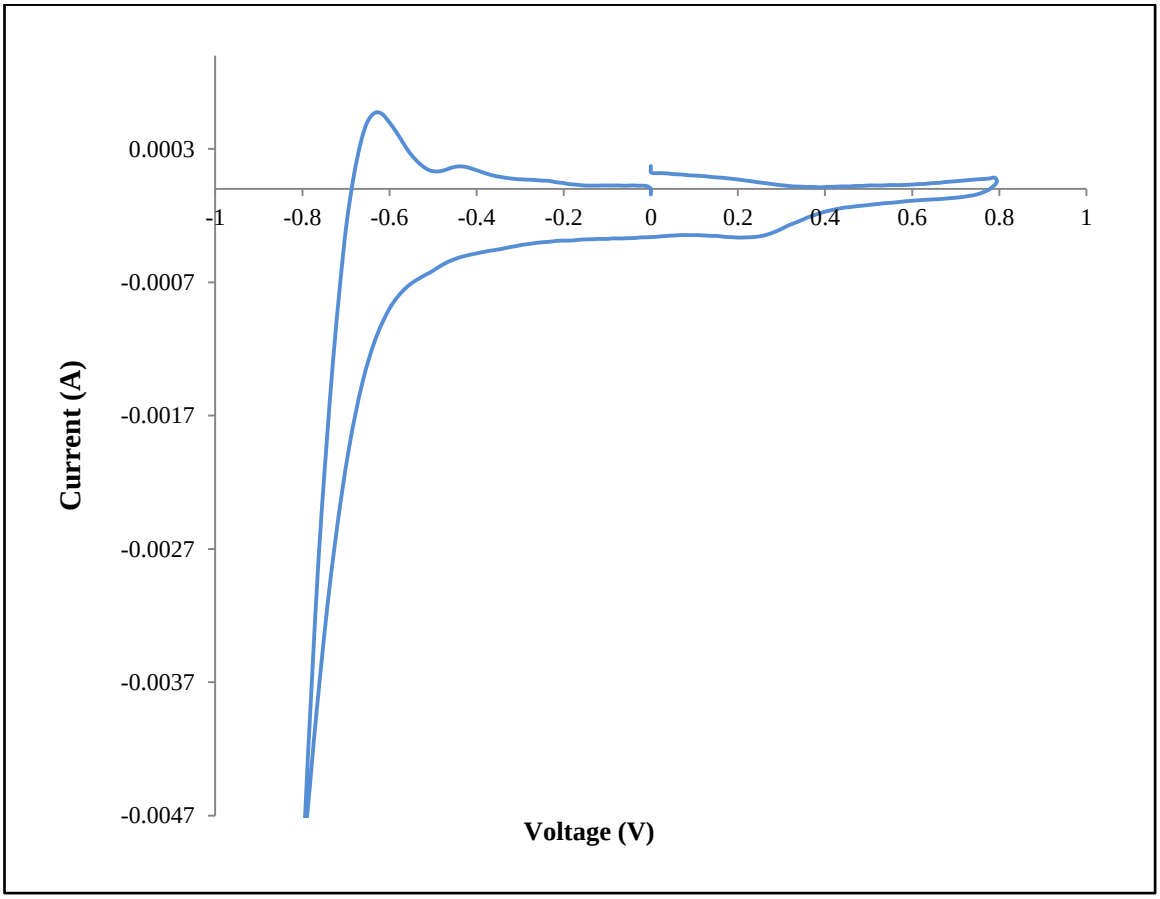

Figure 4.8. Cyclic voltammetry responses of platinum electrodes obtained from 5mM glucose (pH 7.4) with a scan rate of 50mV/s.

The results in Figure 4.8 confirms the electron transfer and catalytic activities of PtVCC and plain platinum sheet electrodes in glucose solution, where (a) displays small cathodic 0.5 mA and anodic -0.33mA peak currents at -0.65v and -0.28v potentials respectively. While PtVCC electrode in Figure 4.9 is obtained with greater cathodic and anodic peak currents of 8.27mA and -14 mA at 0.55v and -0.31v potentials respectively for a reversible reaction in glucose solution. The plain platinum electrode exhibited limited redox reaction in glucose solution, but the PtVCC electrode with its micro-porous nature, in combination with platinum nanoparticles, this oxidises glucose better than pure metals, so the current peaks are indicative of the higher capacity and better electrochemical properties of this electrode for electro transfer activities. Though the forward and reverse peak potentials of PVCC are much higher than Pt electrode, suggesting the PVCC requiring more energy than Pt does to oxidise the same solution, PVCC electrode peak

current density are also much higher than Pt electrode, which is directly proportional to the amount of glucose oxidised.

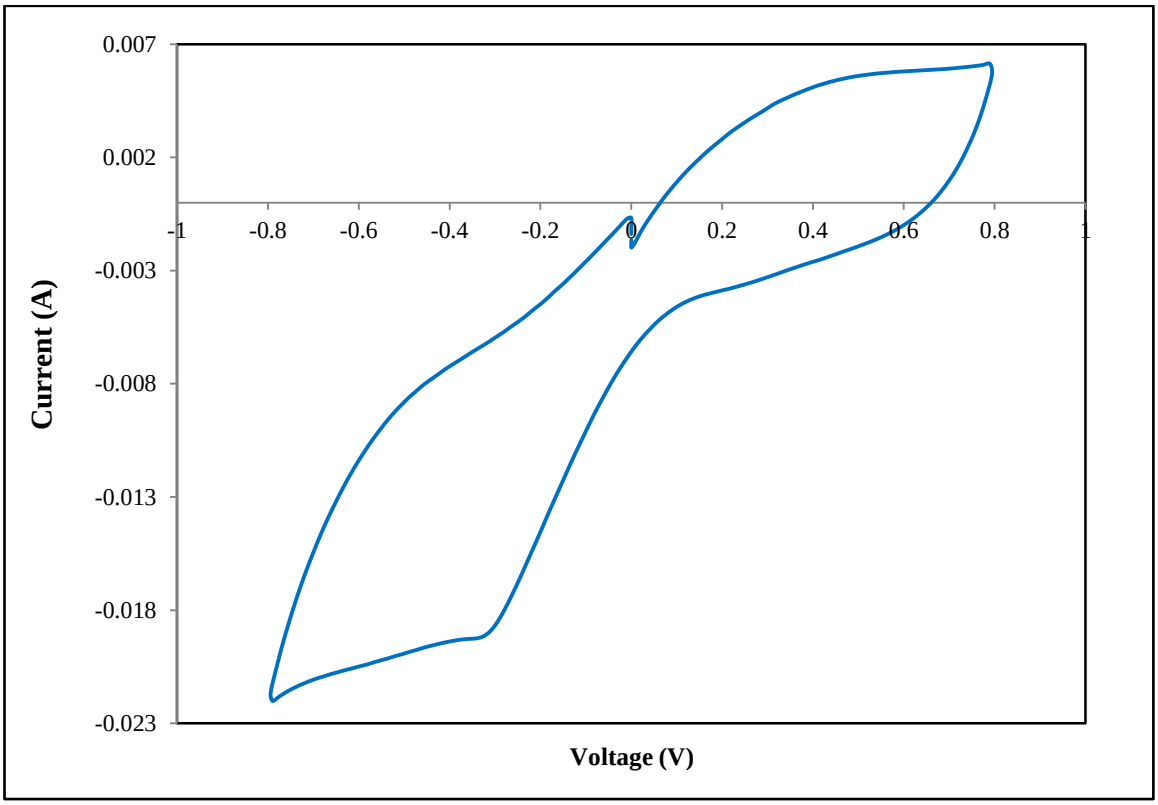

Figure 4.9. Cyclic voltammetry responses of PtVCC electrodes obtained from 5mM glucose (pH 7.4) with a scan rate of 50mV/s

Figures 4.7 and 4.9 show the polarization curves illustrating the electrical properties, catalytic and conductivity properties of plain platinum sheet and PtVCC electrodes obtained from potassium Ferricyanide and glucose solutions separately.

The CV experiments were carried out using a scan rate of 50mV/S and it was noted that the redox reactions peaks of PtVCC in glucose solution could increase with increasing scan rate. And the plots in Figure 4.9 have the expected i_{pc} and i_{pa}, peak cathodic (reduction) and anodic (oxidation) currents respectively, for a reversible reaction. The recorded CV test of PtVCC in glucose solution meets the well-defined characteristics of a reversible electrochemical reaction by displaying a voltage separation between current peaks where the positions of peak voltage did not alter as a function of voltage scan rate and the ratio of the peak currents can be calculated to be greater than one ($i$pa / $i$pc = 1.7) and are proportional to the square root of the scan rate, and the resulted electro-active surface area of PtVCC in glucose solution is 18 times greater than the apparent area.

By analysing the variation of peak potentials (E_{pc}, E_{pa}) and peak currents (i_{pc}, i_{pa}) of the cathodic and anodic peaks respectively, directly as a function of scan rate from the plot of Figure 4.9, it is possible to estimate the electron transfer rate constants, and calculate I_{pa}/I_{pc}, ΔE (potential difference) and the electro-active area were calculated, as shown in Table 4.3.

The CV experimental tests of both Pt and PtVCC electrode in 5 mM glucose solution were carried out using scan rate of 50mV/S. Compared to Pt electrode, PtVCC electrode showed much more profound reduction and oxidation of glucose solution in the reverse scan, compared to Pt electrode, indicating higher electrocatalitic activity of PtVCC electrode in glucose solution.

The obtained redox reaction of PtVCC electrodes in glucose solution in Figure 4.9 show its electron transfer and catalytic activities being greater than in Figure 4.8 the plain platinum electrode material in the same glucose solution, and the resulted electro-active surface area of PtVCC electrode is > 2.43, acting as an electrode material with good electron transfer and catalytic activities in glucose solution.

Table 4.3. Electrochemical properties of Pt and PtVCC electrodes based on the cyclic voltammetry results

Electrode	Solution	Ipa (mA/ cm^2)	Ipc (mA/ cm^2)	Ipa/Ipc (mA/ cm^2)	E_{pa} (V)	E_{pc} (V)	ΔE (V)	Apparent Area (cm^2)	Active Area (cm^2)
Platinum	Potassi. Ferricy.	1.3	1.45	0.95	370	450	80	0.84	1.6
PtVCC	Glucose	-14	8.27	1.7	-310	550	-860	1	18

The electro-active surface area is calculated from the Randles-Sevcik equation (12) using cyclic voltammetry results:

$$\text{Ipa} = 2.69 \times 10^5 \times A \times \sqrt[2]{D} \times \sqrt[2]{N^3} \times \sqrt[2]{\gamma} \times C \qquad (12)$$

Where Ipa is the anodic peak current, A represents the electro-active surface area (cm^2), D is the diffusion coefficient of the molecule in solution ($6.7x10^{-6}$ cm^2s^{-1}), N is the number of electrons participating in the redox reaction, which is equal to 1, γ is the scan rate ($50mV^{-1}$) and C is the concentration of probe molecules in solution = 5 mM.

The calculated electro-active surface areas in Table 4.3 are greater than the actual working areas and the PtVCC electro-active responses in glucose solution show higher responses compared to plain platinum electrode in potassium ferricyanide solution.

As the principles of CV test in potassium ferricyanide and glucose solution are different, it was necessary to perform two separate tests to analyse the typical redox electrochemical reaction in the potassium ferricyanide solution as a classic reaction to test the electrode activity of platinum and PtVCC individually.

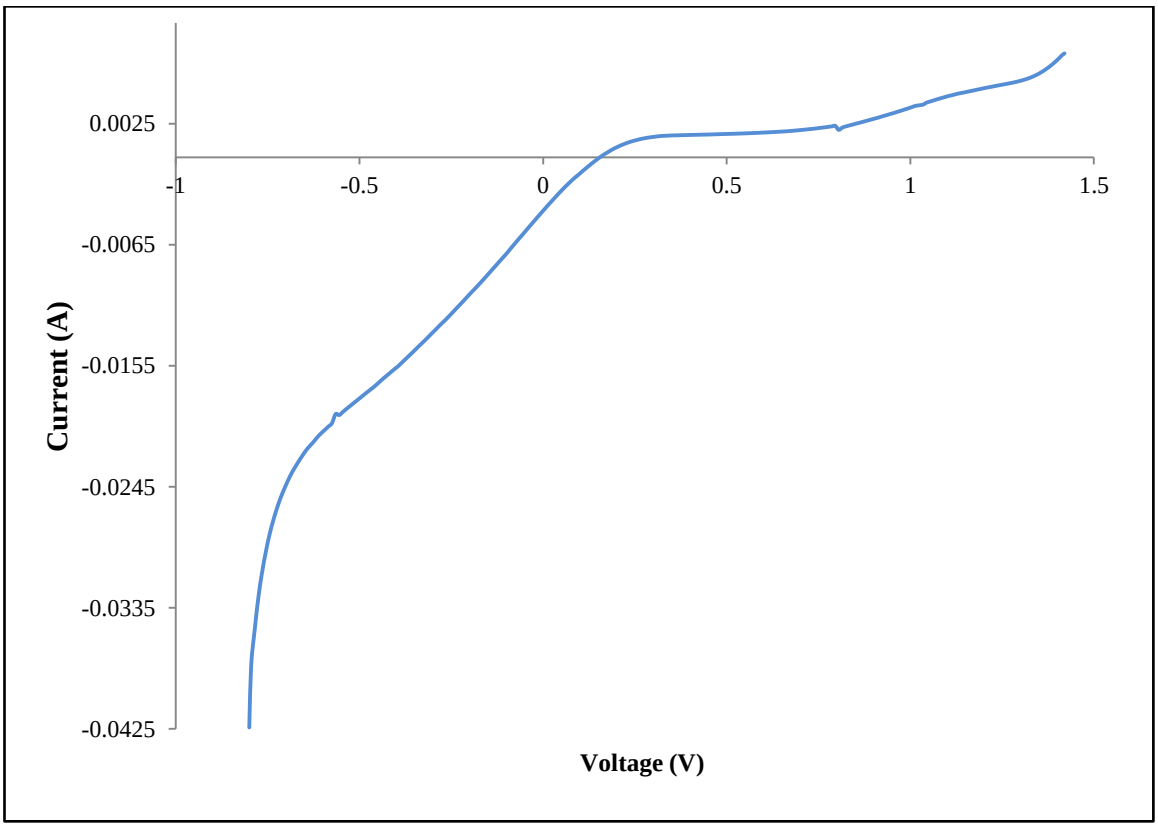

Figure 4.10. Current vs. Potential tests (I/E) responses obtained from 5mM glucose (pH 7.4) of PtVCC

The results of PtVCC electrode materials in glucose solution shown in Figure 4.10, with an applied voltage ranging from -0.8 V to +0.8 V produced current responses of more than 2.3 mA, maximum current value obtained when the positive potential when it reached 0.8 V, however the current value at negative polarity when potentials reached -0.8v was over (-42mA). Therefore PtVCC electrodes show great electron conductivity at the negative potential where maximum electron transfer takes place.

4.1.3. Direct GFC Characterisation Results

Based on these electrochemical test results, a direct GFC was designed as shown in Figures 3.5, 3.6 and 6.7, using PtVCC electrode to catalyst the glucose solution. A two cells electrode configuration on IM6 (electrochemical station) was used to measure all states of current and potentials of the fuel cell in the Lab.

4.1.3.1. Polarization phase of direct glucose fuel cell

This required measuring current vs. time or voltage vs. time. In this experiment the electrochemical measurement using potentiostat/galvanostat (IM6) was set as current or voltage meter to measure current or voltage, similar in principal to measuring a working battery cell.

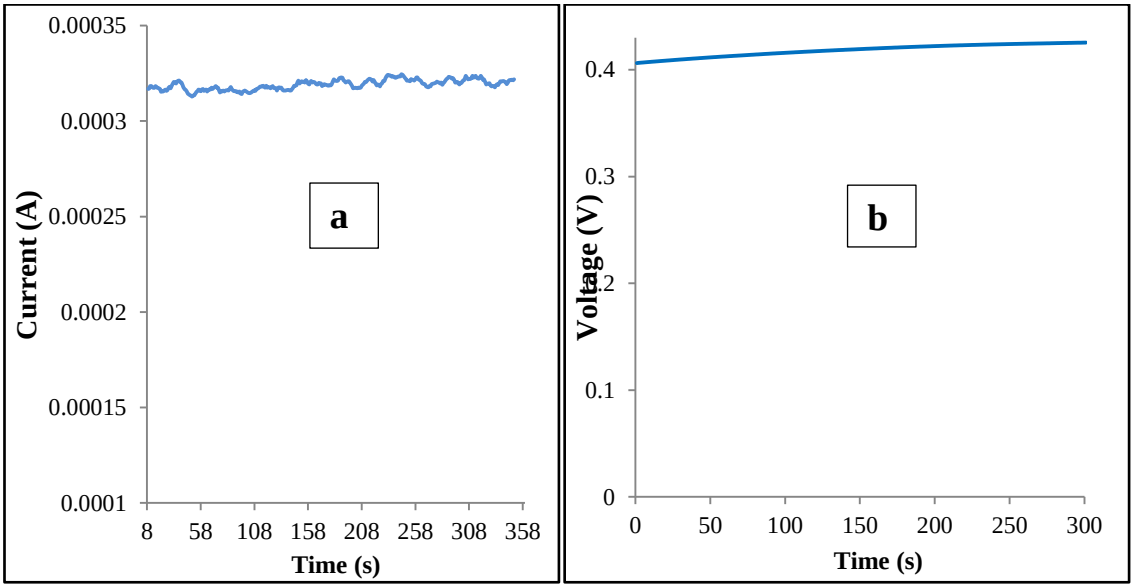

Figure 4.11. Responses obtained from 5mM glucose (pH 7.4) of PtVCC, (a): Current (b): Potential.

Figure 4.11(a) displays the current response obtained with PtVCC electrode in glucose solution with circuit current response above 332μA, as a result PtVCC catalytic electrode shows great improvement and good conductivity in glucose solution compared to plain platinum electrodes.

Figure 4.11 (b) shows the potential response of a PtVCC electrode consistently increasing over 300 sec. This was obtained from a glucose solution that resulted in a

maximum open circuit potential of over 0.43 V. This shows that the PtVCC electrode exhibits the same voltage response as plain platinum electrode.

Having obtained the maximum current and voltage responses of the fuel cell, the power consumption was obtained by applying different load resistances and recording the current consumption.

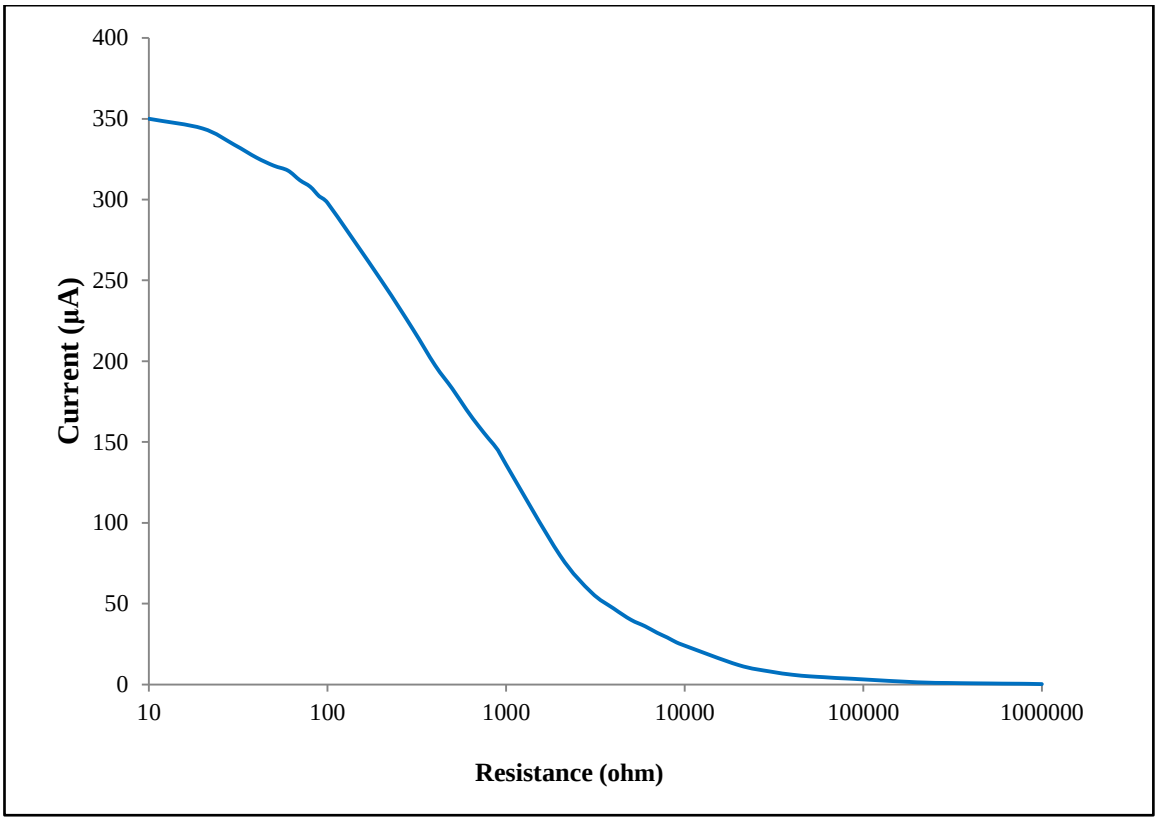

Figure 4.12. Direct GFC current response from 5mM glucose (pH 7.4) obtained by applying different load resistances

Figure 4.12 displays the initial output current response of GFC at its maximum current of 350 µA when the resistive load is 10 Ω, and starts to drop with an increase with load resistance. At 1 kΩ load resistance the current consumption dropped to 140µA, while at 10 kΩ, the current dropped further to 30µA. Figure 4.13 illustrates this as a series of current steps, where a step increase in load resistance from 1 kΩ to 10 kΩ in steps of 1 kΩ, giving responses reflecting the current consumption at each step, as a result providing the ideal load resistance that should be used as an optimum GFC output power density.

Furthermore, chrono-polarization measurements we carried out in order to confirm the improved electro-activity of GFC (PtVCC electrode) in glucose solution by conducting impedance matching for power output optimisation. This measurement was determined with the steady-state power output of the GFC when driving a range of resistive loads, as shown in Figure 4.13 and the step changes of current over time, and consequently the ideal working load corresponding to current consumption is shown in Figure 4.14.

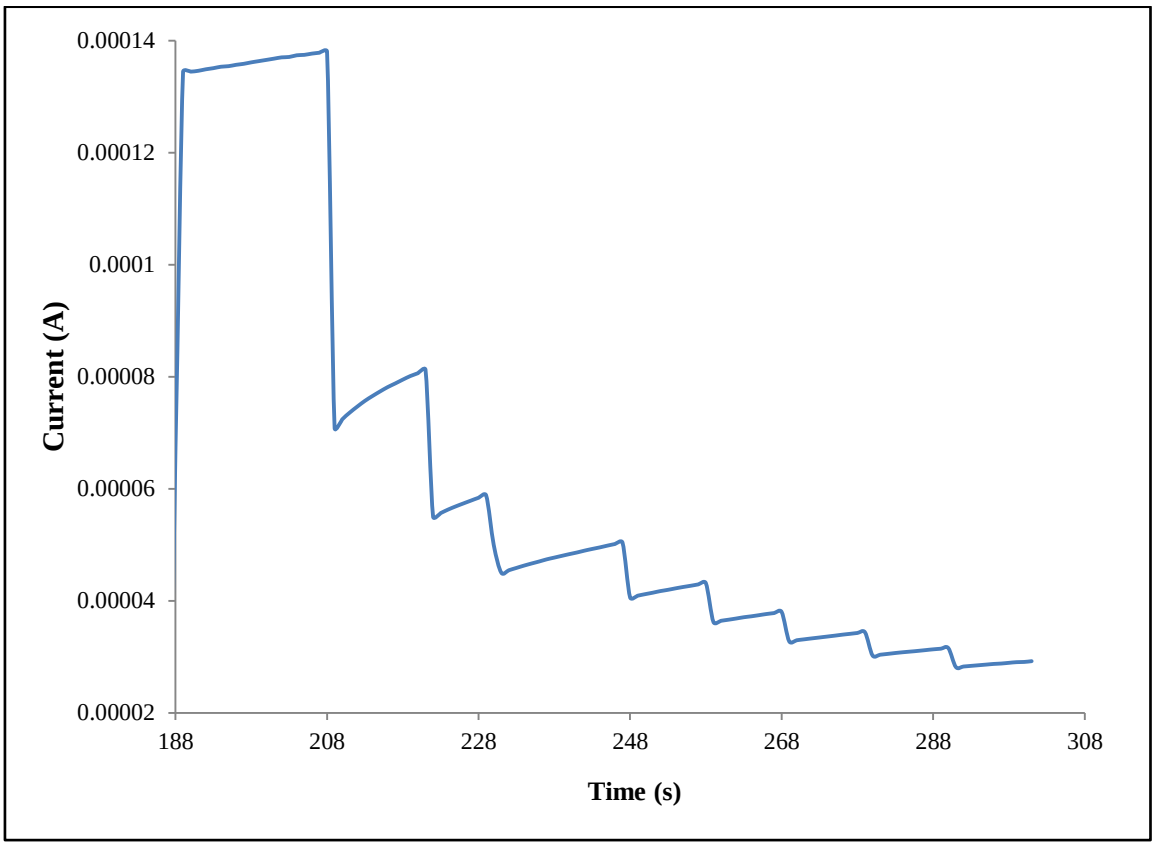

Figure 4.13. Direct GFC current step response from 5mM glucose (pH 7.4) obtained by applying different load resistances from 1 kΩ to 10 kΩ in steps of 1 kΩ

Furthermore in Figure 4.13 the graph shows big drop in current from 140µA (at 10 kΩ) to almost half at 80µA when the load resistance is doubled from 1 kΩ to 2 kΩ. The current then dropped below 60 µA when the load was again increased to 3 kΩ. The maximum load resistance at this stage was 10 kΩ, where the current dropped to 30µA. The current responses from (a) was used to calculate the power consumption of the GFC, and then plotted the result in (c) as a function of different resistive loads. This show the highest GFC working power density of 18.5 µW is obtained at 1 kΩ load.

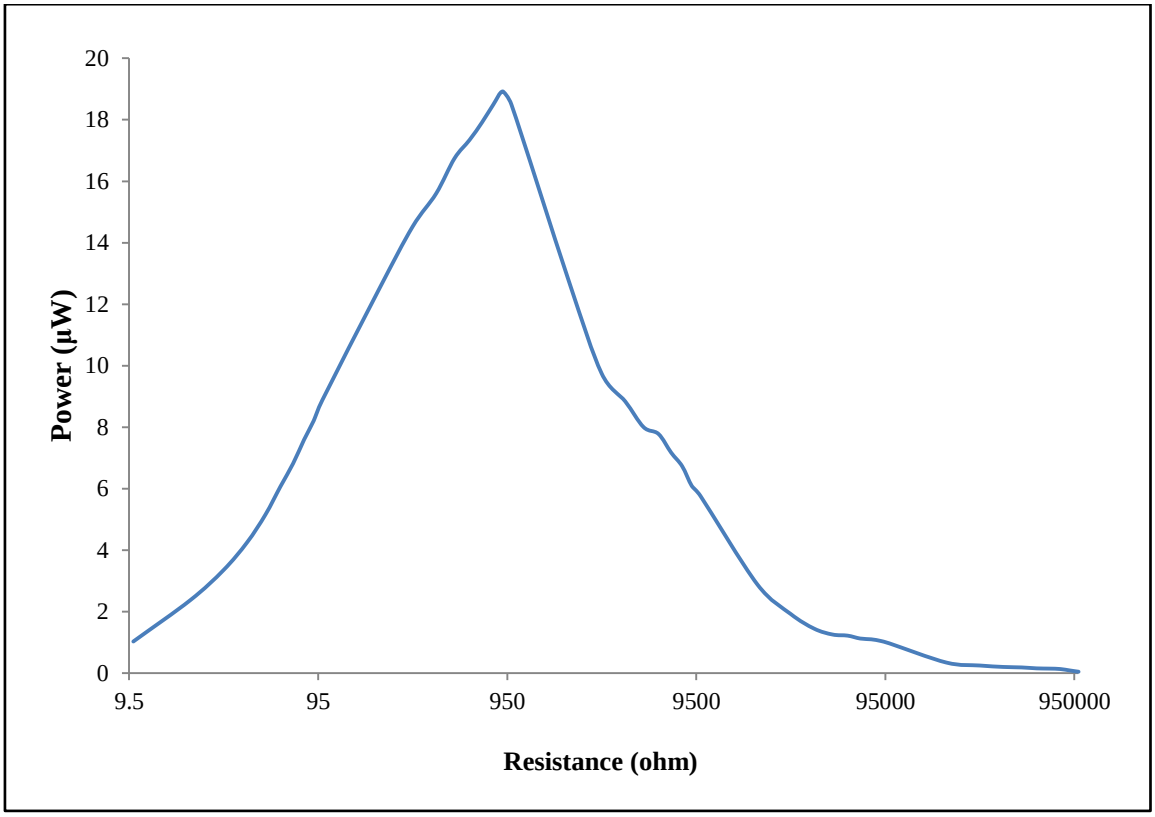

Figure 4.14. Power responses from 5mM glucose (pH 7.4) of DGFC obtained by calculating current vs. resistance responses

The current step responses from Figure 4.13 were used to calculate the power consumption from the PtVCC fuel cell and then plotted as a function of resistance shown in Figure 4.14. This clearly shows that the highest working power recorded of 20 µW was obtained with a 1 kΩ load.

As potential IMDs power supply, these fuel cells are flexible enough to be made into almost any arbitrary shape, harvest readily available body fluid within tissues which contains glucose of typically 5mM concentration (Van, 2012). The GFC electrodes react with oxygen to form oxidised products and water. When the oxidation is complete, CO_2 and water are resultant by-products (Van, 2012).

Because platinum electrode materials are known for their excellent electro-catalytic effect in glucose sensing, and Pt nanoparticles provide the enhanced electrochemical activities on the oxidation of hydrogen peroxide. The combination of two ideal electrochemical electrode materials such as Pt nanoparticles and carbon cloth, presents an excellent platform for glucose sensing, and glucose fuel cell designs (Xie, 2007). At this

stage we report on design, fabrication and test of PtVCC catalytic electrode based fuel cell for glucose oxidation. The PtVCC fuel cell produced comparatively higher output current and power at a lower cost than other conventional fuel cell designs, potentially in the favourable body fluid to power IMDs, in combination with an intermediate circuitry (DC-DC convertor) to boost the GFC output voltage.

4.2. GFC Design Results

To our knowledge, the presented work is the first attempt to investigate the influence of PtVCC material on the performance of three-electrode biofuel cells as a glucose reduction/oxidation catalyst for IMDs. Most of the investigated open circuit potential and current performances were significantly increased because of three-electrode GFC based on two-anode PtVCC electrode configuration design, indicating the increase of direct electron transfer. These results prove that two anode PtVCC electrodes improve the catalytic performance, which contributes directly to glucose oxidation. This work therefore presents a direct GFC that catalyses glucose ($C_6H_{12}O_6$) very slowly, resulting in no changes to the solution, although heat maybe produced by the process. The electron transfer reaction may also produce a low amount of hydrogen and/or oxygen gas, however since platinum and carbon can both be stable even when implanted, these will not oxidise to produce hydroxide and, throughout these experiments, the PtVCC specimens did not show any characteristic changes on their surfaces.

4.2.1. Three-electrode GFC Fabrication and Assembly

We assembled a polymer membrane based fuel cell, Figure 3.6, with nafion membrane placed between the cathode and anode electrodes. Nafion membrane is porous, and this acted as the insulator and at the same time providing glucose diffusion across the membrane.

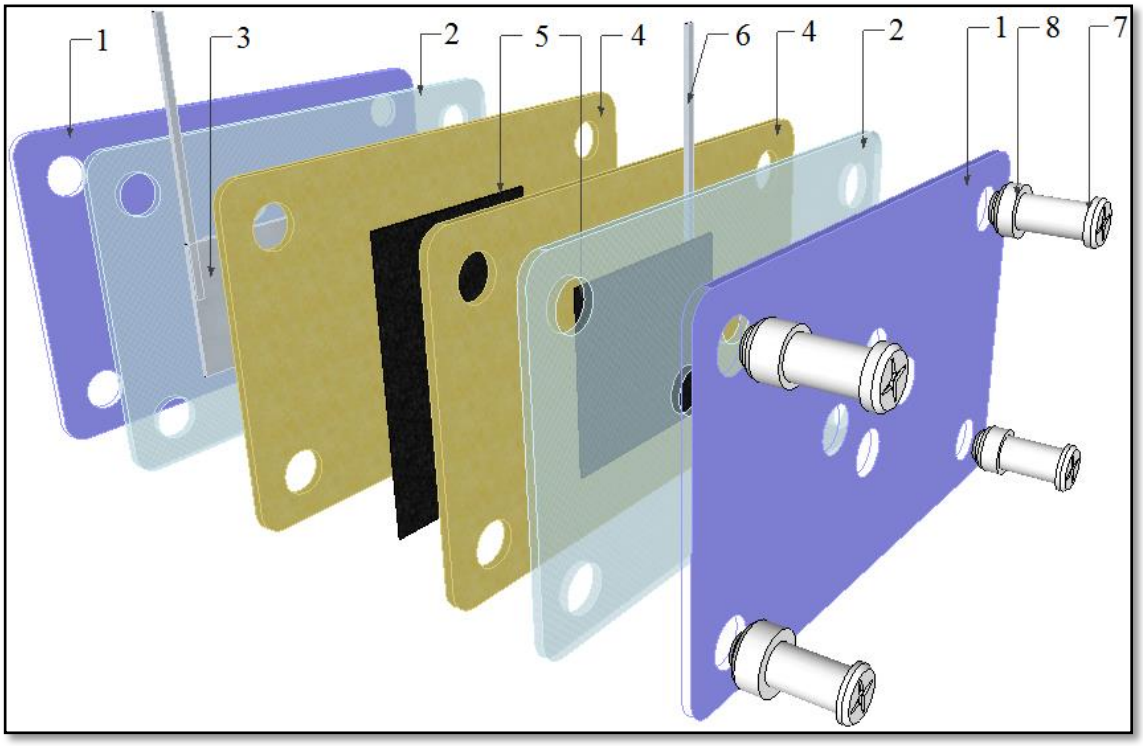

Figure 4.15. Sandwich design concept of a direct GFC, with open illustrations; (1) Polycarbonate Frame, (2) Silicone Rubber Gasket, (3) Platinum sheet (anode electrode), (4) Nafion Membrane Separator, (5) PtVCC, (6) Cathode Current Collector, (7) Nylon Screw and (8) Nylon Nut.

Figure 4.15 illustrates a sandwich type of a direct GFC assembly, where the anode is based on PtVCC material, and the separator as nafion membrane; which is an electrically insulated polymer and has the ability to diffuse glucose. When fabricating the direct GFC we applied additional PtVCC as anode material. All materials involved are bio-compatible with good conductivity and electron transfer capabilities.

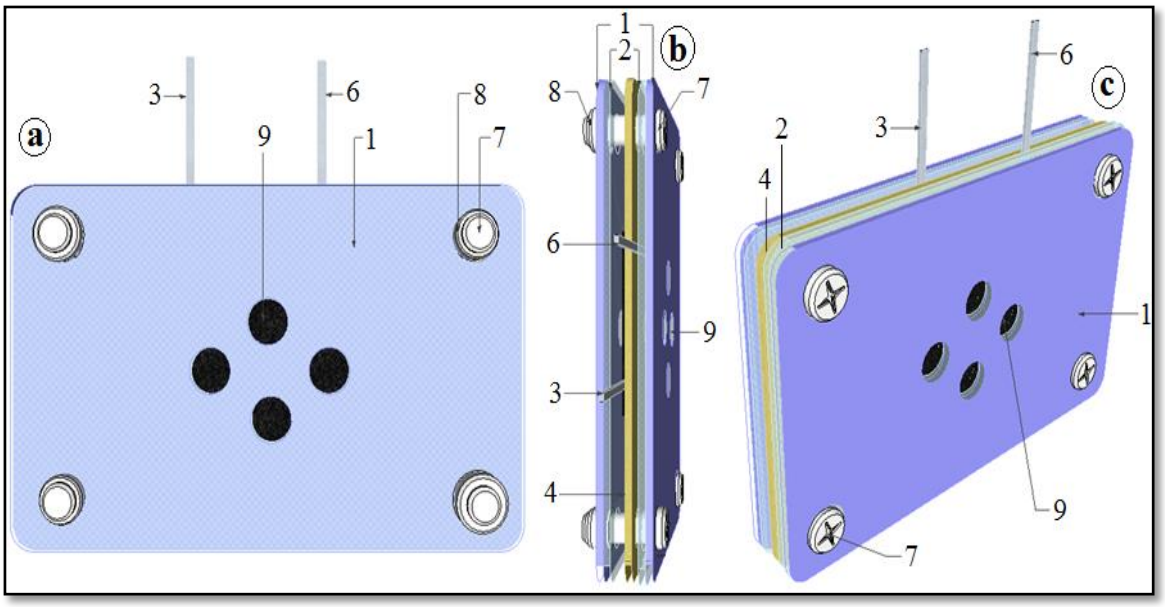

Figure 4.16. Sandwich design concept of a direct GFC mechanisms with (a), (b) and (c) views of Closed illustrations; (1) Polycarbonate Frame, (2) Silicone Rubber Gasket, (3) Platinum sheet (anode electrode), (4) Nafion Membrane Separator, (5) PtVCC, (6) Cathode Current Collector, (7) Nylon Screw, (8) Nylon Nut, (9) Glucose Intake.

We have considered rapid assembly fittings, to which electrodes and membranes can be stacked between silicon rubber gaskets and thick polycarbonate frame and backing. The whole assembly in Figure 4.16 is clamped together with nylon screws. Since the cathode is comprised of PtVCC and platinum sheet, which is catalytic in nature, while the anode only contained Pt film/mesh, this were manually pressed together with the plastic covers. The final thickness of the fuel cell, including the contribution from cathode, anode nafion separator, silicon rubber and polycarbonate was 8mm. More electrodes could be stacked together to obtain higher current or voltage. Polycarbonate frames and silicon rubber gaskets both provided mechanical support to the electrodes while damping the pressure effects due to the clamp. This cell design proposition was validated with dimensions designs recommended for implantable fuel cell devices discussed in chapter two; commonly the active electrodes are required to be limited by size of typically $1cm^3$.

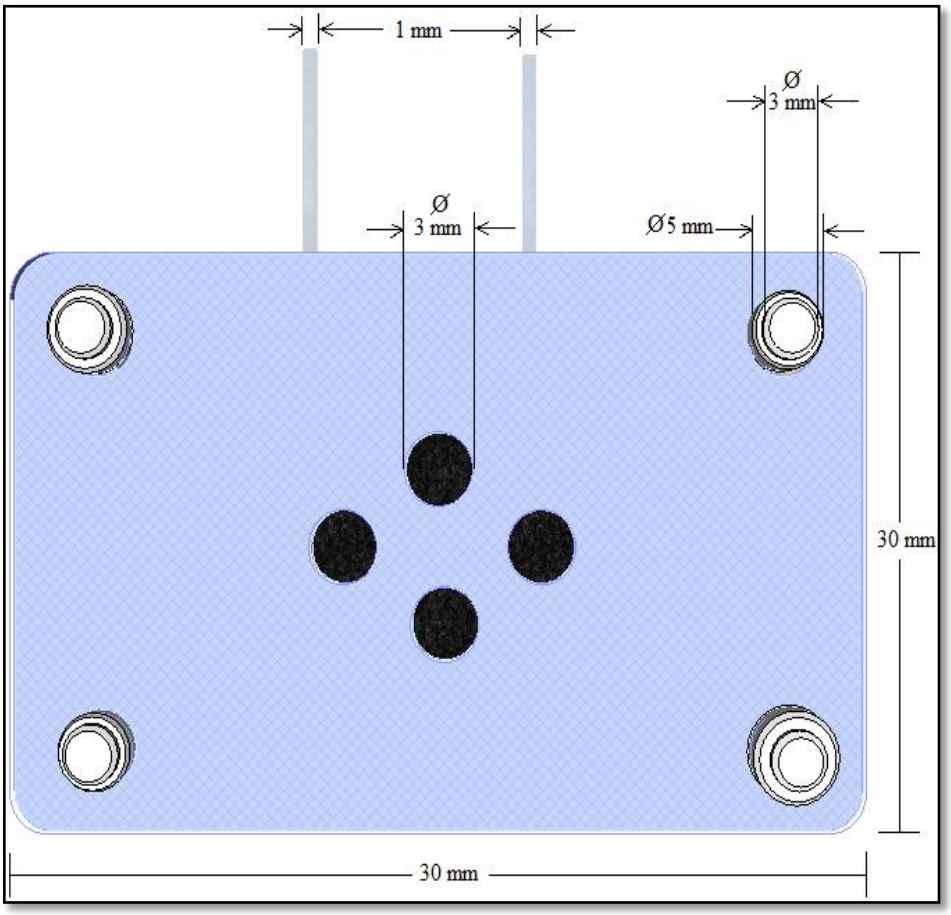

Figure 4.17. Direct GFC assembly dimensions.

Figure 4.17 illustrates the geometric sizes of the fuel cell components. The platinum film current collectors for anode and cathode have widths of 1mm, while the glucose intake holes have 3mm diameter, also 3mm diameter for nylon nuts, 5mm diameter nylon bolt and 30mm^2 Polycarbonate Frames, nafion and silicon rubbers, while PtVCC and Pt sheet were cut not larger than 1mm^2. The Polycarbonate Frames were cut with laser in the laboratory from a computer aided design (CAD) drawing fabrications.

The focus of this design was to deliver a direct GFC, and there were many steps taken to reduce the challenges found on practical aspect of fabrication and assembly GFC, by providing an easy-to-use assembly system with reduced structures that use construction techniques needing only two casing pieces only requiring fastening.

While there are other choices of PtVCC material compositions in development involving different physical proprieties, the PtVCC material with diffusion layers made of electrically conductive porous materials, presents good catalytic proprieties that were

selected to construct a proficient direct GFC, that presented stable design and fabrication method with consistent performances carried out in laboratory experiments for the sole purpose of producing high output current to power IMDs.

In terms of volume-normalized current density, the three-electrode GFC based on two-anode PtVCC electrodes, exhibited higher values of open circuit current and voltages: 350μA cm^{-2} and 0.42V respectively from a single cell. CV tests proved PtVCC has catalytic capabilities and other tests demonstrated the PtVCC having a faster response time and higher sensitivity than traditional electrodes in glucose solution. Because the PtVCC diffusion layers are made of electrically conductive porous materials, the three-electrode GFC design and fabrication based on two-anode PtVCC proprieties has shown long-term stabilities in the laboratory, and has produced high currents, confirmed in numerous tests using IM6 (electrochemical station), including oscilloscope displays that confirmed all states of potentials of the GFC capable of powering IMDs when combined with a voltage boosting device.

Table 4.4 GFC performances results

Anode - O_2 (reduction)	**Cathode Oxidation**	**Separator or Membrane**	**Fabrication Method**	**Fuel Source**	**Fuel Type**	**Power Output**	**Experiment Duration**	**Reference Papers**
PtVCC	Pt film / sheet	Nafion	Mechanical. Confined	In vitro	Glucose /O_2	20μW cm^{-2} (0.4V)	6 months	This work

Table 4.5. GFC performances results from a design experimental that only required glucose to be topped-up for the duration of 6 months.

Output	**Oct 2015**	**Nov 2015**	**Dec 2015**	**Jan 2016**	**Feb 2016**	**Mar 2016**
Current (μA)	230	142	108	92	61	50
Voltage (V)	0.31	0.31	0.35	0.35	0.3	0.3

Tables 4.4 and 4.5 are the 6 months continues performance results of the proposed GFC design. During this observations, the proposed GFC design required only glucose solution to be topped-up at intervals of once per week. The GFC power out reduced with decreasing glucose solution overtime, due to evaporation, but the power out resumed back to normal with every glucose topped-ups.

In addition we have presented the abiotic catalytic, three-electrode sandwich type GFC approach with 3 cells in parallel connected to a DC-DC converter, a voltage boosting circuit that produced higher output voltage > 4.0 V; ten times greater than the input value, enough to power most efficient electronic devices. This suggests that the direct GFC design based on PtVCC electrode is a promising solution for powering small electronic IMDs.

4.2.2. Increasing and controlling the electrical potential generated by the GFC

Powering IMDs circuits requires >2 V, while the designed GFC is able to deliver maximum of 0.4 V from each cell, therefore required a DC-DC converter to increase the output potential to a value greater than the required IMD input. The DC-DC converter consequently provides enough power to the microcontroller, sensor and transmitter. The power management circuitry to supply the wireless temperature sensor or a glucose sensor that should at later stages will be integrated into the design of the custom glucose monitoring module.

As covered previously, individual cells of GFCs could not be connected in series while sharing the same glucose solution, in attempt to multiplying the output voltage, because these cells being in the same glucose solution will essentially produce the overall voltage or current no greater than the single cell output. This problem is partially overcome by connecting the cells in parallel; but this only increases the output current, yet keeping the output voltage the same as a single cell. For that reason, the voltage produced by the GFC is required to be increased and controlled to provide the require operating voltages to drive IMDs, so boosting DC-DC converter circuit is required to increase the output voltage >2 V. Practically all electronic components available on the market require working potentials higher than those delivered directly by GFCs. And because the

potential of GFCs varies with time, then the potential developed by the GFC needs to be stepped up and stabilised by an energy management system to power any IMD.

4.2.3. GFC Power Management System

Previously simplified block diagram of power supply module with power management shown in section 3, was comprised only of GFC as energy source, a DC-DC power conversion module and an IMD, without any intermediary energy storage (rechargeable battery) device.

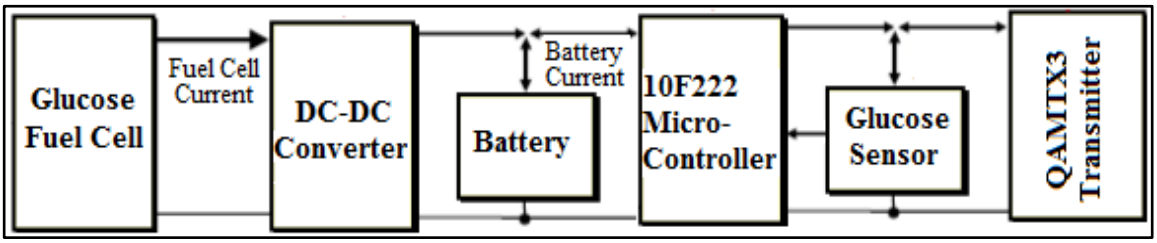

Figure 4.18. Block diagram of GFC power supply and the power management system connected to IMD system.

The block diagram in Figure 4.18 shows the block diagram of a complete system, planned power management arrangement capable of providing power to drive IMD's transmitter system using GFC for energy conversion. The energy storage device required for the power management is a rechargeable battery, and a DC-DC converter required to boost the 0.4V input potential from GFC to a potential sufficient to power the microcontroller, glucose sensor and the transmitter.

Electrical energy produced by fuel cells can be stored in various ways, the most common is to be stored by rechargeable batteries, this have been proven to provide suitable power levels for various applications including IMDs, of which this works intends to capitalise the use of rechargeable batteries instead of ultra-capacitors, because batteries have much higher energy density storage capability compared to ultra-capacitors.

Table 4.6. Different DGFC connection set-up and DC-DC converters outputs

Fuel Cell Outputs	Single Cell	Double Cells In Series	Double Cells In Parallel	Triple Cells In Series	Triple Cells In Parallel	LTC3105 DC-DC converter	NCP1400 A DC-DC converter
Voltage (V)	0.42	0.4	0.4	0.35	0.4	4.033	4.012
Current (μA)	350	300	500	290	700 - 1200	~300	~280

Table 4.6 show the outputs of 5 different DGFC connection configurations. Each design setup was connected in turn to a DC-DC converter, to either LTC3105 or NCP1400A to boost the lower input voltage to an output voltage sufficient to drive an IMD. Though, only the three cell design in parallel provided sufficient input current >700 μA, enabling the DC-DC converter (LTC3105) to switch the 0.4 V input to an output to voltage > 4.0 V. This DC-DC converter was also capable of providing small boost to the input voltage from two cells in parallel; which resulted to output voltages up to 1.5 V only.

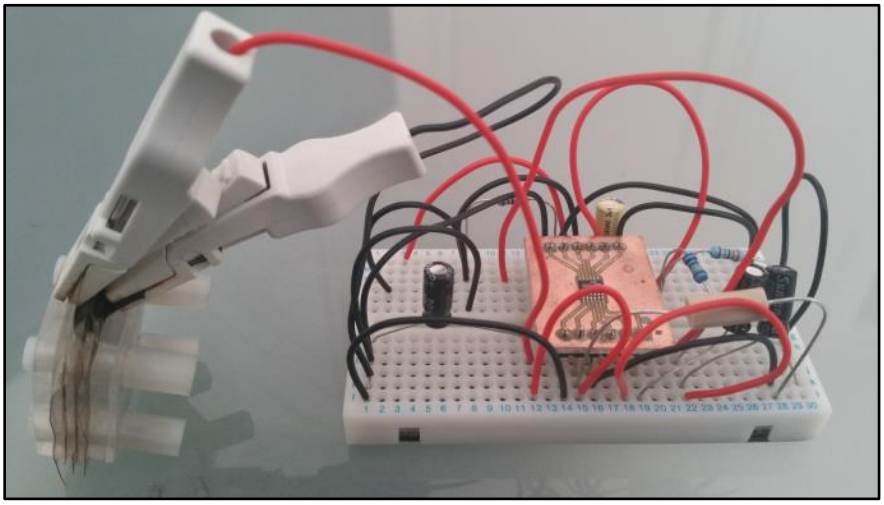

Figure 4.19. A DGFC connected to a DC-DC converter (LTC3105) voltage boosting circuit

Figure 4.19 show the DC-DC converter (LTC3105) circuit used in setup with 3 DGFC in parallel to boost the input voltage from as low as 0.225V to an output voltages > 4.0V, but this required high input current > 900μA to operate, as a result, the boosted output voltage was dropping below 4.0 V once the DGFC current settled below 800μA.

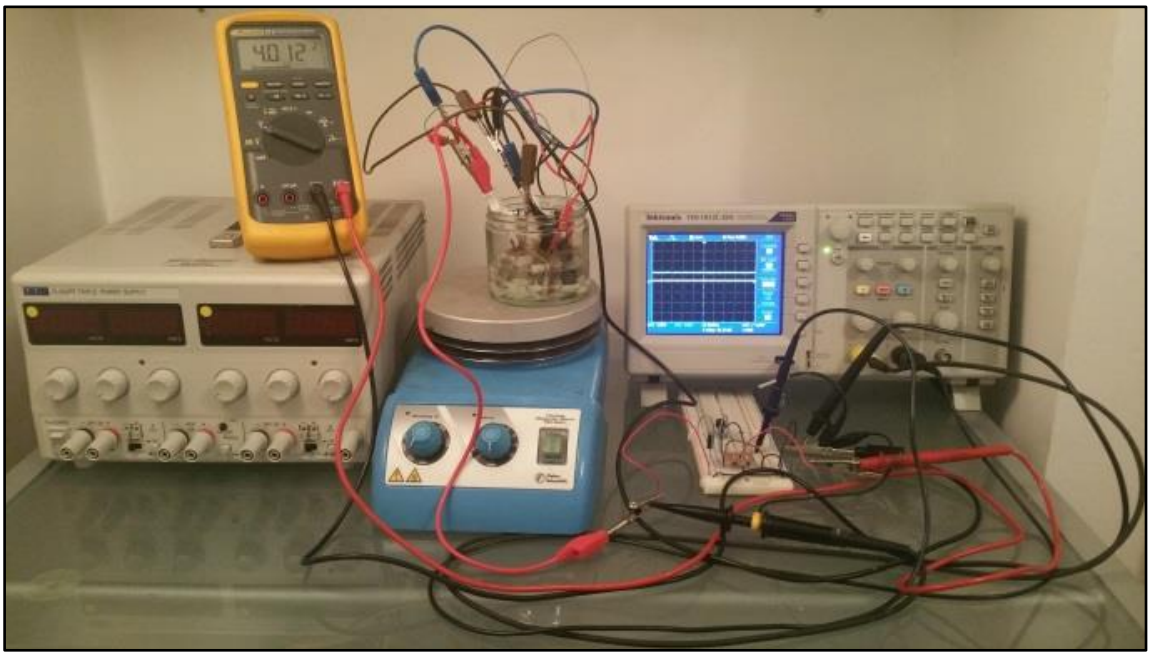

Figure 4.20. Three GFC connected in parallel to a DC-DC converter (NCP1400A) circuit that boosted the 0.4 V to 4.012V, input and output voltage respectively being displayed on the oscilloscope, while only the output is displayed on the digital meter (fluke meter)

On the other hand, the DC-DC converter (NCP1400A) circuit shown in Figure 4.20, with its input and output voltages captured from an oscilloscope display (Figure 4.21), this circuit worked in the opposite manner to the LTC3105 convertor, requiring instead higher input voltages >0.97 V (though this devices is designed to start up with a cell voltage of 0.8 V and could still operate thereafter down to voltages less than 0.2 V), and with current as low as >500μA.

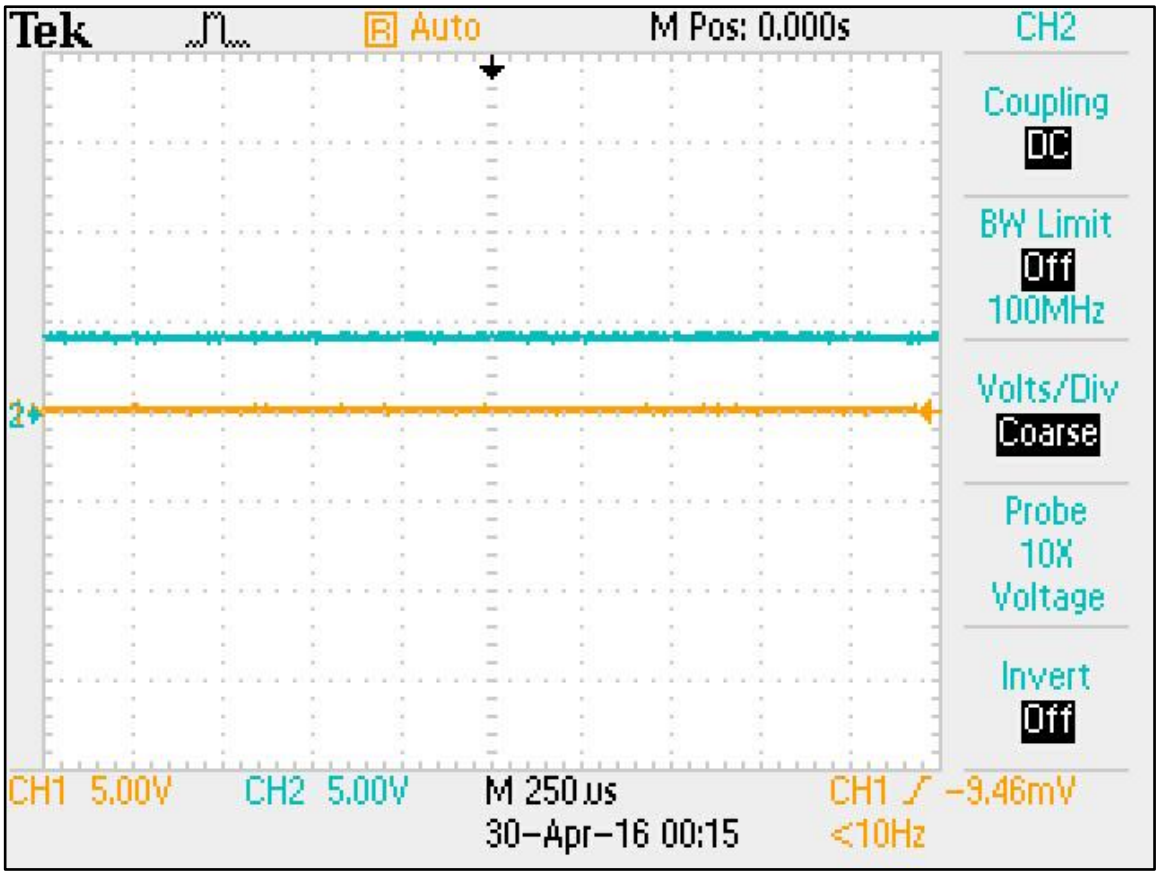

Figure 4.21. The oscilloscope display of input voltage 0.4 V (orange), and the boosted voltage 4.012 V (Aqua blue) from a DC-DC converter (NCP1400A) circuit output

While Figure 4.20 shows the system connections between the measuring devices, the voltage boosting device, and 3 GFCs connected in parallel, including display of the input voltage (0.4V) and the boosted output (> 4.0V) captured by the oscilloscope, displaying adequate output voltage required to power most small electronic devices, including low power microcontrollers, sensors and transmitters, which require minimum stable potential of 1.8V.

Since each GFC is capable of only producing low voltages and currents of 0.4 V and 350µA respectively, the only configuration practicable was to connect the 3 DGFCs in parallel, as a result, only the DC-DC converter (LTC3105) boosting circuit seemed suitable to for this kind of fuel cell setup, however, it only provided shorter boosting time due to fuel cell rapid current drop over time. Whereas, the DC-DC converter (NCP1400A) circuit operated much longer with the same arrangement of 3 DGFCs connected in parallel, but it required an external battery to start-up the DC-DC converter (NCP1400A) circuitry by providing the needed voltage above 0.97 V. On this

experiment, it required to connecting an external battery for less than 0.5 second to the input of the DC-DC converter (NCP1400A) for it to start-up and boost the input voltage from the DGFC which provided an efficient boosted output voltage >0.4 V.

Because of the limitation covered previously relating to the individual fuel cells should not be connected in series while sharing the same glucose solution, there was no other alternative apart from attempting to increase the set-up to 4 or more cells in parallel, to increase and maintain the current > 1500 μA instead. However, since the IMD could be designed with a recharge battery as illustrated in Figure 5.16, this same battery should be used to initially start-up the DC-DC converter (NCP1400A) and then use the power management switching techniques, to recharge the same battery and then power the IMD. The circuit designs of Figure 4.19 and Figure 4.20 will subsequently be assembled and tested on PCB.

4.2.4. GFC Power Management Applications

The designed power management system was used to control the energy generated by GFC, and stored in the rechargeable battery, and this energy was used only when the level of the stored energy was adequate to deliver enough power to the implantable microcontroller, containing the sensor and the transmitter.

To demonstrate the usefulness of the power management system, a commercially available temperature sensor, transmitter and receiver was used, and transmitted the measured temperature data wirelessly from the sensor to a remote receiver. When the GFC charged the battery to 1.2 V, the DC-DC converter was activated to produce a 3.3Voutput; which was then used to drive the microcontroller and control the sensor and the transmitter.

After few data transmissions, the voltage in the battery was decreases, causing the potential to decrease below 1.2 V, and these results in the microcontroller system switching to sleep mode until the battery voltage reaches 1.2 V, which restates the same process again to be boosted the DC-DC converter. Selecting the potential of 1.2 V as the potential at which the system was changed to active mode was arbitrary; the lower the selected potential, the shorter the charging time for the battery. Although the DC-DC

converter required only 0.9 V to operate, therefore the switching regulator was used to charge the battery to 1.2V from the GFC. As soon this voltage was reached the DC-DC converter operating value, this was activated to deliver an output voltage of 5V, required to be supplied to the implantable microcontroller, sensor and the transmission modules.

4.2.5. Recharging Thin-Film Micro-Energy Cell (THINERGY MECs) Battery

The existing energy generated by GFC requires to be stored by a recharging battery which could then power the IMD, this is because the amount of power generated by a single GFC is very small and cannot sustain the continuous operation of IMD circuitry, as a result, the use of rechargeable battery will accumulate the charge, and compensate for any peak power demands that might be required by the IMD system. As a result, a recharge-ability feature of the storage device is crucial for this application, so the THINERGY MEC is smaller, thinner, and lighter design with optimum duty cycle that allows the implant device to only use the required amount of energy it needs, and yet it can be recharged with multiple cycles, with little damage to the battery life and performance; yet capable of holding charge well, and has a charging acceptance from 1 μA of current and allows only 1nA of leakage current. In addition, since THINERGY MECs can be recharged beyond 10,000 cycles, and are therefore perfect for dribble charge (Wei, 2008 and Martinez-Catala, 2009), constant recharge from an integrated energy harvesting GFC.

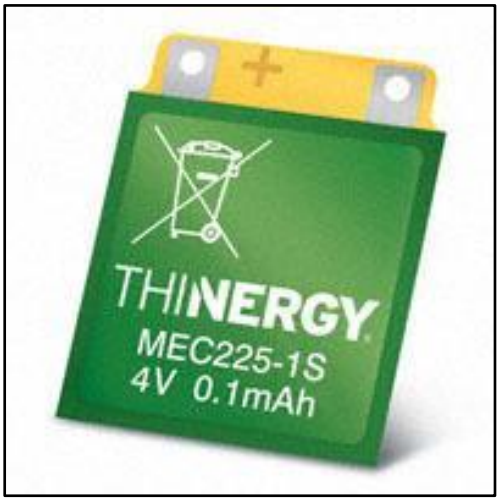

Figure 4.22. THINERGY™, Thin-Film Micro-Energy Cell (MEC225-1S) Solid-State, Flexible, Rechargeable Battery (THINERGY MEC225 Data Sheet and Infinite Power Solutions in the Appendix E)

A THINERGY rechargeable battery in Figure 4.22; is more appealing compared to a super-capacitor and other energy storage technologies (Infinite Power Solutions), due to its thin energy storage mechanism which can be completely incorporated into IMD chip or be embedded into rigid or flex PCBs, as it can withstand variable temperatures, pressure better that other storage devices. In addition, rechargeable batteries have the lowest cost with less maintenance costs, with a long-life lasting application, since it can be trickle charged and reused several times over, with constant-voltage recharge with no current limiting.

Battery charging mode is ideally needed to be done with constant voltage charge. Since the charging current will always be limited, this required using a charge-limiting resistor. And charge the battery at voltage lower than the upper limit, to maintain the electrical characteristics of the battery including the discharging capacity.

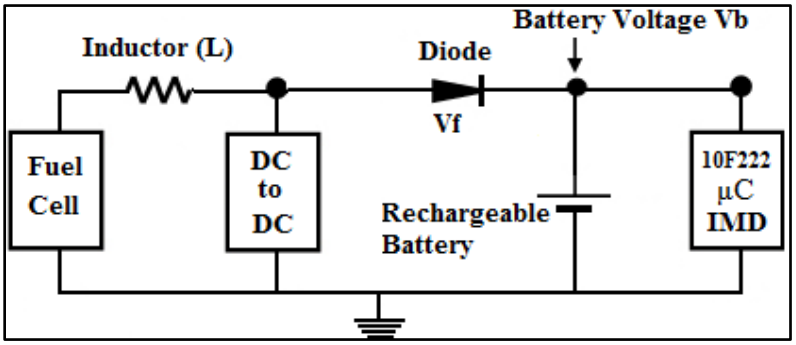

Figure 4.23. Block diagram of power management of energy harvesting principle, incorporating GFC, DC-DC convertor, battery and IMD.

Figure 4.23 could incorporate THINERGY battery, which (Infinite Power Solutions) claim to be used in a wide range of medical devices including implantable devices, such as glucose monitors and implantable insulin pumps. THINERGY MECs provide the highest energy density package with virtually limitless lifetime performance in a safe, solid-state package that can be implanted for life and recharged unobtrusively within the body with GFC energy conversion to:

a. provide continuous back-up power
b. limit the need for battery replacement and patient surgeries
c. enable integrated, smaller and thinner devices

(Infinite Power Solutions) also claims that THINERGY battery reduces the need for additional components such as charging capacitors, because of high pulse current capability of THINERGY MECs, which is capable of charging from zero to 90% capacity in only 15 minutes. The recharge is simple from a regulated 4.1V source and there are no external current limiting components. MECs are much smaller than coin cell batteries and super capacitors, and provide backup power for up to 20 times longer than other thin-film batteries. Estimated backup times range from weeks to months. Managing the harvested energy from the GFC has been used significantly to extend the life of the IMD, by managing the small harvested and stored into a rechargeable battery to reach power required to drive any IMD, and enough power to extend the life of the any IMD.

To guaranty that the IMD system does not drain the energy stored in the rechargeable battery deriving from the GFC because of high power consumption during operations; the IMD is required to be disconnected from the GFC by the power management until the energy builds up in the rechargeable battery reaching enough level for operation again. Once again, to guaranty sufficient power to drive the implant systems (IMD), the designed energy management system provides two modes of operations; sleep and active modes, with low power electronic device monitoring the voltage level of the energy storage device, and adequate power to the sensor device when required.

4.3. QAM TX3 and RFM12 based RF micro-systems

4.3.1. QAM and RFM12B systems design features

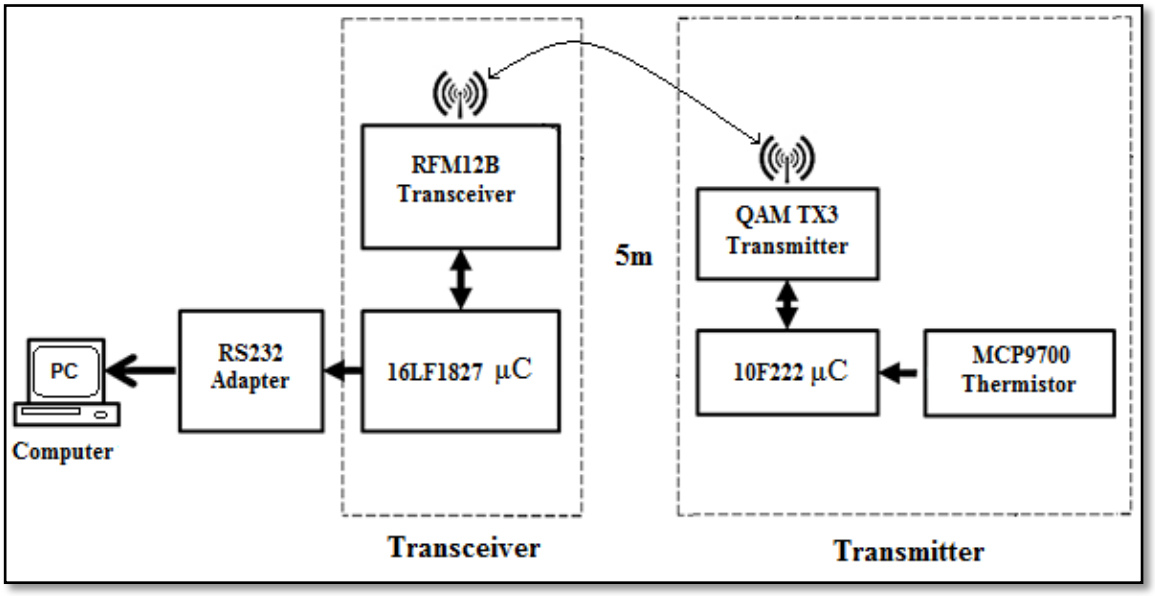

Figure 4.24. Functional block diagram of a QAM based RF micro transmitter based systems that transmit sensory data to a reader microcontroller interfaced to a PC.

In Figure 4.24, the external reader unit comprises the RFM12B transceiver, the RS232 adapter (RS232 Serial port converter) and a computer desktop running on Hyper Terminal (RFM12B Transceiver datasheet), a Microchip 16LF1827 microcontroller chip (Microchip 16F1827 datasheet) and a 3V DC coin cell battery; while the transmitter could be placed up to 5 m away from the external transceiver, consist also of a QAM TX3 transmitter described in Table 4.7, a Microchip 10F222 microcontroller, a Microchip MCP9700 thermistor (Microchip MCP9700 datasheet) and a 3V DC coin cell battery. The transmitter and the transceiver have each an attached λ/4 (single copper wire) antenna. On power up, the external transceiver microcontroller initiates and configures the external RFM12B transceiver for polling (receipt of data from the internal transmitter). Sensed temperature data received by the external transceiver from the immersed transmitter situated 5 m away are then logged and displayed on the computer desktop Hyper Terminal screen.

At each stage, the immersed transmitter was powered using a 3 V button cell instead of the developed GFC for an efficient prove of concept; running at 433 MHz using 4.8 kbps

Frequency-shift keying encoding (a variation pattern in which digital information is transferred over separate frequency changes of a carrier signal), and programmed to transmit at 0 dBm (1 mW) resulting in a measured received power level in air, over 5 m, of -24 dBm (4 μW). The tests required the transmitter to be fully packaged and immersed in the beaker containing either, air, deionised (DI) water or glucose solutions only. This resulted in no data corruption (in this case sensing the surrounding temperature) recordings and no noticeable power loss at the receiver was recorded during the experiments. The experiments were carried out without transmission cables attached to the probes, and this facilitated the deployment and monitoring tests in standard test vessels simply by immersing the wireless systems, while a desktop computer was connected to an external reader device that was used to capture the readings from the sensor probes continuously by interrogating it wirelessly.

Table 4.7. QAM TX3 transmitter operating proprieties

Types of tests	Declarations
Operational mode	The QAM TX3 transmitter in the immersed system are software-configured for sending of sensed temperature data while the external RFM12B transceiver receives and logs the multiple data and displays them on a computer desk-top Hyper Terminal.
Small Antenna	The QAM TX3 transmitter has an attached (single copper wire) antenna
Frequency selection	Taking into consideration RF attenuation resulting from the conductivity of the test in glucose solution as well as Electromagnetic compatibility (EMC) due to the operation of the magnetic stirrer (Berelli, 2013; Behzadi, 2013 and Boughriet, 1999) the selected operational frequency is 433 MHz. This is in the unlicensed RF spectrum that has good penetration in liquid media and is suitable for short range applications (FCC, 2014).
Compatibility and packaging	Available chemically inert probe enclosure materials include: PTFE (Dupont Teflon PTFE) and Acetal (Typical properties of Acetal).

4.3.2. QAM and RFM12B systems setup

The initial laboratory experimental test set-up involved the transmitter to fully be submerged in a 1 litre volume laboratory glass beaker (placed inside a laboratory fume hood) containing the test glucose solutions (5mM at 7.4 pH). The magnetic stirrer and

hot plate options were implemented by placing the beaker on top of a Fisher Scientific; heating magnetic -stirrer FB15001 (Fisher Scientific).

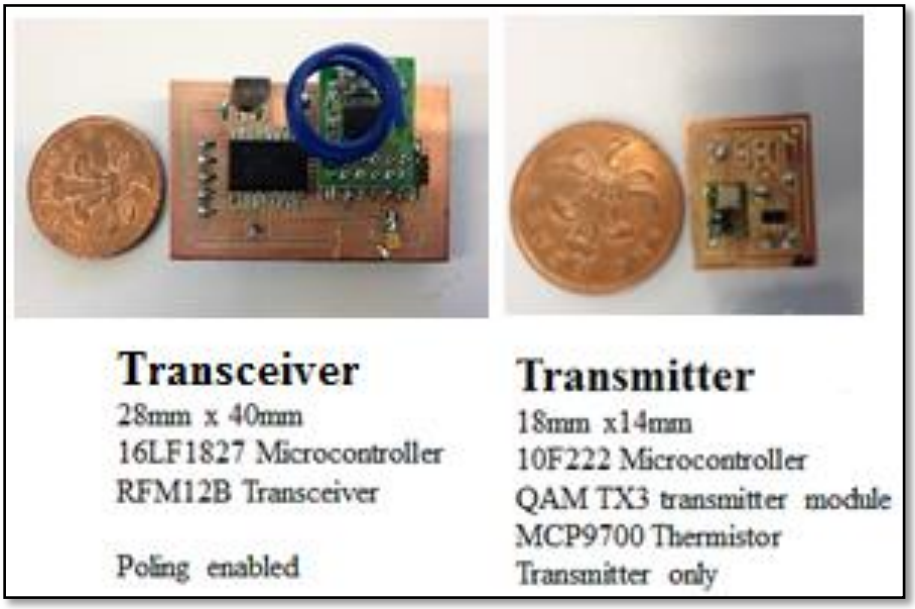

Figure 4.25. Transceiver and the transmitter based circuits

Figure 4.25 shows both the transceiver and the transmitter have a small outline integrated circuit (SOIC) packaging (the two pictures have the same 2p coins, the only problem is the difference in picture sizes), hence the transceiver circuit has 28 mm x 40 mm in size, comprising the RFM12B transceiver with a 16F819 microcontroller, while the transmitter has a size of 18 mm x 14 mm, comprising a 10F222 (Microchip 10F222 datasheet) microcontroller and the QAM TX3 transmitter module (QAM TX3 datasheet) and enabled for transmission mode only. Therefore the sensed temperature data received from the transmitters by the external transceiver is poled, logged and displayed as shown in the Hyper Terminal screen shot in Appendix C.

4.3.3. QAM TX3 system based temperature results

The sensed temperature data received by the external RFM12B transceiver from QAM TX3 transmitter placed 5 m away in a glass beaker, with either no solution present (i.e. in air), in DI water or in glucose solutions, are shown in Table 4.8.

Table 4.8. Test results of temperature transmissions

Time	NO Stirred Air (A)	Stirred Air (B)	DI Water Set (C)	DI Water Tested (D)	Glucose Set (E)	Glucose Tested (F)
0	22.8	22.8	22	23	23	24
5	23	23	23	23	24	25
10	23	23.2	24	24	25	25.8
15	23	23.4	25	25	28	30
20	23	23.6	26	28	30	33
25	23	23.8	27	30	35	43
30	23	24	28	31	39	45
35	23	24.2	29	32	44	52
40	23	24.4	29	33	50	59
45	23	24.6	29.3	33	58	65
50	23	24.8	29.5	34	62	70
60	23	24.9	29.8	35	70	78

The above Table 4.8 data comparison results are simplified by plotting the output results on graph shown in Figure 4.26, comparing the change differences between tested results in all stages involving Air (stirred and non-stirred), DI water and glucose (set and tested temperature values).

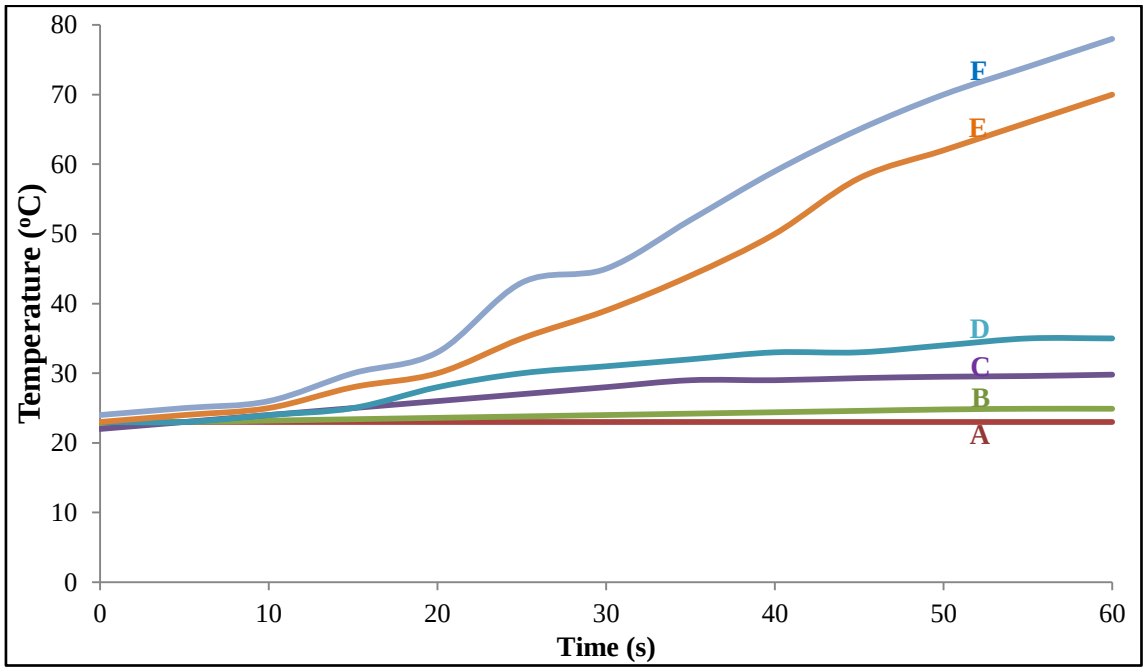

Figure 4.26. Test results of temperature transmissions; (A) NO Stirred Air, (B) Stirred Air, (C) DI Water Set temperature, (D) DI Water Tested temperature, (E) Glucose Set temperature, (F) Glucose Tested temperature.

4.3.3.1. Air transmission test

The graphs in Figure 4.5 show the sensed data received versus time, comparing the data between a magnetic stirrer being switched on or off, while the hot plate was set to maximum of 23^{o}C for a time period of 20 minutes before being switched off throughout the readings. Whereas the sensed temperature maintained between 23 and 24 ^{o}C (i.e. room temperature), this further indicates that over a time period of 60 minutes, only a temperature change of about 1^{o}C is experienced despite the magnetic stirrer set on maximum. Indicating that there is little or no electromagnetic impact at tested transmission frequency of 433 MHz.

4.3.3.2. DI water transmission test

Immersing the transmitter in a beaker filled with DI water with a resistivity of 18 MΩ.cm, where the hot plate temperature was increased randomly from 22 degrees room temperature to achieve a perfect final value of 30 degrees within the 60 minutes of the test. These sensed temperature data were received with the magnetic stirrer set on maximum.

The data received shown in Figure 4.5 is higher than the actual set temperature. This occurred after 15 minutes of the test, and this may be attributed to high battery drain as well as the effects of temperature changes to the ADC. Though the hot plate was reached a value of 30^{o}C after 60 minutes, the actual temperature sensed is about 35^{o}C after an hour; correctly tracking the temperature changes within the liquid DI water.

4.3.3.3. Glucose transmission test

Received sensed temperature data from the transmitter fully immersed in a beaker containing glucose solution, where the hot plate temperature was increased from room temperature at 22 degrees to final value of 70 degrees in increments of 5 minutes duration. It can be noted that in spite of the change of solution from DI water to glucose, the measured temperature was still between 23 and 25^{o}C (at room temperature for the first 10 minutes), once again confirming that the probe correctly monitors the temperature even if the conductivity of the solution varies.

During experimental tests, the actual temperature readings were recorded using a digital thermometer inserted inside the beaker, with or without solutions. Most measured results can be noted being higher than the actual set data values and this occurred from after 10 minutes of each test, this can be attributed to the high drain of the off-the-shelf button cell battery. Additionally, the V_{ref} of the ADC in the transmitter Microcontroller is subject to temperature changes; manifesting in the variations observed in the transmitted sensed data. These were taken into consideration during calibration of the next design iterations.

4.3.4. QAM TX3 and RFM12B based RF systems summary

RF signals propagation and sensed temperature data transmission through air, water and glucose solution has been obtained using immersed transmitter and the external (receiver) transceiver powered by a single 3 V DC button cell and transmitting at 433 MHz, achieved an operation range of 5 m between the two devices, at power of 9mW. To enable poling i.e. the logging of data received from multiple transmitters, the RFM12B transceiver was used. The immersed transmitters system, consisted of a Microchip 10F222 microcontroller chip, a QAM TX3 transmitter, a Microchip MCP9700 thermistor and a 3 V button cell battery, were all encased in an ABS box and then fully immersed in water or glucose solution to carry out the test. This experimental test demonstrates the transmission of sensed temperature data only; other physical properties such as glucose level can also be monitored by the inclusion of the appropriate glucose sensor and associated signal processing. As the size of the immersed transmitter is critical, design iterations using alternative microcontroller packaging were explored as well as fabricating transmitter-only circuits using the QAM TX3 transmitter module with a form size of just 18 mm by 14 mm. As a result, this test result provided the background to designing a complete Self-Powered Bio-Sensing Platform with Glucose Energy Harvesting Fuel Cell, comprising of IBFC system, with power management and energy storage including a backup recharging micro-energy batteries, as expanded on the next chapter.

4.4. Implant Solution System

Prototypes of implant solution system were made with commonly available discrete components presented in previous section. The tested bio-implant circuitries consist of

temperature sensors, but a glucose sensor is desired in this case for the purpose to be implanted inside human's body to monitor changing glucose levels. The implant solutions have mainly been presented in four main parts: power source, sensor, data sampler and data transmitter.

At this stage, we address two main important parts of this implant solution; first is the implantable microcontroller circuitry containing the transmitter and the monitoring sensor; as tested and discussed on previous sections, while the second part presents the IGFC as the main power source proposed for this work. The integration between these two parts forms an assembly combination between a suitable micro-power source and an associated low-power circuitry to form the Self-Powered Bio-Sensing Platform with Glucose Energy Harvesting Fuel Cell.

Table 4.9. Comparison between RF transmission (with/without oscillator) and power consumption of existing circuits and proposed circuit.

References	Oscillator Based Transmitter	Running Frequency (Hz)	Supply Voltage (V)	Power Consumption (µW)	Technology CMOS (µm)
This work	Yes	433M	2	120	NA
This work	No	31K	2	310	NA
(Betancourt-Zamora, 1997)	Yes	200M	3	1500	0.5
(Cong, 2009)	Yes	433M	2	300	1.5
(Lasanen, 2005)	Yes	32K	1 - 1.8	3	0.35
(Haider, 2010)	Yes	500	1.5	400	0.35
(Mohseni, 2004)	Yes	6k	3	2200	1.5
(Beach, 1999)	No	304M	3.7	0.32	NA

Based on the experiments carried out using different microcontroller system setups involving either an oscillator or a clock-less based transmitter (microcontroller with or without an oscillator respectively), as a result, Table 4.9 illustrates few existing RF transmitters and their power consumption circuits compared to this work's systems. Despite this work's clock-less based microcontroller transmitter facilitated the possibilities of transmitting the temperature data at lower frequency and without an oscillator, yet this attempt did not improve the current consumption, by running at 310 µW, while the microcontroller circuit with an oscillator, in spite of running at higher frequencies 433MHz, still consumed lower power 120 µW. In addition, based on the

accuracy of data transmitted, and the simplicity of circuit design with fewer components and ease of implementation, the QAM TX3 and RFM12B based RF microcontroller systems was chosen to be powered by GFC derived from this work, with the integrated power management circuit to form a Self-Powered Bio-Sensing Platform with Glucose Energy Harvesting Fuel Cell device.

4.5. Data Recovery

The first challenge was to adequately manage the small energy generated by the GFC, to power a Self-Powered Bio-Sensing device. The second challenge was to successfully demonstrate the data being transmitted to a remote receiver (data recovery) test systems carried successfully in section 4.

The design of Self-Powered Bio-Sensing device functions included efficient power management for all components in the system; proficient implanted sensors, adequate data storage and accurate wirelessly transmitters. The design of the Self-Powered Bio-Sensing Platform data recovery system also required extra attention to balance requirements, namely on how to interface between the implant microcontroller, sensing device, processing and transmission of sensed data, while managing power distribution effectively.

Between the two microcontroller circuits designs tested in section 4, the design comprising of RFM12B transceiver and QAM TX3 transmitter module, which presented the best result for an implantable solution system, based on simple and compact design, easy-to-use, easy to assembly and integrate with other systems. The integrated was circuits composed of a reliable communication interface between the Self-Powered Bio-Sensing Device (transmitter circuit) and detector (reader circuits), and have an easy-to-use data coding and decoding required for glucose sensing analysis. The selected QAM TX3 transmitter module, was chosen to build Self-Powered Bio-Sensing Platform with Energy Harvesting GFC system, because of many advantages it presented over the Clock-Less Pulsed RF transmitter, such by having lower power consumption capabilities, long distance transmission, compact size design, faster transmission and much easy to integrate to CMOS design because of fewer components.

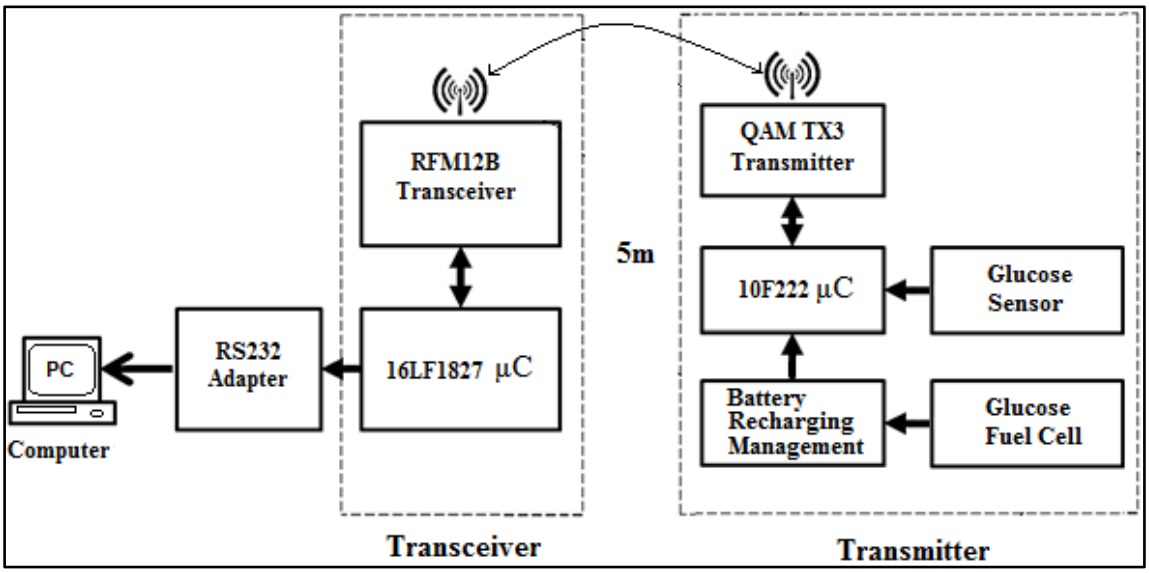

Figure 4.27. Functional block diagram of a Self-Powered Bio-Sensing Platform with Energy Harvesting GFC *systems that transmit sensory data to a reader microcontroller interfaced to a PC.*

The block diagram of Figure 4.27 above presents a Self-Powered Bio-Sensing Platform, comprising of microcontroller with QAM based RF micro-transmitter, glucose sensor, Energy Harvesting GFC, and the power management block that converts relatively low levels of energy into amounts that are store in rechargeable battery, to later provide power to drive the Self-Powered Bio-Sensing Device. The diagram here presents a complete working system with major components as an autonomous wireless sensor.

The data recovery comprised of prearranged sequence of codes that were sent and checked for errors. For validation purpose, a digital thermometer (instead of glucose) sensor was used, and the temperature was sent as analogue output that was then read by an ADC at the receiver circuit. The Self-Powered Bio-Sensing solution is comprised of all the electronic components that are commercially available from specialised vendors, although some of the electronics had to be designed and added to fit the needs of this work.

The transmitter and receiver microcontroller circuits were programmed to run at 8MHz clock speed, using a C programming language presented in the appendix D section. The 10F222 based transmitter circuits comprised of flash memory microcontroller, and the C program code was to defined pins (B0 and B1), for input temperature sensor and output transmitter (RF TX) respectively. The transmitter circuit's code was also setup to start

with ADC converter and the transmitter pin switched off, while at first reads the input pin (sensor) and presents the value in temperature's most significant bit (MSB) and least significant bit (LSB), evaluates the byte values, the sends the temperature values 3 times before it switches to sleep mode.

The QAM RF transmitter and receiver (RX) function code were programmed with length of (350 uS) zero pulses in delays, and length of (999 uS) one pulses in delays, (525 uS) Midpoint sample time in delays, while the starting pulse of only (10 mS) delay. The temperature values are therefore stored in bytes, and the receiver circuit timer 1 is setup, which is needed to detect received pulse widths (1uS) pulse delay.

The transmitter microcontroller was coded initially to send a start or header bit to the output pin (RF TX) with the starting pulse to the output pin then send a start bit and then the byte three times. While the receiver circuit waits for first positive transition from the RF pin, for the receive data packet, and checks all 3 bytes and accepts the data if 2 out of 3 bytes are equal, and returns false (error) otherwise.

The data recovery was setup with the receiver circuit to receive temperature values sent from the transmitter as 3 equal bytes, with LSB first, and the outputs value is only accepted when any 2 of 3 bytes matches. The receiver circuit's Timer1 is setup to produce a 1uS tic, while temperature value is returned in static signed char receiver byte variable. The transmitted signal or sensed data (temperature) transmitted through a series of tests, demonstrated the operation range capability and the coding efficiency via a wireless connection between the transmitters and the receiver circuits which was the connected to a PC via RS232 interface, displaying the temperature values on HyperTerminal display, which where the signals were validated using Saleae logical analyser within the same computer in Appendix C.

Chapter 5

Conclusion

This work has addressed the requirement for improving the electronic processes and systems for transferring signals / data outside body, and the management of power source inside patient's body to achieve long span monitoring; addressing the requirement for a reliable Self-Powered Bio-Sensing solution using GFC energy harvesting platform for long-life power supply.

5.1. Limitations

The human body being a complex system consisting of many different kinds of tissues, implanting wireless electronic devices inside the body has its challenges, some of which this work could not overcame. As such, the limitation of this work includes the lack of analyses on the behaviour of RF transmission on different layers of tissues as follow:

- The antennas could have been designed considering different layers of tissues environment.
- Estimation of the high dissipation of RF signals due to the body tissues structures.
- Another point which has to be considered is the choice of operating frequency. The frequency band of 402–405 MHz is allocated for implantable medical devices in ETSI, while the proposed device operates at the frequency of 433 MHz, which has no particular disadvantage compared to frequencies 402–405 MHz band (Werber, 2006).
- The proposed IMD cannot be inserted in the brain, but instead in the legs, arms and stomach.

It can also be recognised that through the limitations of research, this work has followed the same path to many other published IMDs prototypes and proof-of-concepts, by focusing mainly on validating performance, typically in a perfect model environment not similar to the difficult implantable environment. In addition, this research study only deals with monitoring of disease or health conditions, but not the control of medication delivery. Regarding the power source relating to GFC energy harvesting technique, which have been promised to one day replace batteries, nonetheless this studies concludes that there is still a long way before glucose fuel cells can replace batteries from IMDs, and overcome the most challenges IMDs face in relation to long-term reliability of its power supply.

5.2. Contributions

Though it's acknowledged that all the above element of studies make up for a very complex system that a particular researcher will possibly not possess the knowledge and the essential equipment or services required to satisfy all of the requirements to successfully design an innovative IMD. Nevertheless, this work offers a proof-of-concept of a Self-Powered Bio-Sensing solution using GFC energy harvesting platform for continuous power supply, to overcome some of existing limitations with IMDs, this work specifically presents analysis and techniques for self-sustainable, low-power, wireless and efficient data transfer technique from both theoretical and practical points of view. To restate, the investigatory contributions from this work includes the following:

- Innovative design model that produced energy harvesting glucose fuel cells with selective bio-compatible materials that meets the implantable requirements, in addition, proving higher output power compared to the existing designs.

- Low power microcontroller based transmitter system capable of sending data accurately while immersed deeply in liquid solutions, without requiring further amplification.

- Accurately sent data wirelessly with a transmitter designed with minimum hardware control-circuit; involving only a microcontroller without oscillator and a copper wire antenna.

- Successfully obtained power management design system capable of capturing, storing and distributing the energy generated by glucose fuel cells to power IMD.

- Confirmed overall system performance using multiple analytical and data displaying tools, and consequently, confirmed performance on effective data transmission, detection and decoding mechanism with accuracy.

Much investigation efforts have been targeted on improving the power output of IGFC, as such, the new 3 electrodes configuration design method and electrode assembly

technique has been presented that promises solution to obtaining higher power efficiency with the use of PtVCC.

- This work results confirms that the presence of PtVCC on both anode and the intermediate of a 3 electrodes configuration; improved the fuel cell's performance by providing greater tolerances of oxygen at the anode, and glucose at the cathode, yet this could not prevent fuel cell's performance from degrading over the time.

- This work confirms also that fuel cell's design is more complex than other energy convertors for powering IMDs, as compared to vibrational or thermal energy harvesting techniques, in terms of reliable material selection and consistent generation of output power.

- It can be concluded that current progress with IGFCs design are still incapable of providing reliable output power without any additional help of power management system to drive IMDs as a self-sustainable monitoring device that can last the lifespan of the patient's life.

- The presented abiotic catalytic GFC based on PtVCC electrode approach with 3 cells connected in parallel to a DC-DC converter (voltage boosting) circuit produced higher output voltage > 4.0 V; ten times greater than the input value, thought enough to power most efficient electronic devices, but this required a battery to start-up the existing converter circuit. This indicates that an improved ultra-low-power (start-up current and voltage) DC-DC converter circuit is required to efficiently manage the output voltage from the fuel cells.

It can then be recognised that the prototype proof-of-concept involving Self-Powered Bio-Sensing system using GFC energy harvesting platform with continuous power supply should not remain restricted to research, due to boundless miniaturisation possibilities, consistent high power supply output, and good reliable interface between implant sensor and external reader device.

The successful implementation of Self-Powered Bio-Sensing Platform with Energy Harvesting GFC solution was realised by involving 3 crucial areas, 1: energy conversion,

management and storage, connecting GFC, DC-DC converter and rechargeable battery respectively, 2: transmitter circuit (including microcontroller and sensor) and 3: receiver circuit (including microcontroller and the PC). The circuits of Self-Powered Bio-Sensing Platform with Energy Harvesting GFC solution design emphasises on maximising the device's active life by focussing on low power data sampling and transmission, with the final goal of integrating the design into a sub-micron CMOS IC that operates on ultra-low power.

5.3. Future work

The experiment results proved that an effective implementation of power management circuitry is able to provide the possibilities of powering any kind of sensor and communication system using body fluid based GFCs. However, long-term and in vivo testing of this system were not carried out in the laboratory, but will need to be done in the future in order to determine the long term reliability of this system in an implantable environment.

Platinum electrode (cathode) could be produced using clean-room lithography technology, which can produce minimum feature lengths of nano-meters when fabricated on thin silicon wafers. These would result in a further degree of miniaturisation and will produce electrodes having greater catalytic capability that correlate with theory.

Further investigations could be made to develop a more efficient transmitter circuit to ensure maximum data transmission at ultra-low power. Additionally, the design of GFC in a clean room environment and encased in bio-compatible material to meet the implantable requirements system would be valuable.

Further funding, could have helped to carry out in vivo tests of the system in animal and then in human, which could have provide the opportunity to determine the characteristics and properties of this prototype's interface within real life IMDs applications.

Since subcutaneous operations are safe due to the negligible power of the transmitted data. Potential applications of Self-Powered Bio-Sensing Platform with GFC Energy Harvesting solution would include a variety of embedded solutions for general purpose

monitoring, where software modifications could be made to support additional protocols and improve patient data privacy.

Future recommendation is to develop application specific control-circuits that have only essential hardware functions for the purpose further improving power consumption, for example; ultra-low power oscillator/clock, integrated comparator and ADC, including integrated DC-DC converters into a single CMOS design.

Finally, although the backgrounds of this work falls into biomedical sector, future works can cover the use of this prototype interface system into other industry applications.

List of Written Papers

Journal paper under consideration (Journal of Applied Electrochemistry):

Bunga, S., Vilches, A. and Song, W. *"Three-Electrode Glucose Fuel Cell Design Based on Platinum Nanoparticles Supported on Vulcan Carbon Cloth for Powering Implantable Medical Devices,"* 2016

Conference paper (UK cconference under consideration):

Bunga, S. and Vilches, A. "*Simple low power externally triggered transmitter for subcutaneous bio-implants*," 2016

References

Alam, S.B. (2009) *Single Compartment Micro Direct Glucose Fuel Cell.* Thesis, Helsinki University of Technology, Available online at: http://lib.tkk.fi/Dipl/2009/urn100110.pdf (Accessed 22 May 2016)

AHRQ (2011) Agency for Healthcare Research and Quality. *Critical Appraisal of Systematic Reviews of Implantable Medical Devices.* Department of Health and Human Services. Available online at: https://www.pharmamedtechbi.com/~/media/Supporting%20Documents/The%20Gray%20Sheet/37/51/_AHRQ_systematic_MedicalDevices_DraftReport.pdf (Accessed 14 May 2016)

Anastasi, G., Conti, M., Francesco M. Di, & Passarella, A. (2009) *Energy conservation in wireless sensor networks: a survey*, Ad Hoc Networks, vol.7, no.3, pp. 1-58

Bartona, S.C., Gallaway, J. & Atanassov, P. (2004) *Enzymatic Biofuel Cells fo Implantable and Microscale Devices.* American Chemical Society, vol. 104, pp. 4867-4886

Bartona, S.C. & Atanassov, P. (2004) *Enzymatic biofuel cells for implantable and micro- scale devices.* Chem. Soc., Div. Fuel Chem., vol. 49, pp. 476-477

Bazaka, K., Jacob, M.V. (2013) *Implantable devices: Issues and challenges*. Electronics Vol 2, pp.1-34

Beach, R.D., K¨uster, F.V. and Moussy, F. (1999) *Subminiature Implantable Potentiostat and Modified Commercial Telemetry Device for Remote Glucose Monitoring*. IEEE Transactions On Instrumentation And Measurement, vol. 48, no. 6, pp. 1239 - 1244

Behzadi, G. & Fekri, L. (2013) *Electrical parameter and permittivity measurement of water samples using capacitive sensor*, Int. J. Water Resources and Environmental Sciences , vol. 2, pp. 66-75

Belleville1, Fanet, M.H., Fiorini, P., Nicole, P., Pelgrom, M.J.M., Piguet, C., Hahn, R., Hoof, C.Van & Vullers, R. (2009) *Energy Autonomous Sensor Systems: State and Perspectives of a Ubiquitous Sensor Technology*. IEEE, Advances in sensors and Interfaces, pp. 134 – 138

Belleville, M., Cantatore, E., Fanet, H., Fiorini, P., Nicole, P., Pelgrom, M.J.M., Piguet, C., Hahn, R., Van Hoof, C., Vullers, R. and Tartagni, M. (2009) *Energy Autonomous Systems: Future Trends in Devices, Technology, and Systems.* CATRENE Working Group on Energy Autonomous Systems.

Berelli, G. & Pozzabori, A. (2013) *RFID under water: technical issues and applications*. InTech, Chpt. 18

Betancourt-Zamora, R.J., Hajimiri, A., Lee, T.H. (1997) *A 1.5mW, 200MHz CMOS VCO*

for Wireless Biotelemetry. Allen Center for Integrated Systems, Electrical Engineering Department, Stanford University, pg. 1-2.

Bettin, C. (2006) *Applicability and feasibility of incorporating microbial fuel cell technology into implantable biomedical devices*. Thesis, Dept. of Food, Agricultural and Biological Engineering. The Ohio State University, Ohio, USA

Bloom, D., Canning, D., & Fink, G. (2011) *Implications of population aging for economic growth. Available online at:* http://www.hsph.harvard.edu/pgda/WorkingPapers/2011/PGDA_WP_64.pdf (Accessed 22 May 2016)

Boughriet, A., Wu, Z., McCann, H. & Davis, L. (1999) *The measurement of dielectric properties of liquid at microwave frequencies using open ended coaxial probes*, 1st World Congress on Industrial Process Tomography, Buxton, Greater Manchester

Burleson, W., Clark, S.S., Ransford, B. & Fu K. (2012) *Design Challenges for Secure Implantable Medical Devices.* University of Massachusetts Amherst.

Cadei, A., Dionisi, A., Sardini, E. & Serpelloni, M. (2014) *Kinetic and thermal energy harvesters for implantable medical devices and biomedical autonomous sensors.* IOP Science, pp. 1-14.

Campi, T., Cruciani, S., Feliziani, M. & Hirata, A. (2014) *Wireless Power Transfer System Applied to an Active Implantable Medical Device.* IEEE, pp. 134-137.

Chen, J., Zhao, C.X., Zhia,M.M., Wang, K., Deng, L. & Gu Xu, G. (2012) *Alkaline direct oxidation glucose fuel cell system using silver/nickel foams as electrodes*. Elsevier, Electrochimica Acta, vol. 66, pp. 133– 138

Chiara, B., Andrea C., Davide, D. & Roberto, V. (2009) *An overview on wireless sensor networks technology and evolution*, MDPI, Sensors, vol.9, pp.6869-6896.

Chlistunoff ,J., Sansiñena, J.M. (2014) *Effects of axial coordination of the metal center on the activity of iron tetraphenylporphyrin as a nonprecious catalyst for oxygen reduction*. American Chemical Society. Journal of Physical Chemistry, vol.118, pp.19139−19149.

Cinquin, P., Gondran, C., Giroud, F., Mazabrard, S., Pellissier, A., Boucher, F., Alcaraz, J.P., Gorgy, K., Lenouvel, F., Mathe, S., Porcu, P. & Cosnier, S. (2010) *A Glucose BioFuel Cell Implanted in Rats.* PLoS ONE, vol. 5, pp. 1-7.

Cleland, J., Louis, A., Rigby, A., Janssens, U. & Balk, A. (2005) *Non-invasive home telemonitoring for patients with heart failure at high risk of recurrent admission and death: the Trans-European Network-Home-Care Management System (TEN-HMS) study*. *J. Am. Coll. Cardiol.*, vol.45, no. 10, pp.1654-64.

Colin, C., Bantin, C., (2007) *Radiation from a Pulse-Excited Thin Wire Monopole*. Antennas and Propagatlon Magazine, Vol. 43, pp. 64-6.

Cong, P., Young, D.J., Ko, W.H. (2009) *Wireless Batteryless In Vivo Blood Pressure SensingMicrosystem For Small Laboratory Animal Real-Time Monitoring*. Thesis for the degree of Doctor of Philosophy. Department of Electrical Engineering and Computer Science, Case Western Reserve University, pp. 13-14.

Cuevas-Muñiz, F.M., Guerra-Balcázar, M., Esquivel, J.P., Sabaté N., Arriaga, L.G. & Ledesma-García, J. (2012) Glucose microfluidic fuel cell based on silver bimetallic selective catalysts for on-chip applications. Elsevier, Journal of Power Sources, vol. 216, pp. 297-303

Cunci, L, Velez, C.A., Perez, I., Suleiman, A., Larios, E., José-Yacamán, M, Watkins, J.J., Cabrera, C.R. (2014) *Platinum electrodeposition at unsupported electrochemically reduced nanographene oxide for enhanced ammonia oxidation. American Chemical Society.* Appl. Mater. Interfaces, vol.6, pp.2137−2145.

Khan, A.S.A., Ahmed, R., Mirza, M.L. (2010) *Performance evaluation of platinum-based catalysts for the development of proton exchange membrane fuel cells.* Turkish Journal of Chemistry, vol.34, pp.193 – 206.

Daly, D. & Chandrakasan, A.P. (2007) *An energy-efficient OOK transceiver for wireless sensor networks.* IEEE JSSC, vol. 42, No. 3. pp. 2-3

Dong, K., Jia, B., Yu, C., Dong, W., Du, F. & Liu, H. (2013) *Microbial fuel cell as Power supply for implantable medical devices: Anovel configuration design for simulating colonic environment.* Biosensors and Bioelectronics, vol. 41, pp. 916–919

Dupont Teflon PTFE properties handbook. Available online at: http://www.rjchase.com/ptfe_handbook.pdf (Accessed 14 April 2016)

FCC online table of frequency allocations (2014) Available online at: http://transition.fcc.gov/oet/spectrum/table/fcctable.pdf (Accessed 14 April 2016)

Fisher Scientific; heating magnetic -stirrer FB1500. Available online at: http://akribis.co.uk/fisher-scientific-magnetic-stirring-hotplate-fb15001.html. (Accessed 20 May 2016)

FuelCellsEtc. Available online at: http://fuelcellsetc.com/store/ (Accessed 22 May 2016)

Fuel Cell Store. Available online at: http://fuelcellstore.com/fuel-cell-components/gas-diffusion-electrode/03-ptc-cloth-electrode. (Accessed 22 May 2016)

Gollakota, S., Hassanieh, H.AL, Ransford, B., Katabi, D. & Fu, K. **(**2011) *IMD Shield: Securing Implantable Medical Devices.* Avaliable online at: http://groups.csail.mit.edu/netmit/IMDShield/ (Accessed 22 May 2016)

Gollakota, S., Hassanieh, H., Ransford, B., Katabi, D. & Fu, K. (2011) *They Can Hear Your Heartbeats: Non-Invasive Security for Implantable Medical Devices.* Massachusetts Institute of Technology.

GOV.UK (2013) *Custom-made medical devices* - Medicines, medical devices and

blood regulation and safety – guidance. Medicines and Healthcare products Regulatory Agency. Available online at: https://www.gov.uk/government/uploads/system/uploads/attachment_data/file/398428/Custom_made_devices.pdf (Accessed 14 May 2016)

Guerra-Balcázara, M., Cuevas-Muniz, F.M., Álvarez-Contrerasc, L., Arriaga, L.G. & Ledesma-García, J. (2012) Evaluation of bimetallic catalyst PtAg/C as a glucose-tolerant oxygen reduction cathode. Elsevier, Journal of Power Sources, vol. 197, pp. 121-124

Gupta, S.K. & Sinha, P. (2014) *Overview of wireless sensor network: a survey*., International Journal of Advanced Research in Computer and Communication Engineering (IJARCCE), vol.3, pp. 5201-5207

Hached, S., Trigui, A., Khalloufi, I. El, Sawan, M. Loutochin, O. & Corcos, J. (2014) *A Bluetooth-based Low-energy Qi-compliant Battery Charger for Implantable Medical Devices.* IEEE ISBB, pp. 1-4.

Haider, M.R., Islam, S.K., Mostafa, S., Zhang, M. & Oh, T. (2010) *Low-Power Low-Voltage Current Readout Circuit for Inductively Powered Implant System.* IEEE Transactions on Biomedical Circuits And Systems, vol. 4, no. 4, pp 205

Halámková, L. (2012) *Cyborg snail produces electricity.* American Chemical Society. Avaliable online at: http://phys.org/news/2012-03-cyborg-snail-electricity.html (accessed 14 April 2016)

Han, Y., Yu, C. & Liu, H. (2010) *A microbial fuel cell as power supply for implantable medical devices.* Biosensor Bioelectronics, vol. 25, pp. 2156-60

Hareland, S.A. & Radtke, L.P. (2013) *Prognostic Opportunities and Limitations in Implantable Medical Devices.* IEEE PHM, pp. 1-7.

Hogg, A., Uhl, S., Feuvrier, F., Girardet, Y., Graf, B., Aellen, T., Keppner, H., Tardy, Y. & Burger, J. (2014) *Protective multilayer packaging for long-term implantable medical devices.* Elsevier, Surface & Coatings Technology, vol. 255, pp. 124–129.

Hussein, L., Rubenwolf, S., Stetten, Fvon., Urban, G., Zengerle, R., Krueger, M. & Kerzenmacher, S. (2011) *A highly efficient buckypaper-based electrode material for mediatorless laccase-catalyzed dioxygen reduction.* Biosensors and Bioelectronics, vol. 26, pp. 4133-4138

Infinite Power Solutions. Available online at: http://www.cytech.com/products-ips (Accessed 23 May 2016)

Ivanov, I., Vidaković-Koch, T. & Sundmacher, K. (2010) *Recent Advances in Enzymatic Fuel Cells: Experiments and Modeling.* MDPI, Energies, vol. 3, pp. 803-846

Jiang, Z., Pajic, M. & Mangharam, R. (2011) *Cyber-Physical Modeling of Implantable Cardiac Medical Devices.* Proceedings of the IEEE, vol. 100 , pp. 122 -137.

Joung, Y.H. (2013) *Development of Implantable Medical Devices: From an*

Engineering Perspective. International Neurourol Journal, vol. 17. pp. 98-106.

Justin, G.A., Zhang, Y., Sun, M., & Sclabassi, R. (2004) *Biofuel Cells: A possible power source for implantable electronic devices.* IEEE, IEMBS, vol. 2, pp. 4096-4099

Kerzenmacher, S., Ducree, J., Zengerle, R. & Stetten, F.von (2008) *An abiotically Catalysed glucose fuel cell for powering medical implants: Reconstructed manufacturing protocol and analysis of performance.* Elsevier, Journal of Power Sources, vol. 182, pp. 66-75

Kerzenmacher, S., Ducre, J., Zengerlea, R. & Stettena, F. von (2008) *Energy harvesting by implantable abiotically catalyzed glucose fuel cells.* Journal of Power Sources, vol. 182, pp.

Kerzenmacher, S., Kräling, U., Metz, T., Zengerle, R., , F.von (2011) *A potentially implantable glucose fuel cell with raney-platinum film electrodes for improved hydrolytic and oxidative stability.* Elsevier, Journal of Power Sources, vol. 196, pp. 1264-1272

Kerzenmacher, S., Kräling, U., Schroeder, M., Brämerc, R., Zengerle, R. & Stetten, F.von (2010) *Raney-platinum film electrodes for potentially implantable glucose fuel cells. Part 2: Glucose-tolerant oxygen reduction cathodes.* Elsevier, Journal of Power Sources, vol. 195, pp. 6524-6531

Kerzenmacher, S., Schroeder, M., Brämerc, R., Zengerle, R., Stettena, F.von (2010) *Raney-platinum film electrodes for potentially implantable glucose fuel cells. Part 1: Nickel-free glucose oxidation anodes.* Elsevier, Journal of Power Sources, vol. 195, pp. 6516–6523

Khan, W., Muntimadugu, E., Jaffe, M. & Domb, A.J. (2014) *Implantable Medical Devices.* Springer, *pp. 33-59.*

Kiani, M. & Ghovanloo, M. (2012) *Pulse Delay Modulation (PDM) A New Wideband Data Transmission Method to Implantable Medical Devices in Presence of a Power Link.* IEEE Biomedical Circuits and Systems Conference (BioCAS), pp. 256-259.

KIETMA (2013) *Keithley Instrumentation for Electrochemical Test Methods and Application.* Tektronix. Available online at: www.tek.com/dl/KI%2520eChem%2520Methods_ApplicationsAppNote_0.pdf (Accessed 14 April 2016)

Kjeanga, E., Djilali, N. & Sintona, D. (2009) *Microfluidic fuel cells: A review.* Elsevier, Journal of Power Sources, vol. 186, pp. 353-369

Kloke, A., Biller, B., Kräling, U., Kerzenmacher, S., Zengerle, R. & Stetten, F.von (2011) *A single layer glucose fuel cell intended.* Fuel Cells, WILEY-VCH, vol. 11, pp. 316-326

Lasanen, K. & Kostamovaara, J. (2005) *A 1-V Analog CMOS Front-End for Detecting QRS Complexes in a Cardiac Signal*. IEEE Transactions on Circuits And Systems, vol. 52, No. 12, pp. 2584 – 2594

Liang, Z., Chen, W., Liu, J., Wang, S., Zhou, Z., Li, W., Sun, G., Xin, Q. (2004) *FT-IR Study of the microstructure of Nafion membrane*. Journal of Membrane Science, vol 233, pp. 39–44

Marques, M.P.C. & Fernandes, P. (2011) *Microfluidic Devices: Useful Tools for Bioprocess Intensification.* MDPI, *Molecules, vol. 16, pp.* 8368-8401

Marusak, R.A., Doan, K. & Cummings, S.D. (2007) *Introduction to cyclic voltammetry*. Wiley, Integrated Approach to Coordination Chemistry: An Inorganic Laboratory Guide, pp. 235-240

Martinez-Catala, R.V. & Barrett, J. (2009) *A Modular Wireless Sensor Platform with Fully Integrated Battery*. IEEE Transactions on Components and Packaging Technologies, vol 32, Issue 3, pp. 617 – 626

McDonald, J., Dean, S., Niewolny, D., Garcia, D., Chhabra, N. & Chang, L. (2011) *Integrated Circuits for Implantable Medical Devices.* Freescale Solutions for the Medical Market, pp. 1-8.

MEDDEV (2010) *Medical devices: guidance document.* European commission dg health and consumer. 2. 4/1 Rev. 9, pp. 1-51.

Meng, E. & Sheybania, R. (2014) *Insight: implantable medical devices.* The Royal Society of Chemistry, vol. 14, pp. 3233–3240.

Microchip 10F222 microcontroller datasheet. Available online at: http://www.farnell.com/datasheets/1669382.pdf (Accessed 14 April 2016)

Microchip 16F1827 microcontroller datasheet. Available online at: http://ww1.microchip.com/downloads/en/DeviceDoc/41391D.pdf (Accessed 14 April 2016)

Microchip MCP9700 Thermistor datasheet. Available online at: http://ww1.microchip.com/downloads/en/DeviceDoc/21942e.pdf (Accessed 14 April 2016)

Mohseni, P. and Najafi, K. (2004) *Wireless Multichannel Biopotential Recording Using An Integrated FM Telemetry Circuit*. IEEE, IEMBS 26th Annual International Conference, vol. 2, pp. 4083-4086

Mousavi, M.R., Chamanian, S., Ahadzadeh, I., Bahrami, M. & Hosseini, M.G. (2011) *Fabrication and simulation of implantable glucose fuel cell.* IEEE Computer Society, 21st International Conference on Systems Engineering, pp. 315-318

National patient Safety Agency (2008) *Approval for medical devices research.* Health Research Authority, National Research Ethics Services. Available on line: http://www.hra.nhs.uk/documents/2013/09/approval-of-medical-devices-research-version-2-april-2008.pdf (Accessed 22 May 2016)

Niederländer, C., Wahlster, P., Kriza, C. Kolominsky-Rabas, P. (2013) *Registries of*

implantable medical devices in Europe. Elsevier, Health Policy, vol. 113, pp. 20-37.

Olivo, J., Carrara, S. & Micheli, G.De (2011) *Biofuel cells and inductive powering as energy harvesting techniques for implantable sensors.* Science of Advanced , vol. 3, pp. 420-425

Olivo, J., Carrara, S. & Micheli, G.De (2011) *Energy harvesting and remote powering for implantable biosensors*. IEEE Sensors journal., vol. 7, pp. 1573-1586.

Oncescu, V. & Erickson, D. (2011) *A microfabricated low cost enzyme-free glucose fuel cell for powering low-power implantable devices*. Journal of Power Sources, vol 196, pp. 9169- 9175

Oncescu, V. & Erickson, D. (2012) *High volumetric power density, non-enzymatic, Glucose fuel cells.* Scientific Reports, vol. 3, pp. 1-6

Pan, C., Fang, Y., Wu, H., Ahmad, M., Luo, Z., Li, Q., Xie, J., Yan, X., Wu, L., Wang, Z.L. & Zhu, J. (2010) *Generating electricity from biofluid with a nanowire-based biofuel cell for self-powered nanodevices.* Advance Material, vol. 22, pp. 5388–5392

Pan, C., Li, Z., Guo, W., Zhu, J. & Wang, Z.L. (2011) *Fiber-Based Hybrid Nanogenerators for/as Self-Powered Systems in Biological Liquid.* Wiley-VCH, Angew. Chem. Int., vol. 50, pp. 11192 –11196.

Pan, C., Wu, H., Wang, C., Wang, B., Zhang, L., Cheng, Z., Hu, P., Pan, W., Zhou, Z., Yang, X &, Zhu, J. (2008) *Nanowire-based high-performance. Micro fuel cells: One nanowire, one fuel cell.* Advanced Materials, vol. 20, pp. 1644-1648

Peisino, M. (2013) *Deeply implanted medical device based on a novel ultrasonic telemetry technology*. Thesis No 5730. Suisse, pp. 1-122.

QAM TX3 transmitter module datasheet. Available online at: http://www.farnell.com/datasheets/54127.pdf (Accessed 20 May 2016)

Rabaey, J.M., Ammer, J., Karalar, T,. Suetfei, L., Otis, B., Sheets, M. & Tuan, T. (2002) *PicoRadios for wireless sensor networks: The next challenge in ultra-low power design*. IEEE *International,* Solid-State Circuits Conf., vol. 1, pp. 200–201

Rapoport, B.I., Kedzierski, J.T. & Sarpeshkar, R. (2012) *A glucose fuel cell for implantable brain–machine interfaces*. PLoS one, vol. 7, pp. 1-15.

Reid, P.P., Compton, W.D., Grossman, J.H. & Fanjiang, G. (2005) Building a better delivery system: a new engineering/health care partnership. Available online at: http://www.nationalacademies.org/onpi/030909643X.pdf. (Accessed 22 May 2016)

RFM12B Transceiver datasheet. Available online at: http://www.hoperf.com/upload/rf/RFM12B.pdf (Accessed 14 April 2016)

Rouf, H.K., Costen, F. & Garcia, S.G. (2009) *3D Crank-Nicolson finite difference time*

domain method for dispersive media. ELECTRONICS LETTERS, Vol. 45, No. 19, pp. 1-2

RS232 Serial port to TTL converter MAX3232, 3V adapter datasheet. Available online at: http://datasheets.maximintegrated.com/en/ds/MAX3222-MAX3241.pdf (Accessed 14 April 2016)

Sagan, D. (2007) *RF integrated circuits for medical applications: meeting the challenge of ultra-low power communications*," Available online at: http://stf.ucsd.edu (Accessed 22 May 2016)

Schmidt, C.L. & Scott, E.R. (2011) *Energy Harvesting and Implantable Medical Devices.* IEEE International Electron Devices Meeting, pp. 243-246.

Sharma, T., Hu, T., Gopal, A., Stoller, M., Lin, K., Ruoff, R.S., Ferrari, M. & Zhang, X. (2009) *Nanoporous silica as membrane for implantable ultra-thin biofuel cells.* Power MEMS, vol. 1, pp. 522-525

Stetten, F.Von, Kerzenmacher, S., Lorenz, A., Chokkalingam, V., Miyakawa, N., Zengerle, R. & Ducrée, J. (2006) *A one-compartment, direct glucose fuel cell for powering long-term medical implants.* MEMS, vol. 1, pp. 934-937

Tao, H., Hwang, S.W., Marelli, B., An, B., Moreau, J.E., Yang, M., Brenckle, M.A., im, S., Kaplan, D.L., Rogers, J.A. & Omenetto, F.G. (2015) *Fully implantable and resorbable wireless medical Devices for postsurgical infection abatement.* IEEE, MEMS, pp. 168-171.

THINERGY™ MEC225, Solid-State, Flexible, Rechargeable Thin-Film Micro-Energy Cell. Preliminary Product Data Sheet. Available online at: http://datasheet.octopart.com/MEC225-1P-Infinite-Power-Solutions-datasheet-11041087.pdf (Accessed 23 May 2016)

Typical properties of Acetal. Available online at: http://www.wshampshire.com/pdf/psg_acetal.pdf (Accessed 14 April 2016)

Vaddirajua, S., Tomazosb, I., Burgessc, D.J., Jain, F.C. & Papadimitrakopoulos, F. (2010) *Emerging synergy between nanotechnology and implantable biosensors: A review.* Biosensors and Bioelectronics 25, pp. 1553–1565.

Van, H.C.N. (2012) *Implantable Miniaturized Glucose Fuel Cell.* MSc Thesis. Dept. Electrical Engineering and Computer Sciences, University of California, Berkeley, USA

Villafuerte, F.L., Schiller, J.H., Rodríguez, E.T., Ramirez, M. & Valdemar, E. (2008) *Evaluating parameters for localisation in wireless sensor networks: a survey*, Guadalajara University, Mexico

Wang, X., Liu, J., Song, J. & Wang, Z.L. (2007) *Integrated Nanogenerators in Biofluid.* American Chemical Society, Nano Letters, vol. 7, pp. 2475-2479

Wei, J., Liang, P. & Huang, X. (2011) *Recent progress in electrodes for microbial fuel cells.* Elsevier, Bioresource Technology, vol. 102, pp. 9335-9344

Wei, X. & Liu, J. (2008) *Power sources and electrical recharging strategies for Implantable medical devices*. Frontiers of Energy and Power Engineering in China, vol.2, no.1, pp.1-13

Werber, D., Schwentner, A., & Biebl, E.M., (2006) *Investigation of RF transmission properties of human tissues:* Advances in Radio Science, 4, 357–360.

Werner, C. (2003) *Analyst reports medical device market flourishes. Available online at:* http://findarticles.com/p/articles/mi_m0BPC/is_4_27/ai_100484234/ (Accessed 22 May 2016)

WHO (2004) World health organisation. *The global burden of disease*. Available online at: www.who.int/healthinfo/global_burden_disease/GBD_report_2004update_full.pdf (Accessed on 22 May 2016)

Xie, J., Wang, S., Aryasomayajula, L. & Varadan, V.K. (2007) *Platinum decorated carbon nanotubes for highly sensitive amperometric glucose sensing*. Nanotechnology, vol 18, no. 6, pp. 1-9.

Yakovlev, A., Kim, S. & Poon, A. (2012) *Implantable Biomedical Devices: Wireless Powering and Communication.* IEEE Communications Magazine, pp. 152-159.

Appendices

Appendix A: Microcontroller, hardware and software development bench

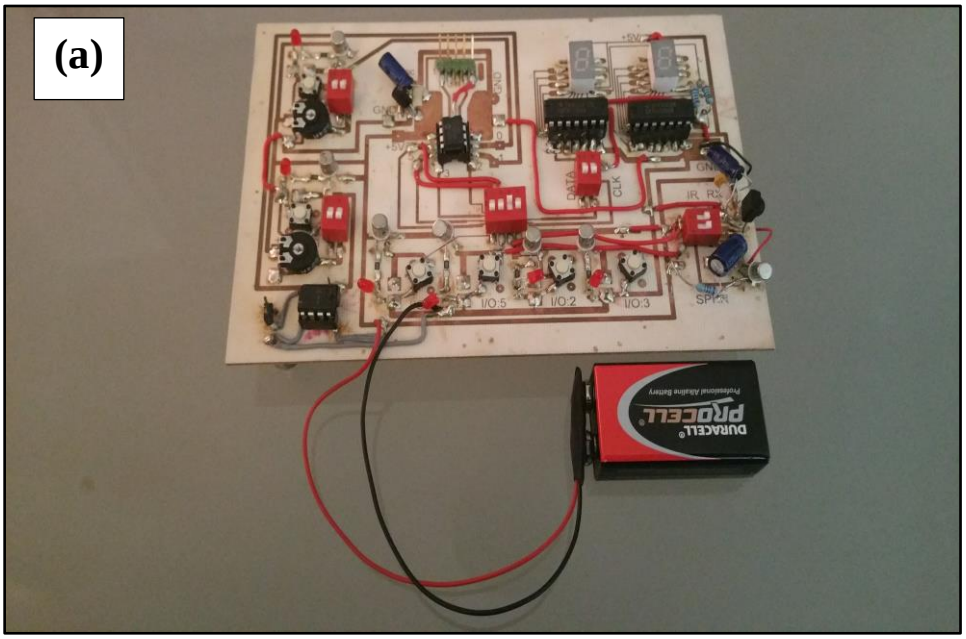

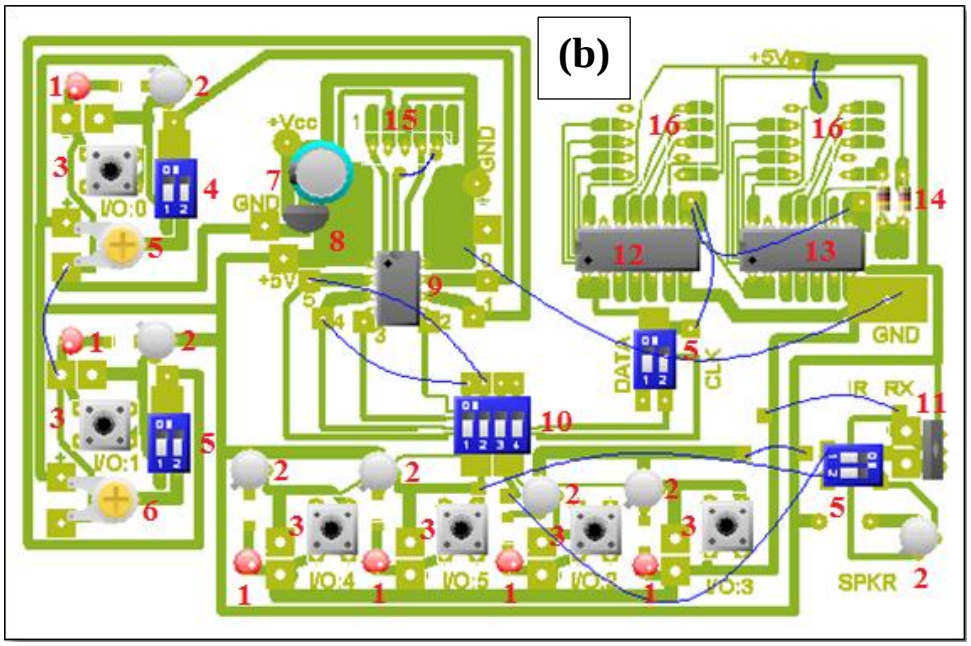

A: PIC microcontroller Testing Bench for hardware development including current consumption and communication protocols – (a) picture view and (b) PCB illustration: (1) LEDs, (2) transistors, (3) push buttons, (4) x2 switches, (5 and 6) variable resistors, (7) capacitor, (8) voltage regulator,(9) Microchip, (10) x4 switches, (11) infrared receiver, (12 and 13) 7-Segment chip register, (14) resistors, (15) PIC programming connections, (16) 7-segments display. (17), (18) with Infrared transceiver and Seven-Segment Display testing board.

Appendix B: Clock-less microcontroller based implant system

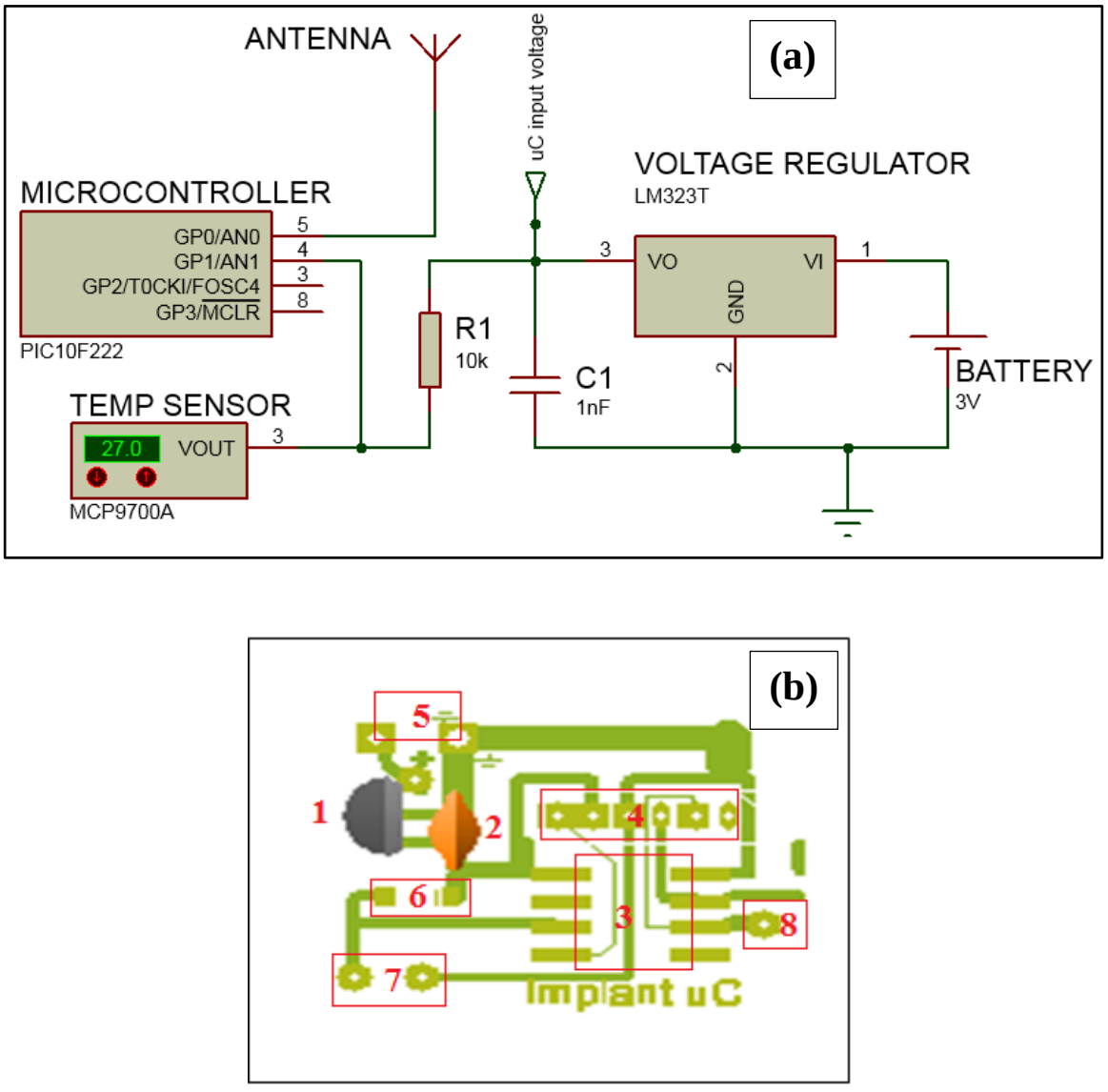

B1: Microcontroller based implant transmitter without an oscillator – (a) *Schematic illustration, (b) PCB designs: (1) voltage regulator, (2/C1) capacitor, (3) PIC10F222 Microcontroller, (4) PIC programming connections, (5) battery supply, (6/R1) resistor, (7) MCP9700 temperature sensor, (8) antenna.*

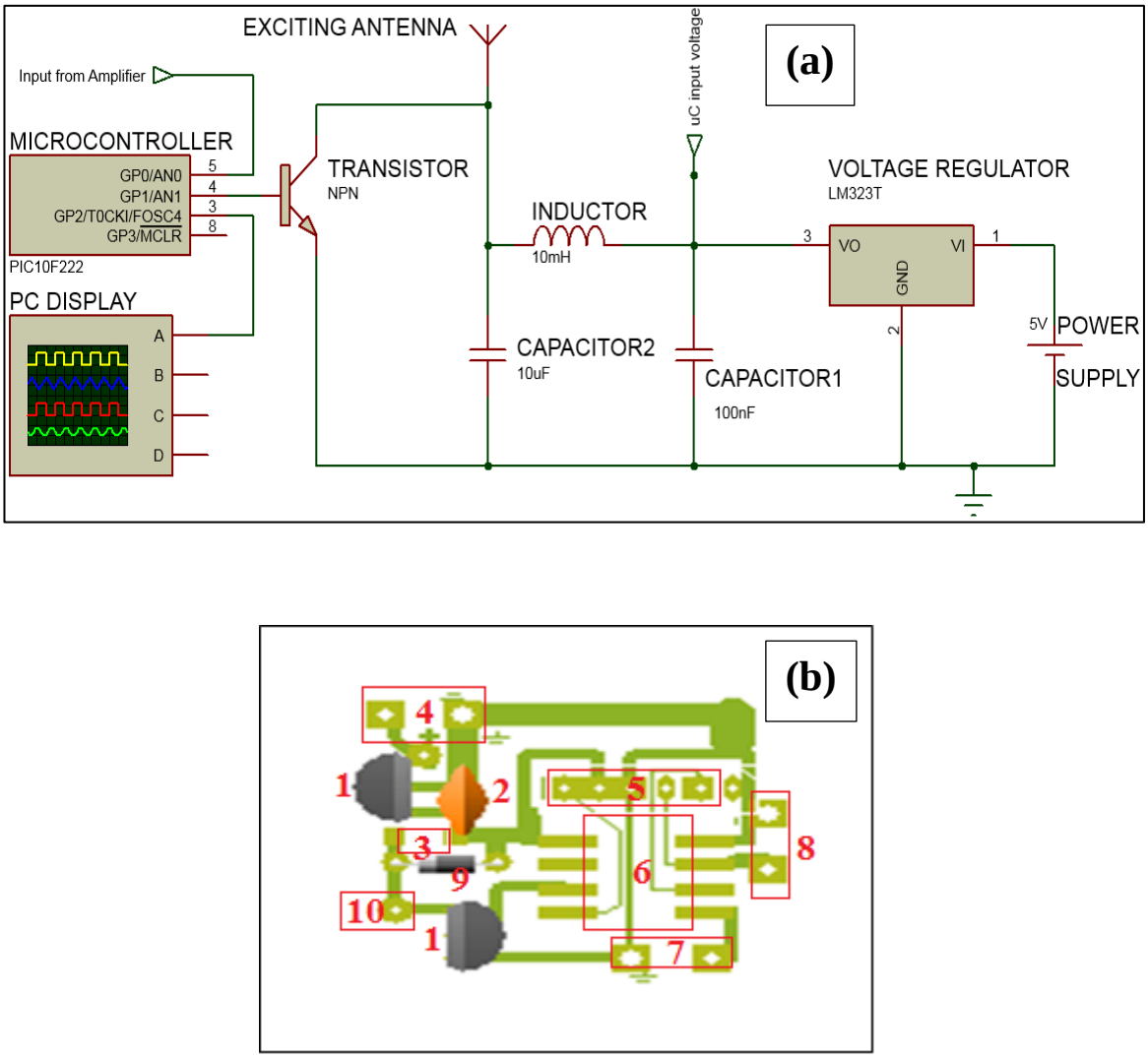

B2: Microcontroller based receiver – (a) Schematic illustration, (b) PCB designs: (1) voltage regulator, (2) capacitor 1, (3) capacitor 2, (4) battery supply, (5) PIC programming connections, (6) PIC10F222 Microcontroller, (6/R1) resistor, (7) RS232 output to PC, (8) switches.

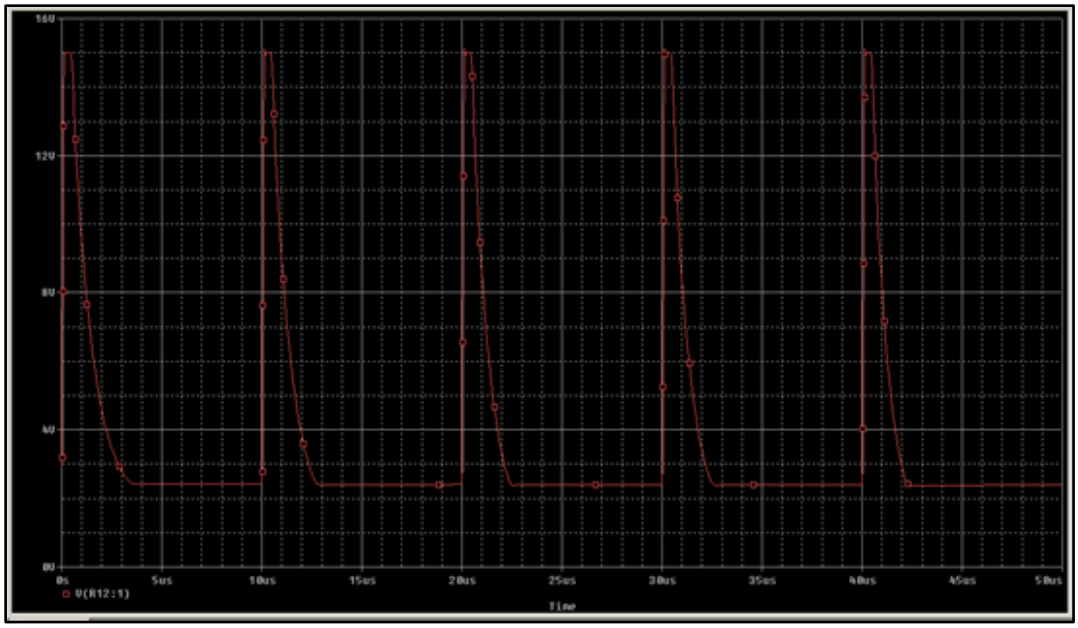

B3: OrCad Cadence; simulated pulse amplifier response to an input pulse that is 0.1uS wide and 15V peak.

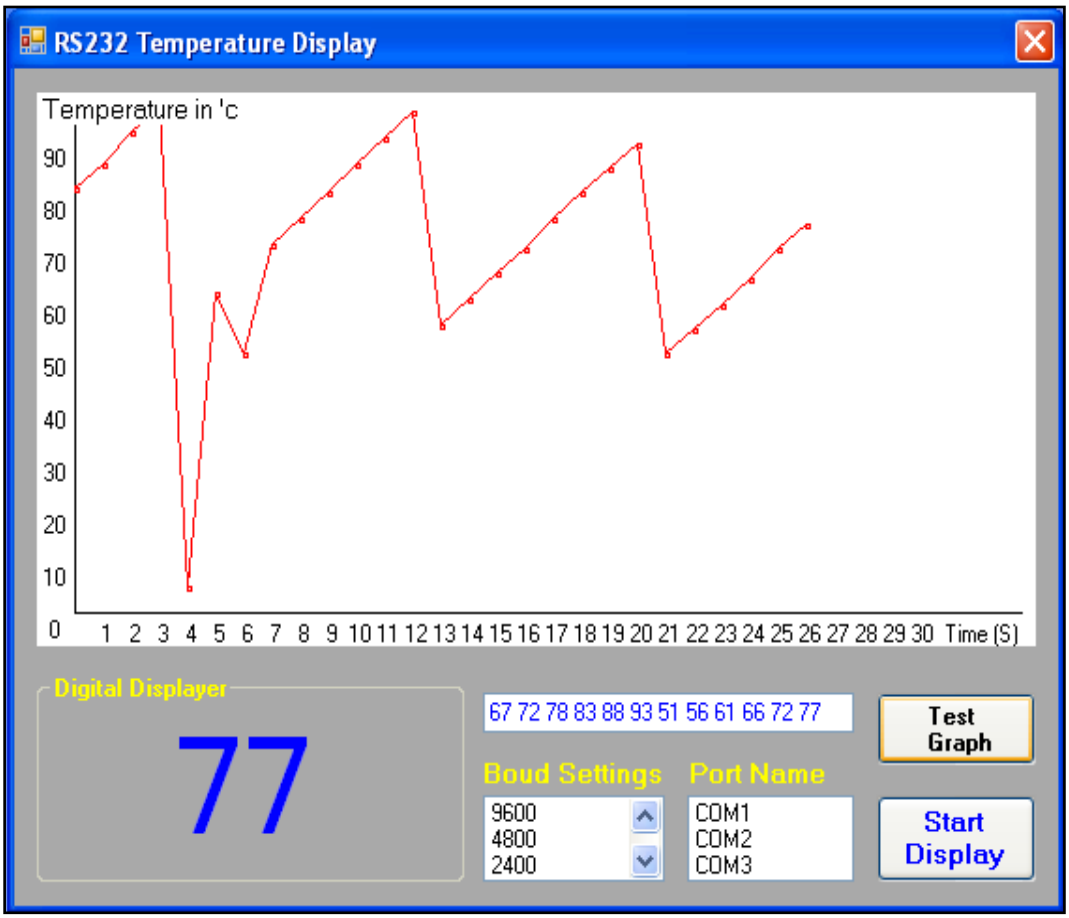

B4: Visual basic graphic (own design and written own codes) for displaying temperature data from the implant microcontroller without an oscillator.

Appendix C: QAM and RFM12B based systems

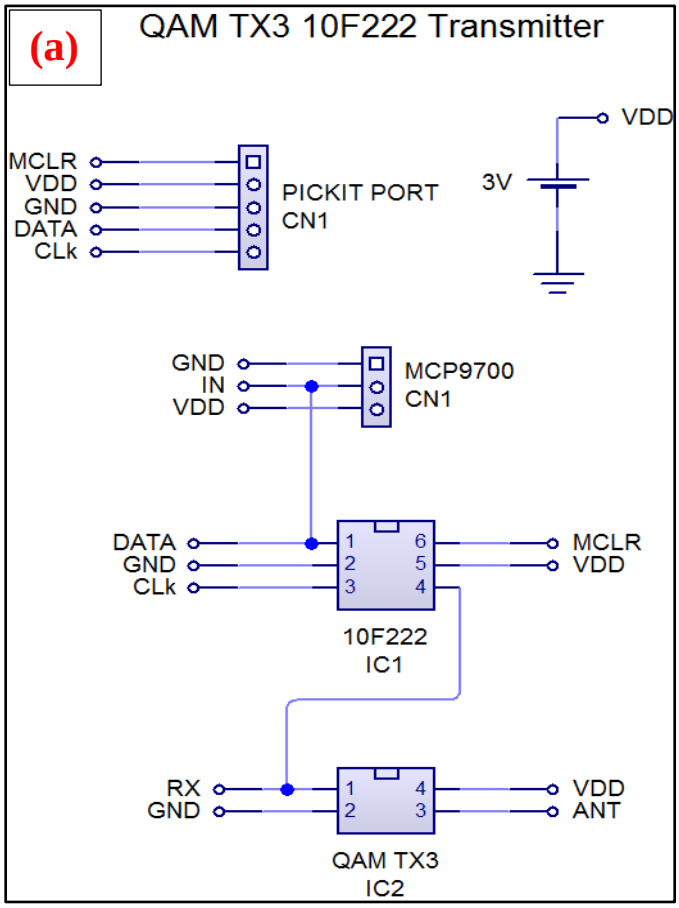

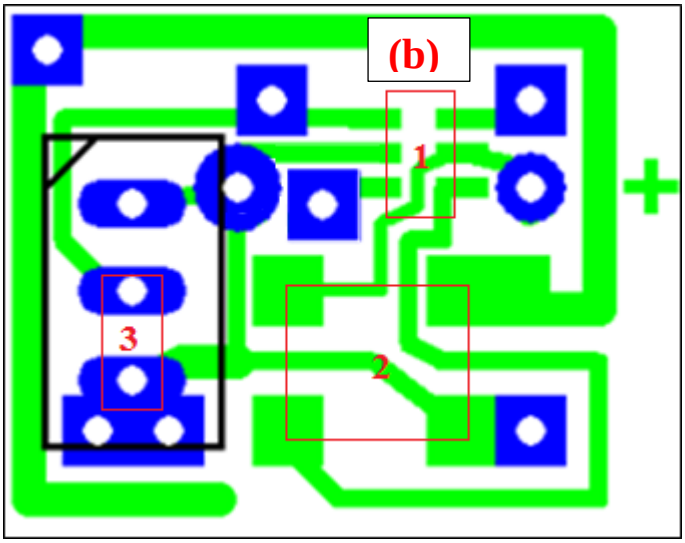

C1: QAM based implantable microcontroller Transmitter – (a) QAM Transmitter circuit Schematic illustration, (b) PCB design: (b) (PICIT port) PIC programming connections, (3V) battery supply, (10F222 / 1) PIC Microcontroller, (QAM3 / 2) transmitter module, (MCP9700 / 3) temperature sensor.

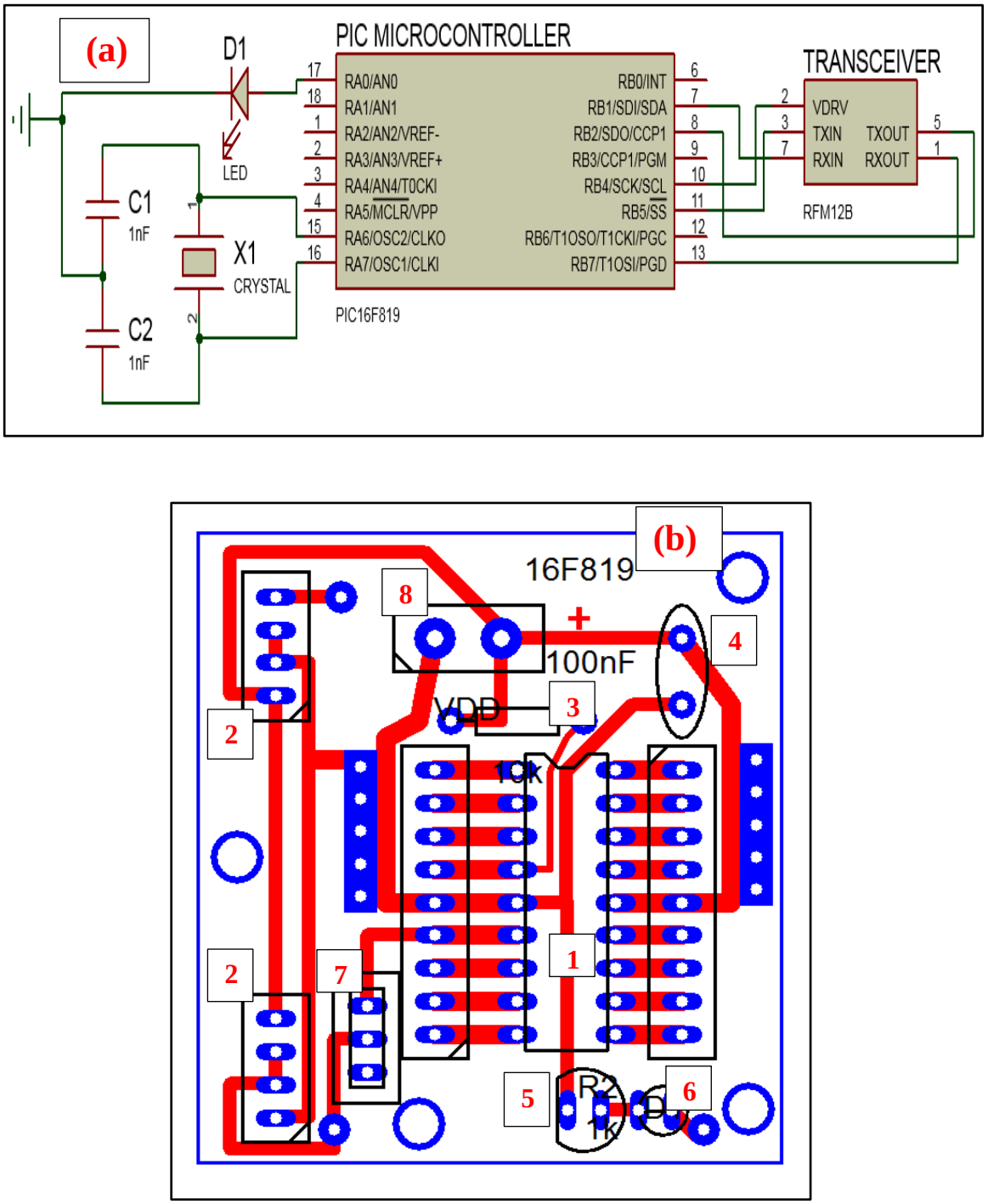

C2: Receiver based 16F819 Microcontroller – (a) Schematic illustration with hidden power supply connections), (b) PCB design: (1) PIC16F819 Microcontroller, (2 / RFM12B) transceiver module, (3) resistor 1, (4 / C2) capacitor 2, (5) resistor 2, (6 / D1) LED 1, (7) switch, (8) power supply, (C1 and C2) capacitors for oscillator, (X1) external oscillator (optional).

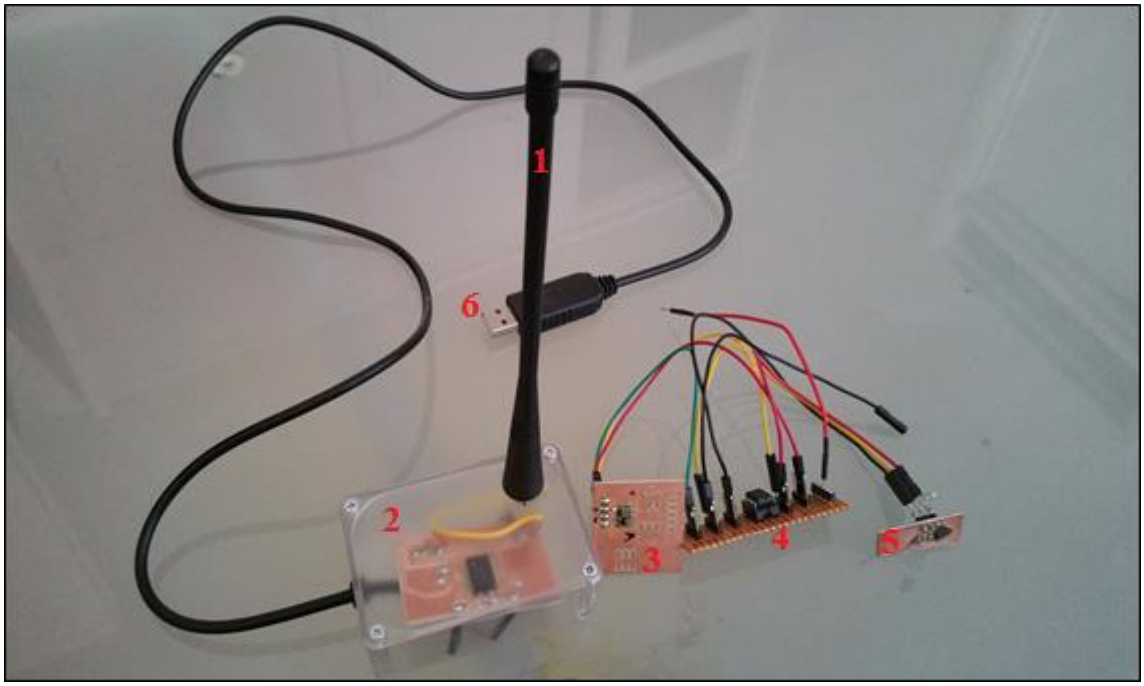

C3: Picture of a Bio-Sensing Platform with wireless microcontroller transmitter and a microcontroller receiver with USB interface for PC communication. (1) Receiver antenna, (2) Receiver based 16F819 Microcontroller with RFM12B transceiver module, (2) QAM3 transmitter module, (4) PIC10F222 Microcontroller, (5) MCP9700 temperature sensor, (6) USB connection for PC interface.

The working PIC10F222 microcontroller with QAM3 transmitter and MCP9700 temperature sensor components where later built on a single board and tested as a Self-Powered Bio-Sensing Device with Energy Harvesting solution using GFC system.

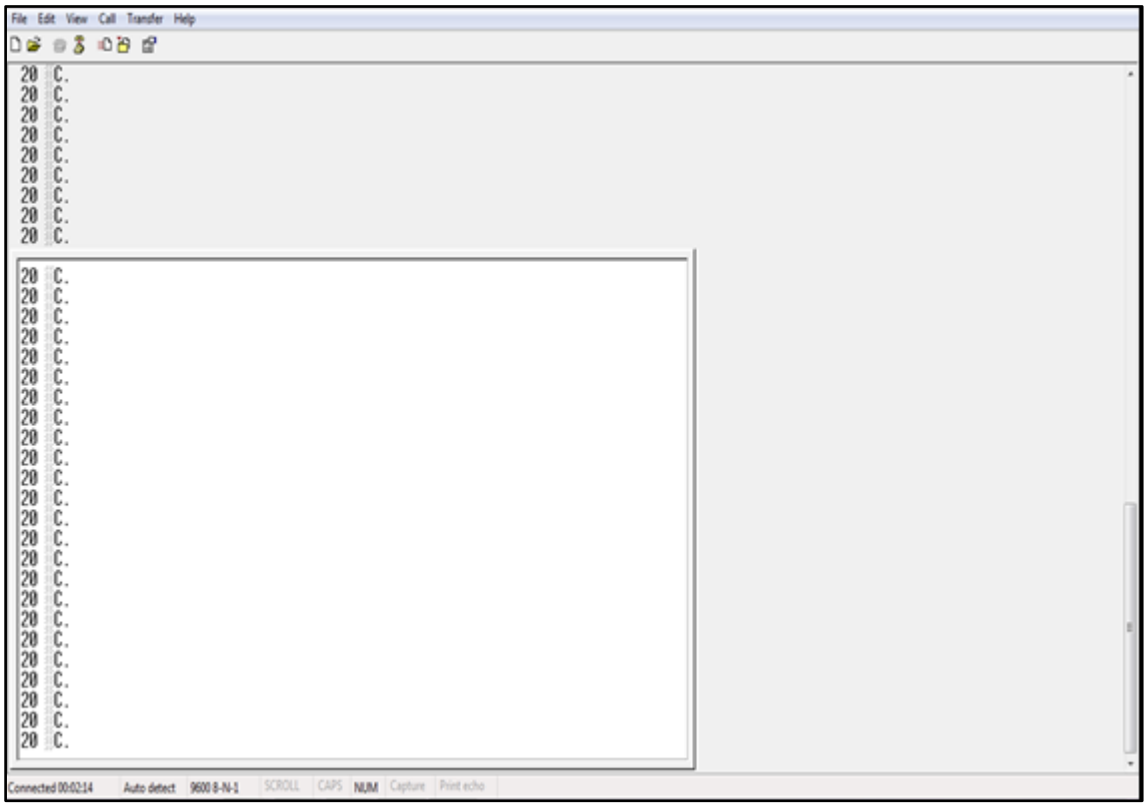

C4: Hyper Terminal print screen shot of sensed temperature data received from the 16F819 Microcontroller based system with the RFM12B transceiver, displaying data sent by the QAM TX3 transmitter systems, demonstrating constant room temperature accurately.

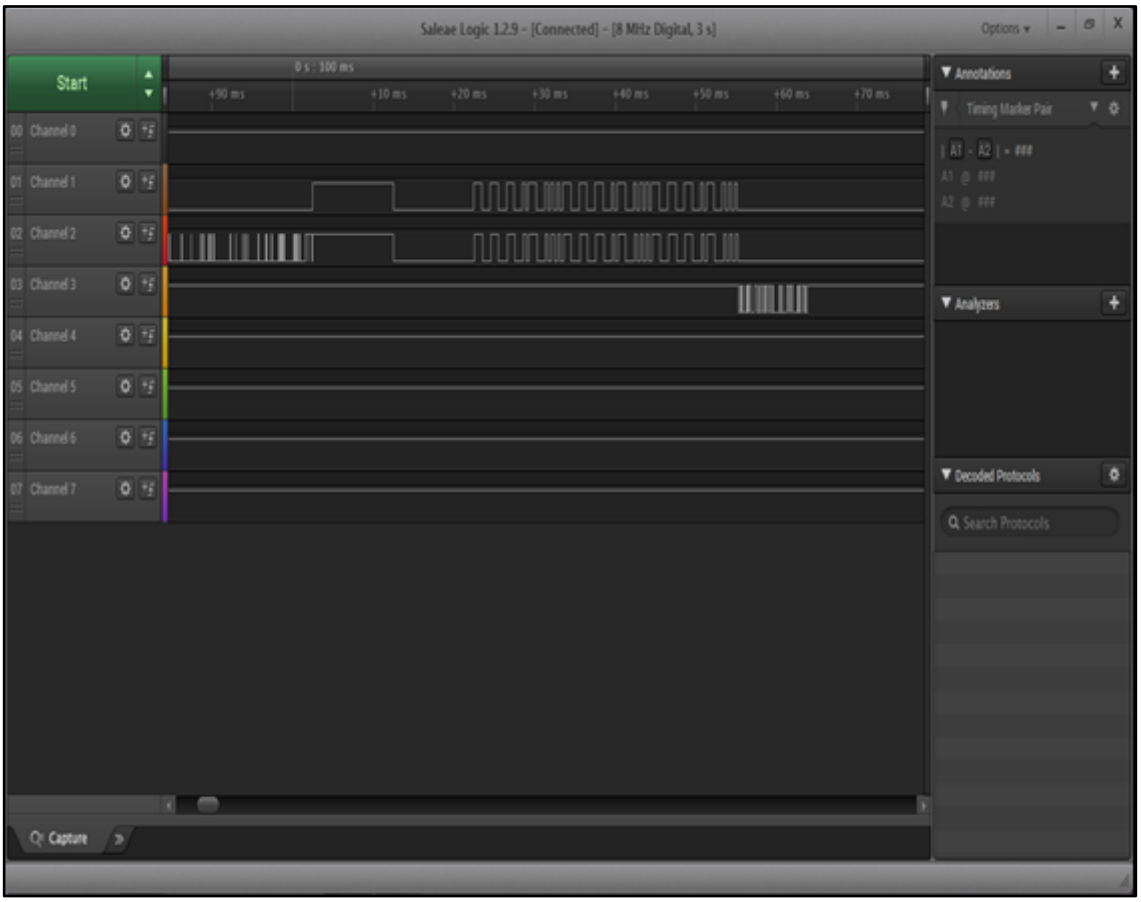

C5: Saleae logical analyser programme displaying and validating the sensed data values from the transmitter circuit (channel 1 - brown), the receiver circuit (channel 2 - Red) and then the output from the receiver circuit to a PC HyperTerminal display (channel 3 - Orange).

Appendix D: C programming code

D1: Test Bench programming code

```
#bit DATAPIN = GPIO.5          //Setup Data and Clock pins
#bit CLOCKPIN = GPIO.4          //const int

character[16]={191,160,118,94,204,218,250,14,255,206,238,248,178,124,242,226};//LE
D character map

void Clockit(){                //Pulse the Clock pin (to shift data in).
                                    CLOCKPIN=1;              //
                                    CLOCKPIN=0;              //
                                                }
                              void ClearLEDS(){              //Blank the LEDs
                                                int c;                  //
                                                c = 7;                  //
                                                while(c > 0){           //
                                                  Clockit();            //
                                                    c--;                //
                                                      }
                                                }
  void DisplayNibble(int value){      //Display a byte on one 7SegLED - 'value' holds the
                                                byte to be displayed
                                                  int b,c;              //
         b = character[value & 0x0f];   //This maps half the byte to be turned into an
                                                alphanumeric character
                                                  c=7;                  //
                                                while(c > 0)   {        //
                                                  if (bit_test(b, 1))   //
                                                  DATAPIN=1;            //
                                                    else                //
                                                  DATAPIN=0;            //
                                                  Clockit();            //
                        b = b >> 1;              //Serially shift data bits into the register
                                                    c--;                //
                                                  }                     //
                                                        }
      void Display(int value){         //'value' must be an integer (a byte) from 0 to 255
                                              DisplayNibble(value);         //
    swap(value);               //This swaps the nibbles in the byte so that each is processed in
                                                        turn
                                              DisplayNibble(value);         //
}


const int character[10]={4,5,6,7,8,9,10,11,12,13};
```

```
void DisplayNibble(int value){ //Display a byte on one 7SegLED - 'value' to be displayed
        int b,c;                //
        b = character[value & 0x0f];    //This maps half the byte to be turned into an
        alphanumeric character
  c=0;
while(c < b){           // stay here while c is less than b

if ((c==0)||(c==b-1)){
output_high(LED);
output_low(LED);
output_high(data);
output_low(data);
     }
c++;
  }
}
void Temperature(int value){        //'value' must be an integer (a byte) from 0 to 255
  DisplayNibble(value);       //
  swap(value);              //This swaps the nibbles in the byte so that each is processed in
turn
  DisplayNibble(value);       //
}
void main(){

float read, temp;

  SETUP_ADC_PORTS(sAN3 | VSS_VDD);      //Sensor on pin 4 with VSS and VDD
as references
  setup_ADC(ADC_CLOCK_INTERNAL);     //Use internal ADC clock
//  INT_PERIPHERAL=1;             //Turn on ADC interrupt
  SET_ADC_CHANNEL(3);           //AN3 channel is 3

#use fast_io(a)
SET_TRIS_a( 0x1A );       //Set PIN3 and PIN1 as an input all others as outputs

while(1){
output_high(sensor);
  read = read_adc();        //read analog input
  temp=((-506.13*read)+297.9);        //convert to degC
      Temperature(temp);        //Display the value in 'count'
       delay_ms(200);        //Wait 200mS
   }
}
```

D2: Transmitter and Receiver programming code

```
#include <10F222.h>
#fuses NOMCLR, NOPROTECT, IOSC8, WDT
#use delay(clock=8000000)

#define ONE_WIRE_PIN PIN_B0          //Define 1Wire pin before
#define RFPIN PIN_B1              //Define RF TX pin

#include "QAM_3byte.h"
#include "ds1820.h"               //calling ds1820 driver

void ADCOFF(){
SETUP_ADC_PORTS(NO_ANALOGS);
SETUP_ADC(ADC_OFF);
}

void main(){
output_low(RFPIN);
setup_wdt(WDT_1152MS);
ADCOFF();

  while(1){
    ds1820_read();                        //Read sensor and stash bytes in Temp_MSB and
Temp_LSB
    Temp_LSB=Temp_LSB>>1;                 //Get rid of half deg bit
    if(Temp_MSB==0xff) bit_set(Temp_LSB,7);       //Set MSBit if MSByte is negative
(- temp)
      else bit_clear(Temp_LSB,7);         //or clear it (+ temp)
    sendPacket(Temp_LSB);           //Send temperature 3 times
    sleep();
    delay_us(1);
  }
}
```

D3: Transmitter and Receiver programming code

```
//QAM RF TX & RX functions

#define pZERO     350                 //Length of Zero pulse in uS
#define pONE    999                  //Length of One pulse in uS
#define pMID    525                  //pZERO + pZERO/2 =Mid point sample time in uS
#define StartBitLength 10             //Length of Start pulse in mS
#define countMin 90                   //(StartBitLength * 10) - 15  = Min length for start bit
test
#define countMax 105                  //(StartBitLength * 10) + 15 = Max length for start bit
test
//#define SAMPLE PIN_A2                 //Sample pin for monitoring

static signed char BRX;                //Byte that stores received Temperature value

//void setupRX();
void sendStartBit();
void sendBit(short n);
void sendByte(unsigned char n);
void sendPacket(unsigned char n);
short RxPacket();
unsigned char RxByte();

/*
Sets up Timer 1 which is needed to detect received pulse widths
void setupRX(){
  setup_timer_1 (T1_INTERNAL | T1_DIV_BY_1);      //1 tic = 1uS with 4 MHz clock
  delay_ms(100);                        //Must use 4 MHz clock or a divisor to ensure
}                                 //1uS tics
*/

//Send a start or header bit
void sendStartBit(){
  output_high(RFPIN);
  delay_ms(StartBitLength);
  output_low(RFPIN);
  delay_ms(StartBitLength);
}

//Send a data bit
void sendBit(short n){
  unsigned long td;
  if(n==0) td=pZERO;
    else td=pONE;
  output_high(RFPIN);
  delay_us(td);
  output_low(RFPIN);
  delay_us(td);
```

```
}


//Send a single byte LSB first
void sendByte(unsigned char n){
  char i;
  for(i=0;i<8;i++) sendBit(Bit_Test(n,i));   //Send all 8 bits
}


//Send a start bit and then the byte three times
void sendPacket(unsigned char n){
  sendStartBit();
  sendByte(n);
  sendByte(n);
  sendByte(n);
}


//Receive data packet
short RxPacket(){
  unsigned char td=0;
  signed char b1, b2, b3;
  while(!input(RFPIN));                  //Wait for first positive transition on RFpin
  while(input(RFPIN)){                   //Count while high
    td++;                          //
    delay_us(91);                        //10 mS is a count of 100
  }

  if((td < countMin) || (td > countMax)) return 0;   //escape function if start pulse < or >
10 mS

  b1=RxByte();                    //Grab all 3 bytes
  b2=RxByte();                    //
  b3=RxByte();                    //

  if((b1==b2)||(b1==b3)){                 //Return b1 if it matches one of the other 2 bytes
    BRX = b1;
    return TRUE;
  }

  if((b2==b1)||(b2==b3)){                 //Return b2 if it matches one of the other 2 bytes
    BRX = b2;
    return TRUE;
  }

  if((b3==b1)||(b3==b2)){                 //Return b3 if it matches one of the other 2 bytes
    BRX = b3;
    return TRUE;
  }
  return FALSE;                         //Return FALSE if at least 2 out of 3 bytes are not
equal
```

```
}

/*

//Receive a data byte
unsigned char RxByte(){
  unsigned long td=0;
  signed char i, value;
  for(i=0;i<8;i++){
    td=0;
    while(!input(RFPIN));                  //Wait for bit to go high
//    output_high(SAMPLE);
    set_timer1(0);
    while(input(RFPIN));
    td = get_timer1();
//    output_low(SAMPLE);
    if(td>pMID)bit_set(value,i);             //Set bit if pulse high time > MID time in uS
      else bit_clear(value,i);
  }
  return value;
}

*/
```

D4: Receiver programming code

```
//Receives temperature sent as 3 equal bytes, LSB first
//Outputs value only if any 2 of 3 bytes match
//Must setup Timer1 to produce a 1uS tic
//Temperature value is returned in static signed char BRX variable

#include <16F819.h>
#fuses INTRC_IO,NOWDT,NOPROTECT,NOMCLR,NOBROWNOUT
#use delay(clock=4000000)
#use rs232(baud=9600, XMIT=PIN_B3, STREAM=PC)            //Setup RS232 here

#define RFPIN PIN_B0                           //Choose RFPIN here
#include "QAM_3byte.h"                          //Include 3 Byte driver file

void main(){
  setupRX();                                 //Called first to setup Timer1 for 1uS tic
  fprintf(PC, "\fReceiving..");
  while(1) if(RxPacket()) fprintf(PC, "\n\r%d °C.", BRX);      //Temperature returned in
static byte BRX
}
```

Appendix E: THINERGY (MEC225) Battery datasheet

Infinite Power Solutions®

THINERGY® MEC225

Solid-State, Flexible, Rechargeable Thin-Film Micro-Energy Cell

DS1014 v1.2 | Product Data Sheet

Features

- Thin Form Factor – 170 µm Thick
- Capacity of 130 µAh
- All Solid-State Construction
- High Discharge Rate Capability
- Ultra-Low Self-Discharge Rate
- Industry-Leading Cycle Life
- Fast Recharge
- RoHS Compatible
- Eco-Friendly/Safe

[actual size]

Applications

- Energy Harvesting Solutions/Self-Powered Systems
- Remote/Autonomously Powered Wireless Sensors
- Memory & Real Time Clock (RTC) Backup
- Semi-Active RFID Tags
- Smart Cards (Including Units with Displays/Biometrics)
- Medical Devices
- High Temperature Applications
- Military/DoD & Aerospace

Benefits

- Lowest Cost of Ownership
  - No maintenance costs
  - Lasts the lifetime of the application
  - Can be recharged and reused over and over
- Ideal energy storage solution for energy harvesting
  - Can be trickle-charged with no memory effect
- Simple constant-voltage recharge with no current limiting required.

Physical Properties

Size:	12.7 mm x 12.7 mm x 0.170 mm [0.5 in x 0.5 in x 0.007 in]
Mass:	125 mg

General Description

The THINERGY® MEC225 is a solid-state, flexible, rechargeable, thin-film Micro-Energy Cell (MEC). This unique device substantially outperforms all other small form factor electrochemical energy storage technologies, including supercapacitors, printed batteries, and other thin-film batteries. The device is fabricated on a metal foil substrate to achieve its flexibility, thin profile, broad operating temperature range, and long life.

The MEC is offered in a unique, patented package design that maximizes the active area of the cell and minimizes the device footprint to deliver the highest energy and power density of any energy storage element of its size and thinness. External terminals in the form of positive and negative nickel-plated tabs are located along the top edge of the cell for easy soldering to printed circuit boards (PCBs). The tabs are supported with a flex circuit for added strength and to keep them planar with the rigid or flex PCBs. Through-holes located in the terminal contacts allow the MECs to be aligned on solder posts for easy connection and cell stacking to create battery modules with higher capacity and current. These tabs also allow easy connection to both terminals from either side of the cell, which is important during automated assembly onto flex circuits and PCBs. The conductive metal tabs allow various connection methods including epoxies, anisotropic conductive film (ACF) materials, and solder. The cells can be oriented to stack in series (to multiply voltage) or in parallel (to multiply capacity and power).

The active materials in the device include a Lithium Cobalt Oxide ($LiCoO_2$) cathode and a Li-metal anode. A solid-state electrolyte called LiPON (Lithium Phosphorus Oxynitride), with its high Li-ion conductivity, is used to provide superior power performance. The extremely low electron conductivity within LiPON results in ultra-low self discharge, making

this technology ideal for applications where energy must be reliably stored for many years without the ability to recharge, or for low-power ambient energy harvesting charging solutions. In addition, this eco-friendly technology contains no toxic chemicals or heavy metals, providing industry-leading safety with absolutely no possibility for chemical leakage, thermal runaway or fire, as experienced with other Li-ion batteries using liquid or gel electrolytes. A proprietary flex-circuit encapsulation methodology is used to achieve the ultra-thin and flexible form factor and to ensure reliability and performance under harsh environmental conditions, far exceeding other micro-energy storage technologies.

The thin form factor, rechargeability, and high discharge rate capability enable applications where conventional coin/button or primary thin batteries are not well suited. Due to its low internal cell resistance, the MEC offers superior charge acceptance, making it an ideal energy storage device for applications where extremely low current recharge sources are available, including various ambient energy harvesting methods. Pulsed or continuous currents as low as 1 µA can be used to effectively recharge this device. The MEC recharges in seconds to minutes, depending on its state of discharge and available charge current.

MECs can be recharged using constant current, constant voltage, pulsed current, or pulsed voltage sources. Any constant voltage (CV) charge greater than cell voltage (not to exceed the maximum specified charge voltage) will result in safe and rapid charging. Unlike conventional lithium ion batteries, MECs do not require temperature monitoring during charge, or current limiting by using a complicated constant-current/constant-voltage (CC/CV) charge algorithm. MECs use a simple CV charge method that is fast and totally safe, regardless of the state of charge. A variety of CV charging methods can be used, such as direct connection to a power supply, wireless recharge via inductive coupling, or energy scavenging solutions that harvest kinetic, solar, RF, magnetic, or thermal energy.

The low self-discharge rate results in decades of shelf life. With its recharge cycle stability, the device offers tens of thousands of recharge cycles for many years of use with no memory effects. The MEC225 provides an extremely safe, reliable, and low-cost energy storage solution that outperforms any other micro-battery or capacitor solution. This component class device is intended to be designed in for the life of the product.

Specifications

Parameter	Options(1)	Rating			Conditions
		Min	Typ	Max	
Capacity(2)	-1	130 µAh			0.05 mA Discharge Rate @ 25°C
Stored Energy(2)	-1	1.8J			
Operating Temperature	All	–40°C		+85°C	(Note 3)
Storage Temperature	All	–40°C		+50°C	
Charge Time:					
to 80% State of Charge	S		15 Min		4.10V constant voltage recharge (min. peak available current of 10 mA)
	P		10 Min		
to 90% State of Charge	S		20 Min		
	P		15 Min		
Max. Continuous Discharge Current (Standard vs. Performance Grade)	S		5 mA		≥25°C
	P		7 mA		
Internal Resistance	S		290Ω		25°C
	P		210Ω		
Cycle Life	-1		100,000		10% depth of discharge with typical application load(4)
			10,000		100% depth of discharge with typical application load(4)
Nominal Output Voltage			3.9V		0.05 mA Discharge Rate @ 25°C
Recharge			4.10V	4.15V	Constant voltage
Shelf Life			15 years		25°C
Discharge Cutoff Voltage(5)		2.1V			For currents of 0.2 mA up to maximum discharge rate
		3.0V			For currents < 0.2 mA
Annual Non-reversible Capacity Loss(6)			1%, 3%, 6%		25°C, 45°C, and 65°C, respectively
Annual Reversible Self-discharge Rate (Charge Loss)(6)			1%, 3%, 6%		25°C, 45°C, and 65°C, respectively

Notes:
1. See Ordering Information.
2. MECs may be shipped in a partially-charged state. Full charging prior to use is recommended.
3. Standard electrochemical degradation is proportional to temperature increase. Contact IPS for performance information regarding higher temperature applications up to 150°C.
4. 80% of rated capacity remaining @ 25°C.
5. Discharging the cell below the specified discharge cutoff voltage will cause permanent battery damage.
6. After first year.
7. MECs cannot be used in reflow or infrared soldering processes. Hand or robotic soldering is required, heating only the MEC terminals.

Typical Characteristics

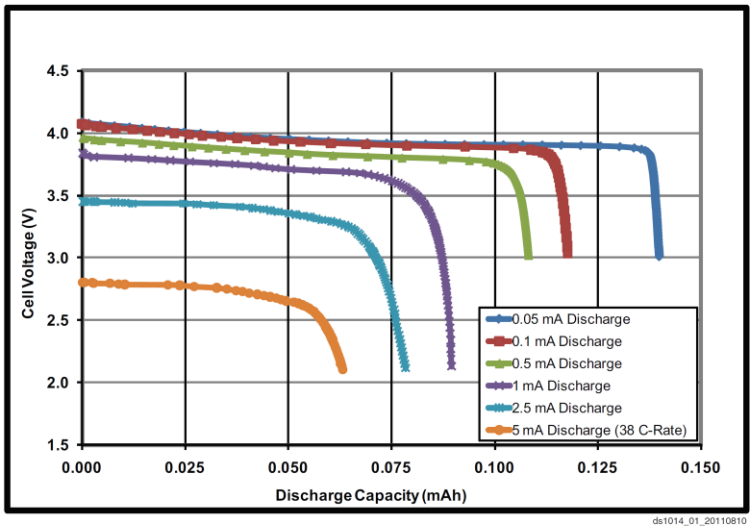

Figure 1: **Typical Discharge Curves @25°C (Standard Grade Cell)**

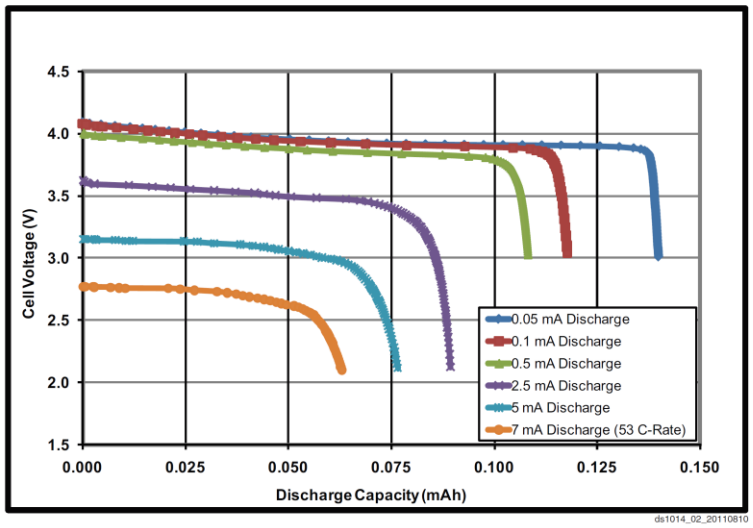

Figure 2: **Typical Discharge Curves @25°C (Performance Grade Cell)**

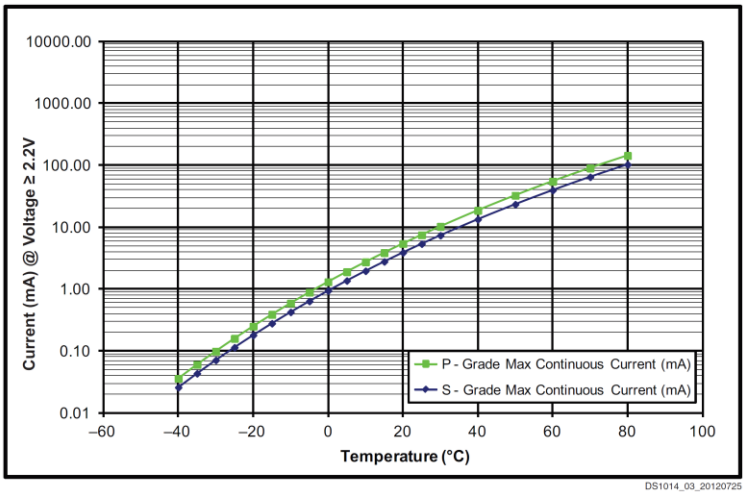

Figure 3: **Typical Maximum Current vs. Temperature**

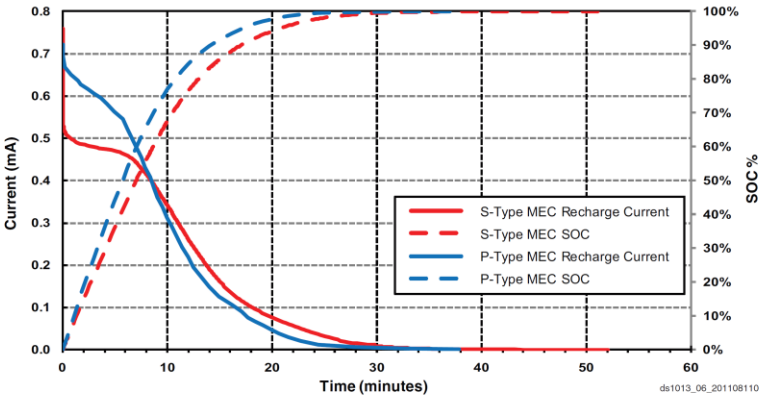

Figure 4: **Typical Charge Curve @ 25°C (Standard and Performance Grades)**

Shelf Life and Self-Discharge Characteristics

Typical energy storage devices such as batteries and super capacitors exhibit self discharge behavior that prevents them from being used in many applications where the stored energy must be retained for periods in excess of ten years or more. Temperature changes that occur in typical applications also have a strong effect on the self-discharge rates of these devices, normally resulting in much higher self-discharge rates as temperature increases. Traditional energy storage devices that have acceptable self-discharge rates at room temperature can easily become unsuitable at elevated temperatures due to elevated self-discharge rates. In contrast, IPS MEC technology consistently demonstrates world leading self-discharge behavior, allowing MECs to be used in place of traditional energy storage devices in applications where decades of use without maintenance are required.

MECs have a distinct advantage over traditional energy storage devices in that they possess a solid state electrolyte. This solid state electrochemical system prevents the high self-discharge rates and premature device failures found in other electrochemical systems using liquid electrolytes.

Shelf life will be determined by the condition of the energy storage device as the open circuit voltage (OCV) decreases over time in the application environment. Device or application failure occurs when the cell voltage drops below the useable cutoff voltage of the application, or when the residual capacity at a given voltage level is no longer sufficient to perform a task demanded by the application without recharge being supplied.

Figure 5 shows the typical MEC state of charge as a function of the open circuit voltage. Note that a great deal of MEC capacity is reserved between 3.9 and 4.0V.

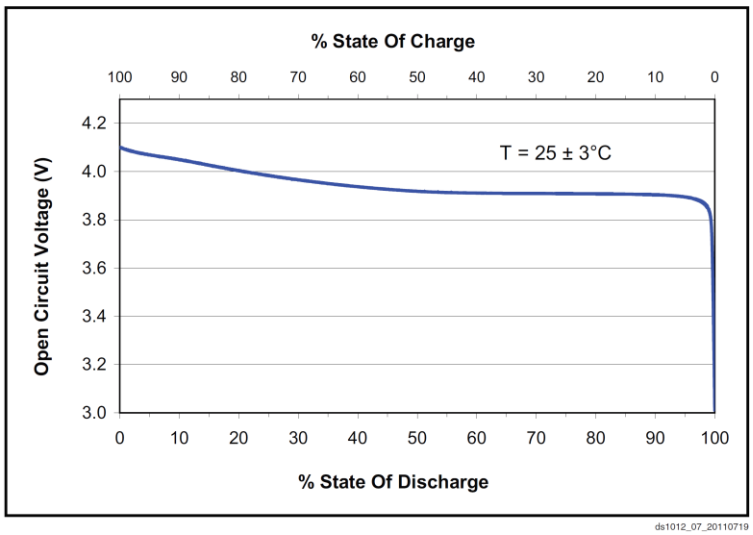

Figure 5: **OCV as a Function of State of Charge at 25°C**

Self-Discharge Performance

In applications where no external load is applied to the MEC, it will experience self-discharge exhibited by an observable decrease in the OCV that is measured on the cell. Figure 6 shows a typical self-discharge curve generated from MEC test data over one year of self-discharge at 25°C. The self-discharge rate increases with temperature, but remains lower than any other energy storage device.

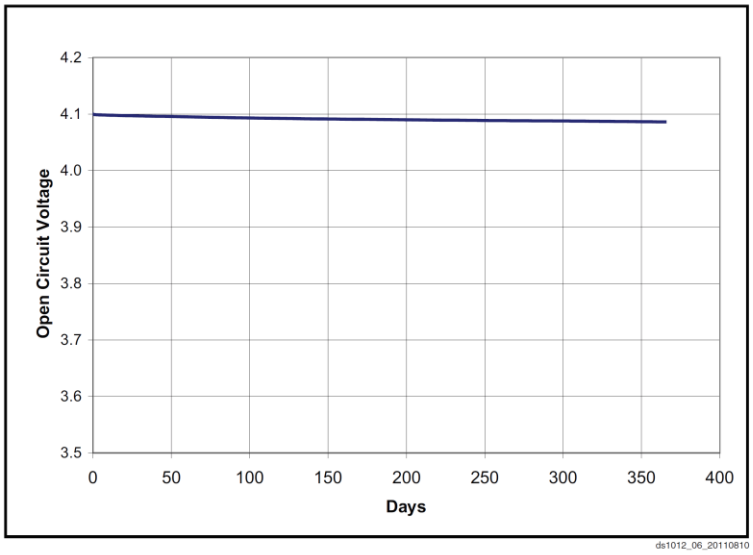

Figure 6: **Typical Voltage Decay over One Year at 25°C**

Figure 7 shows an extrapolated ten year self-discharge curve. Extrapolation is used since no known failure mechanism has been identified in MECs that would cause the discharge curve to deviate from observed normal discharge behavior. As noted previously, the MEC capacity is largely reserved in the voltage region between 3.9 and 4.0V. This demonstrates that the MEC capacity has been reduced by only a fraction, even after ten years of storage at room temperature. Figure 8 shows the extrapolated remaining MEC capacity after 10 years of storage time.

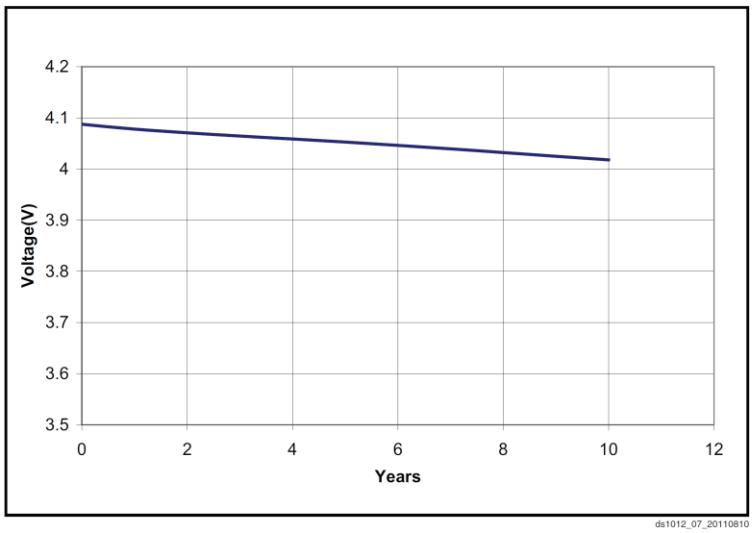

Figure 7: **Ten-Year Extrapolated Voltage Decay at 25°C**

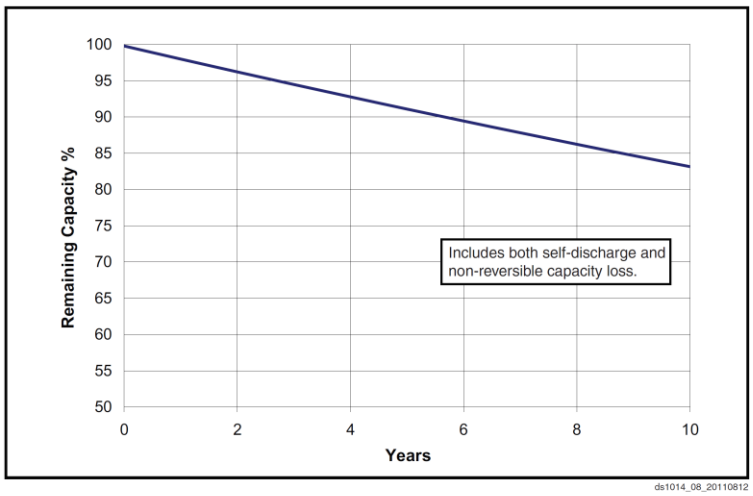

Figure 8: **Extrapolated Ten-Year Remaining Capacity at 25°C**

Package Dimensions

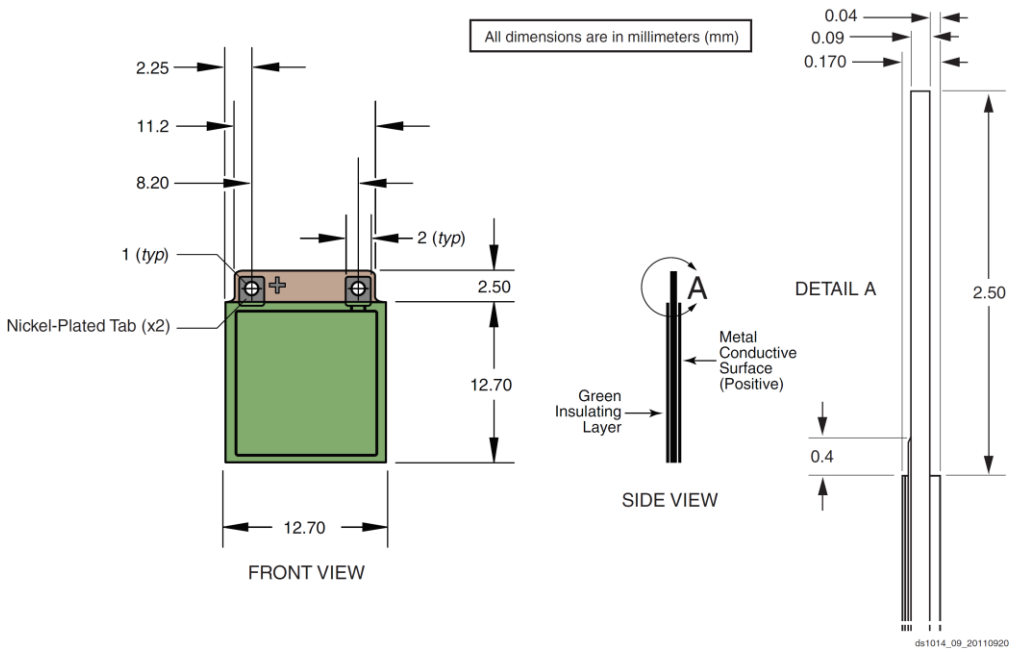

Figure 9: **Front and Side Views**

PCB Land Pattern Dimensions

Drawing (A)
Green (Insulated) Side Up

Dim.	mm	in.
A	3.00	0.118
B	8.20	0.322
C	0.75	0.029
D	2.50	0.098
E	1.00	0.039
F	12.70	0.500
G	14.70	0.578
H	18.20	0.715

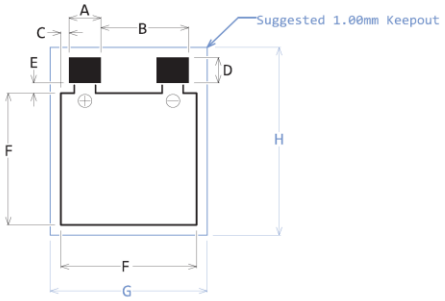

Note: The orientation of this land pattern is such that the MEC225 must be placed with the green (solder mask) side facing away from the board. If your design requires the green (solder mask) side to face the board because of exposed pads, etc., then this land pattern must be mirrored. See Drawing (B) below.

Drawing (B)
Green (Insulated) Side Down

Dim.	mm	in.
A	3.00	0.118
B	8.20	0.322
C	0.75	0.029
D	2.50	0.098
E	1.00	0.039
F	12.70	0.500
G	14.70	0.578
H	18.20	0.715

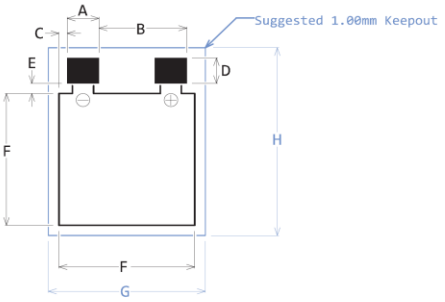

Note: The orientation of this land pattern is such that the MEC225 must be placed with the green (solder mask) side facing toward the board. If your design requires the green (solder mask) side to face away from the board because of cosmetics, etc., then this land pattern must be mirrored. See Drawing (A) above.

ds1014_10_20110810

Figure 10: **PCB Land Pattern**

Ordering Information

The complete IPS part number is as follows:

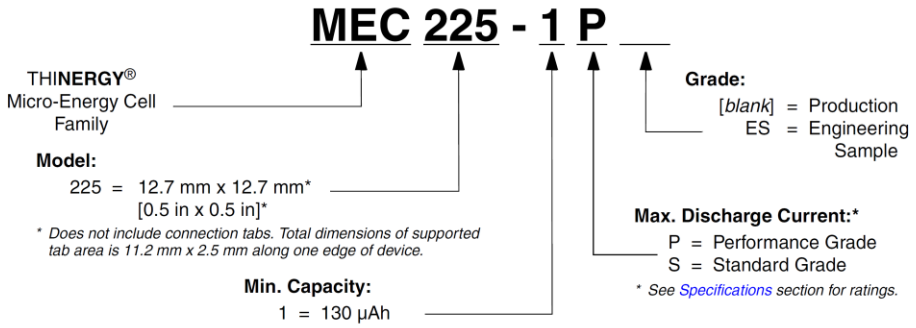

Related Documents

Document	Description
AN1014	*A Guide to Handling, Connecting, and Charging THINERGY® MEC200-Series Micro Energy Cells.*

Related Products

P/N	Description	Capacity	Current	Voltage
MEC201	Micro-Energy Cell (25.4 mm x 25.4 mm)	0.7–1.0 mAh	30–40 mA	4V
MEC202	Micro-Energy Cell (25.4 mm x 50.8 mm)	1.7–2.2 mAh	70–90 mA	4V
MEC220	Micro-Energy Cell (25.4 mm x 12.7 mm)	300–400 µAh	10–15 mA	4V

Available Development Tools

P/N	Description
ADP-201	Application Development Platform (Includes three PCB-mounted MEC devices. Additional PCB-mounted MEC devices can be ordered.)
IPS-EVAL-EH-01	MEC / Energy Harvesting Evaluation Kit Ideal for developing and evaluating various energy harvesting solutions for self-powered applications. Contains THINERGY MEC, Maxim MAX17710 power management IC, and solar cell. Supports any externally connected AC or DC energy harvester.
IPS-EVAL-EH-02	Wireless Environmental Sensor Energy Harvesting Evaluation Kit Complete wireless sensor reference design with solar energy harvesting.

For more information on this and other IPS battery products, visit the IPS web site, or contact us at 303-749-4800 or sales@ipsbatteries.com.

Infinite Power Solutions, Inc.
11149 Bradford Road
Littleton, Colorado 80127 USA
303-749-4800
www.InfinitePowerSolutions.com